Preparation of catalysts on model supports using wet chemical methods and the construction of a device for the in-situ measurement of sum frequency generation spectroscopy at the solid-liquid interface

von

Herrn Rhys Montgomery Dowler, MSc.
geboren in Auckland, Neuseeland

Von der Fakultät II - Mathematik und Naturwissenschaften der
Technischen Universität Berlin
zur Erlangung des akademischen Grades
Doktor der Naturwissenschaften
(Dr. rer. nat.)
genehmigte Dissertation

Diese Dissertation wurde in der Zeit von Juni 2009 bis August 2014 in der Abteilung Chemische Physik am Fritz-Haber-Institut der Max-Planck-Gesellschaft in Berlin unter Anleitung von Prof. Dr. H.-J. Freund angefertigt.

Abstract

The first part of this work details the development and testing of surface science methods for use at solid-liquid interfaces, while the second part of this thesis presents results of surface science investigations into wet chemical catalyst preparation techniques on single-crystalline substrates.

In the first part of this thesis, tests were conducted using an electrochemical scanning tunnelling microscope (STM) and sum frequency generation (SFG) spectroscopy to take in-situ measurements at the solid-liquid interface. Magnesium phthalocyanine was used as a model molecule to be imaged using an electrochemical STM. It was imaged successfully both in-situ and ex-situ on an Au(111) single crystal and ex-situ on an FeO(111)/Pt(111) thin film. This demonstrated that molecular resolution was achievable, even under in-situ conditions using this equipment.

An experimental setup has been designed and built to take sum frequency generation spectroscopy measurements both on samples under ultra-high vacuum (UHV) conditions and at the solid-liquid interface. This was achieved by connecting a liquid cell to a standard UHV chamber via a transfer chamber to allow for clean transfer between UHV and liquid environments without compromising the quality of the vacuum. Initial in-situ measurements were obtained of the spectrum of a self assembled monolayer of octadecanethiol on the Au(111) surface in air, ethanol and water.

In the second part of this thesis, the deposition of palladium and gold particles on iron oxide thin films using wet chemical methods was investigated.

Wet chemical Pd deposition on $Fe_3O_4(111)/Pt(111)$ has been studied previously, but more information was required about the importance of the rinsing step. Rinsing with water until a steady state was reached was found to be sufficient to reduce deposited palladium species to metallic palladium in a manner similar to what is observed from annealing in vacuum. After this rinsing step, small particles could be seen dispersed over the entire surface, confirming the previous model for homogeneous distribution of palladium from solution. Different mechanisms have been proposed for palladium deposited at low and high pH values. Rinsing with water was found to be an effective method for removing chlorine from the surface, although some palladium is lost. In all cases chlorine levels dropped below the detection limit after rinsing until a steady state was achieved.

For gold deposition, a procedure was found for creating small, well dispersed gold particles on an $Fe_3O_4(111)/Pt(111)$ surface. The removal of chlorine through rinsing was found to be critical to maintain dispersion, with significant aggregation observed for unrinsed samples. Gold was deposited on to the surface using a grafting type mechanism similar to what is observed for gold deposition on TiO_2. The deposited gold species were easily reduced either through annealing in vacuum or rinsing with water.

Zusammenfassung

Die vorliegende Arbeit beschreibt einen methodischen und experimentellen Ansatz, der die Untersuchung von nass-chemischen Katalysatorpräparationsverfahren anhand von Modellsystemen und mit oberflächenphysikalischen Untersuchungsmethoden zum Ziel hat. Der erste Teil der Arbeit beschäftigt sich mit der Entwicklung und Erprobung von Methoden zur Untersuchung von fest-flüssig-Grenzflächen, während der zweite Teil die nass-chemische Herstellung von oxid-geträgerten Metall-Nanopartikeln auf einkristallinen Substraten beschreibt.

Summenfrequenz-Erzeugungs-Spektroskopie (SFG) und elektrochemische Raster-Tunnel-Mikroskopie (EC-STM) wurden als in-situ-Methoden zur spektroskopischen und morphologischen Charakterisierung von fest-flüssig-Grenzflächen herangezogen. Die Abbildungsmöglichkeiten des EC-STM wurden anhand der Adsorption von Mg-Phthalocyanin (Mg-Pc) an einkristallinen Oberflächen getestet. Die (Mg-Pc)-Moleküle konnten sowohl ex-situ als auch in-situ, d.h. in einer Toluol-Lösung, auf Au(111) abgebildet werden. Im Fall von FeO(111)/Pt(111), das als Modellsystem für eine Oxidoberfläche verwendet wurde, war eine eindeutige Charakterisierung nur ex-situ möglich.

Für SFG-spektroskopische Untersuchungen wurde ein neuer Probentransfer-Aufbau konzipiert und gebaut, der es erlaubt SFG-Messungen sowohl im Ultrahochvakuum (UHV) als auch in einer geeigneten fest-flüssig-Probenzelle durchzuführen, und die Proben zwischen den beiden Systemen kontaminationsfrei zu transferieren. Erste in-situ SFG-Messungen wurden an selbstorganisierten Monolagen von Oktadekanthiol auf Au(111) an der Luft, in Ethanol, und in Wasser durchgeführt.

Im zweiten Teil der Arbeit, der sich mit Modellstudien zur Katalysatorpräparation befasst, wurde die Abscheidung von Gold und Palladium aus wässrigen, chloridhaltigen Präkursoren-Lösungen auf die Oberflächen von dünnen Eisenoxid-Filmen untersucht. Im Fall von Pd-Fe_3O_4(111)/-Pt(111) konnte gezeigt werden, daßdurch ausgiebiges „Waschen" die auf der Oberfläche adsorbierten Pd-Präkursoren zu metallischem Pd reduziert werden, wobei kleine, gleichmäßig über die Oberfläche verteilte Pd-Partikel entstehen. Weitere Konsequenzen des Waschens, wie der Verlust von Pd oder die Beseitigung von Cl und Na, wurden für verschiedene Proben-Präparationsbedingungen (pH-Wert) unter Verwendung unterschiedlicher Waschlösungen (destilliertes Wasser, Blindlösungen) untersucht. Es konnte gezeigt werden, daßdas Waschen mit Wasser eine effektive Methode zur Beseitigung von Cl darstellt. Letztere ist von Bedeutung für die Dispersion der Pd-Partikel.

Im Fall der Gold-Abscheidung konnte ein Weg gefunden werden, über die nass-chemische Präparation kleine, fein-verteilte Gold-Partikel auf der Fe_3O_4(111)-Oberfläche herzustellen. Wie im Fall von Au-TiO_2 wurde hier die Adsorption der Au-Präkursoren im basischen Milieu über eine Grafting-Reaktion durchgeführt. Die Reduktion der oxidischen Au-Präkursoren erfolgte entweder thermisch oder durch Waschen mit Wasser. Der Einfluss von zurückbleibendem Cl auf die Dispersion von Au-Nanoteilchen auf Fe_3O_4(111) konnte eindeutig nachgewiesen werden.

Acknowledgments

This work would not have been possible without the substantial support I have received from my coworkers, friends and family.

In particular I would like to thank the following people:

Prof. Dr. Hans-Joachim Freund, for giving me the opportunity to come to Germany to continue my career as a surface scientist at the Fritz Haber Institute and acting as my first supervisor for this project.

Prof. Dr. Reinhard Schomäcker, for acting as my supervisor at the Technical University Berlin and helping me to navigate the administrative requirements of that institution.

Dr. Martin Sterrer, for acting as my day-to-day supervisor, allowing me to present my arguments to him when I thought I was right, but sticking to his guns to tell me when I was wrong, and for working with me to tackle the hardest of the technical and scientific challenges that occurred during my research.

Dipl.-Phys. Burkhard Kell, for his technical assistance in piecing together my equipment, teaching me the technical skills necessary to fix and construct things myself and for making sure everything was done in a safe and proper manner within the lab.

A. Prof. Hiroko Ariga, Dr. Matt Brown and Dr. Bill Kaden, for guiding me through the experimental world of surface science, forgiving my foolish questions in the early days of my studies and later when they still came occasionally.

Dr. Andreas Aumer, for showing me the ropes of sum frequency generation and introducing me to the equipment in the lab.

The other members of my workgroup, for the fruitful discussions and camaraderie provided from others in the trenches.

Herrn Klaus-Peter Vogelgesang, for always eagerly springing into action to help with the machining of new parts and dealing with the ever-changing requirements that occur during the construction of new equipment, happy to chat about anything and everything along the way.

The rest of my friends and colleagues at the Fritz Haber institute, your friendly faces and lunchtime conversations helped to buoy me in the occasional difficult times, the outcomes of any scientific conversations notwithstanding.

My parents, for doing their best to keep an eye on me and support me as best as they could from the other side of the world. Thank you for giving me the freedom to follow my dreams, but caring enough to keep in regular contact.

My older brother, Shaun, for trying his best to act like a big brother with his sage advice and insight from a similar time, not long past. I respect your opinions and am always eager to hear your input, even if I don't always agree.

My younger sister, Erin. Shaun already thanked you in his thesis for not talking about his research with him, but I think you know that you are more important than just that.

Zita Hüsges, for being my Zita. You filled the holes left by my family being so far away and helped me to keep my sanity through my studies. I might have made it through to the other side without your help, but it would have been a much darker journey and I would have been poorer for it.

Contents

Chapter 1

Introduction

Heterogeneous catalysts are vital to the modern chemical industry, with an estimated 90% of all chemical processes utilising heterogeneous catalysis [1]. In excess of 80% of all heterogeneous catalysts are produced using the wet chemical methods of precipitation or impregnation [2], but despite this, precious little information is available about the processes occurring at an atomic scale at the solid-liquid interface during catalyst preparation. The material properties and ultimately the effectiveness and efficiency of a catalyst can strongly depend on the preparation method used [3, 4, 5]. For this reason it is absolutely critical to understand these processes.

Investigating these processes in a systematic way requires controlled environments with well ordered samples. Traditional surface science meets these requirements, but the ultra-high vacuum (UHV) environments typically used in surface science [6] are far removed from the liquid environments of catalyst preparation. While much is known about the growth of metal particles on single-crystalline oxide substrates under UHV conditions [7, 8, 9], comparatively little is known about the growth of metal particles deposited from liquid. To properly address the problem of understanding catalyst preparation requires the development of techniques to study the problem in-situ by bringing the well ordered surfaces of surface science into liquid environments.

This work aims to make progress toward this goal of understanding catalyst preparation procedures by developing equipment that can be used for in-situ measurement during catalyst preparation. By preparing well ordered samples under UHV conditions before transferring them into a liquid cell, atomic level information about the processes occurring during catalyst preparation should be obtainable.

Due to the complexity of heterogeneous catalysis, considerable effort has been directed in designing model systems which incorporate the essential features of a particular catalyst of interest, while reducing the complexity of the system [10]. Single crystal surfaces, where only a single crystal plane is exposed for reaction and measurement, are well defined systems where in principle every atomic site on the surface can be defined. Well defined single-crystalline substrates have been used extensively in surface science as they allow effects (such as adsorption, bond cleavage, reactions, etc.) to be unambiguously attributed to specific surface sites.

Many surface science techniques either require or work best with conducting substrates such as metals, but these are not the only materials of catalytic interest. Metal oxides are often used as supports for small metallic particles in catalysis [11] and may even be an important part of

the active catalyst itself [12, 13]. Determining the importance and effect of a particular support requires that the support is also properly characterised [14].

Some metal oxides are insulating, which can lead to charging (for example in XPS), which can in turn interfere with measurement. One potential way to circumvent this problem is to use ultrathin films grown on top of metal substrates. If the film is thin enough that sufficient conduction exists, insulating substrates can be studied using techniques such as scanning tunnelling microscopy (STM) [15]. Using an ultrathin film can also reduce any possible charging effects during measurement.

The complexity of such systems can also be increased in a systematic manner, with initial studies being conducted on metallic single crystals and oxide substrates, before combining the two systems by depositing metal particles on top of an oxide substrate to create oxide supported, highly dispersed metal particle model catalysts [16]. Such model catalysts allow any interaction between metal particles on the surface and the substrate to be investigated. The role of the support for a given catalytic reaction can be critical to its catalytic activity through mechanisms such as the spillover effect or electron transfer. Supported metal particle model catalysts can also be used to investigate the effect of particle size on catalytic activity, which cannot be achieved using single crystals.

These model systems can be used to better understand which features of a catalytic system are important and the mechanisms at work by introducing complexity slowly in a systematic manner. There has been significant research conducted on the catalytic systems used in industrial chemistry, but deeper understanding has been achieved from surface science studies on model catalysts.

Supported metal particle model catalysts were chosen as the focus of this work due to the large body of surface science work conducted in this field [16, 17] and the importance of metal catalysts[18, 19]. Single-crystalline oxide thin film model catalysts are well suited as substrates for studies of catalyst preparation due to the aforementioned advantages of single crystals and their compatibility with surface science methods.

While vacuum based experiments are extremely useful when it comes to gaining initial insight into complex systems, many industrial processes occur in much dirtier environments under much more extreme conditions, such as ambient or even elevated pressures. Ex-situ surface science relies on techniques such as freezing out absorbed molecules to understand their bonding modes during reaction [20] to observe the state of the surface after a process rather than during it. The very act of removing a sample from its environment may change the results of a measurement. It is important to see how a situation of interest can change under these very different conditions.

To this end, traditional surface science techniques have been modified to allow them to work under different conditions, such as the pressures seen inside industrial reaction vessels. Some techniques, such as polarisation modulation infrared absorption spectroscopy (PM-IRAS) and sum frequency generation (SFG) [21], can be applied under high pressure conditions without modification to the technique. This requires an appropriately designed chamber that can retain acceptably low base pressure in a section used for sample preparation with another section which can be brought to higher pressures for in-situ measurement. Ambient pressure SFG has

already been used in order to investigate any differences that may occur in the behaviour of model catalyst samples under higher pressures [22, 23]. STM and atomic force microscopy (AFM) can likewise be applied at ambient pressures [24, 25, 26] and furthermore, have also been demonstrated to work under the same principles in liquid environments [27].

Using differential pumping to keep the pressure low inside the analyser has allowed XPS to be applied to systems at high pressure [28]. With a small aperture at the entrance to the analyser, the pressure can be kept sufficiently low and the mean free path of electrons sufficiently high that measurements can be taken from samples in a pressure of up to 1 Torr.

Using surface science techniques under ambient pressures and more realistic conditions acts as a bridge between the fundamental studies conducted in vacuum and real world catalysis. These kinds of studies are important to ensure that information gained on simpler systems is relevant to what is occurring at reaction conditions. These techniques can be used to understand what is occurring on a surface as it is happening.

Industrial catalyst preparation does not occur under UHV conditions and as such, in-situ surface science techniques are required to properly understand the processes occurring during catalyst preparation. The supported metal particle model catalysts typically used in surface science studies are prepared using techniques such as physical vapour deposition (PVD) [17], which is far removed from industrially used wet chemical methods. While some insight can be gained from ex-situ studies of these processes, a full understanding of the atomic level processes occurring during catalyst preparation requires appropriate in-situ tools which can investigate the processes occurring at the solid-liquid interface.

This thesis specifically addresses this need by detailing the design, construction and testing of equipment for applying in-situ surface science techniques at the solid-liquid interface.

1.1 Aim

The aim of this work was to develop instrumentation for in-situ surface science techniques which could be applied to investigating the processes occurring during catalyst preparation at the solid-liquid interface. This was to be achieved through designing new equipment including load-lock systems which would allow samples to be transferred between UHV, ambient and liquid environments. In this manner samples could be prepared under UHV conditions and then characterised both in-situ and ex-situ in order to understand and follow the processes that occur at the solid-liquid interface during catalyst preparation.

Electrochemical STM is a well established technique which has been used extensively in the past to investigate electrochemical problems [29] and the structures of SAMs on metal electrode surfaces [30], but it has not been utilised in systematic model catalyst studies. This technique was chosen as it provides important real space structural information and can even obtain atomic scale information under the right conditions. Liquid STM could be used both in-situ, to image the initial interaction of catalyst precursors with the substrate surface, and ex-situ, to investigate the effect of post deposition treatments on the deposited metal particles.

To supplement the structural information gained from STM, SFG spectroscopy was chosen to add vibrational information. This technique has already been used to gain information from

model catalyst systems both under UHV and high pressure conditions [20, 31, 32] as well as investigating gas-liquid [33], liquid-liquid [34] and solid-liquid [35] interfaces. SFG is inherently surface selective, making it well suited to investigating processes occurring at a substrate surface during catalyst preparation through a liquid layer. While similar techniques have been applied to polycrystalline catalyst samples [36], in-situ vibrational spectroscopy has not been previously used to investigate catalyst preparation using single-crystalline model catalyst systems.

By marrying these two techniques with a complete UHV preparation and analysis chamber the goal is to create a setup that could be used to investigate the processes that occur during the individual steps of catalyst preparation. The combination of single-crystalline model catalyst substrates with wet chemical preparation methods acts as a bridge between previously conducted surface science studies and real world catalyst preparation to better understand the important processes in catalyst preparation and explain differences observed between UHV prepared model catalyst systems and industrial catalysts prepared by wet chemical methods.

As a first step toward this goal, studies could also be conducted using existing ex-situ surface science techniques. By combining traditional surface science methods housed within the UHV preparation chamber such as XPS and using the STM at ambient pressures, new information could be gained about the interaction of catalyst precursor solutions with single-crystalline model catalyst systems. These first experiments could provide important insight into later experiments using in-situ techniques.

This work attempts to address these questions in the following chapters. Chapter 2 describes the general procedures, applied techniques and equipment used experimentally. Chapter 3 discusses the development of equipment for in-situ surface science on single-crystalline substrates and presents first results from this equipment. Chapter 4 presents results from ex-situ measurements on single-crystalline Fe_3O_4 films on which gold and palladium have been deposited using wet chemical methods.

Chapter 2

Experimental

This chapter outlines the experimental setup used for this work with a description of the physical components used. This is followed by an overview of the iron oxide thin films primarily used in this work and the theoretical background of the major techniques used to characterise the samples produced. The final section outlines the procedures used for liquid deposition experiments.

2.1   Experimental setup

The experiments in this work were conducted inside a purpose built experimental setup consisting of three different chambers, an ultra-high vacuum (UHV) preparation chamber, a UHV/ambient transfer chamber and a high-vacuum/ambient liquid chamber. These chambers were all be separated from each other by gate valves. A detailed account of this setup and its design can be found in section 3.2.1. Sample preparation was conducted inside the preparation chamber which was kept under UHV conditions at all times. A magnetic transfer rod, with an attachment to grab the sample, could be used to remove samples from the manipulator in the preparation chamber (Figure 2.1 (b)) and then transfer them into the transfer chamber on to a second manipulator. After being sealed off from the preparation chamber, the transfer chamber could be purged with an inert gas and the sample then transferred into the liquid chamber or removed from the setup completely through a gate valve.

   The preparation chamber was pumped using a turbomolecular pump (Varian TV 551) and the pressure was measured via an ion gauge (Varian UHV 24). This chamber had a base pressure of 1×10^{-10} mbar. Two evaporators were attached to the preparation chamber for physical vapour deposition (PVD). The first evaporator had three sources and filaments and was set up opposite a quartz microbalance for calibration. The other evaporator had only one filament and source and no quartz microbalance. Cleaning of the sample was achieved through argon ion bombardment using an ion source (Specs IQE 11) and through heating the sample through electron bombardment from a tungsten filament attached to the sample holder (see section 2.1.1). The sputter gun was set up with the correct geometry with respect to a hemispherical analyser (Specs Phoibos 150) which allowed ion scattering experiments to be performed. An x-ray source (Specs XR 50) was situated on the opposite side of this analyser which allowed x-ray photoelectron spectroscopy (XPS) measurements to be made. The chamber
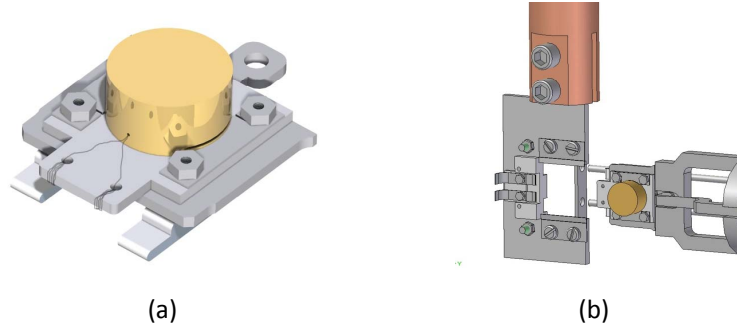
Figure 2.1: Renders of (a) the sample holder and (b) the sample holder on the end of a magnetic transfer rod next to the manipulator in the preparation chamber.

also included a quadrapole mass spectrometer (Pfeiffer QMG 220) for TPD measurements, two direct dosing lines, a valve for backfilling the chamber, a thoriated tungsten filament for electron bombardment, a titanium sublimation pump and low energy electron diffraction (LEED) optics (Specs ErLEED 150).

The transfer chamber was pumped by another turbopump (Pfeiffer TMU 071P), with pressure measured by either an ion gauge under UHV conditions or an absolute capacitance manometer (MKS Barotron 626A) for high and ambient pressure applications. This chamber had a typical operating base pressure of 1×10^{-9} mbar when pumped by the turbopump, although lower pressures could be achieved by baking the chamber out. The manipulator head in this chamber was simple with only one connection for the sample so that it could be grounded or a potential applied. The turbopump could be separated from the chamber via a gate valve and there were additional valves through which the chamber can be backfilled and pumped to high vacuum.

The liquid chamber was pumped using a rotary vane pump (Edwards RV8), which could be separated from the chamber using a valve. The chamber pressure was measured using an absolute capacitance manometer of the same type used in the transfer chamber. Gas could be dosed through an attached valve. This chamber contained within it a liquid cell into which liquid could be introduced and removed through two hose connector inlets. The liquid cell itself consisted of a CaF_2 prism or window pressed up against a Viton ring gasket seal held within a polyether ether ketone housing. The sample was introduced into the liquid cell through an o-ring which sealed against the sides of the crystal.

A scanning tunnelling microscope (STM) stood separately from the rest of the experimental setup and was situated inside an aluminium cube. This cube could be sealed from the environment and the air inside could be replaced by an inert atmosphere. This STM was built by the Wandelt group for electrochemical purposes [37], with the capacity to take measurements in liquid environments with or without potential control. The microscope has undergone some minor adjustments to allow a customised cell to be used, which can accept samples held on

sample

Mo screws M1.2

Mo foil

sapphire plate
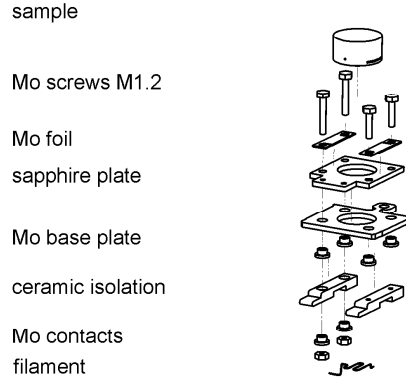
Mo base plate

ceramic isolation

Mo contacts

filament

Figure 2.2: Exploded view of the sample holder.

the sample holder used within UHV. The microscope was placed on top of a benchtop isolator (Halcyonics Micro 40) which rested upon a heavy artificial stone table to reduce the effect of vibrations on imaging.

Sum frequency generation (SFG) experiments were performed using a neodymium-doped yttrium aluminum garnet (Nd:YAG) pulse laser (Ekspla PL501), which was then passed through harmonic crystals (Ekspla H500) to produce the second and third harmonic. The second harmonic was used as the visible beam for SFG spectroscopy. The original infrared (IR) beam and third harmonic were passed into an optical parametric generator/amplifier (Ekspla PG401) to produce a tunable infrared beam, which was then used as the IR component for sum frequency generation spectroscopy. These lasers were situated upon an optical bench which holds mirrors and other optical components to steer the beams to overlap, spatially and temporally, on the sample surface. Two flip mirrors and an additional beam delay allowed the beams to be focused either on a sample within the preparation chamber through two CaF_2 windows or into the liquid cell.

2.1.1 Sample holder and manipulator head

The sample is mounted upon a modified Omicron sample plate (Figure 2.2). Two molybdenum rails are connected to this plate. The first is connected directly to the sample and is used to ground or apply potential to the sample. The other is connected to a tungsten filament which makes several turns before being grounded on the sample plate. Sample heating is achieved via electron bombardment from this filament when the sample is held at high voltage. The sample itself is kept isolated from the sample plate by a sapphire plate. Chromel and alumel wires are spot welded to the side of the sample to act as a thermocouple. These wires are wound around the sapphire plate several times to act as contacts.

The manipulator head has two spring clip contacts made of molybdenum to connect to the rails and a further two spring clips made of chromel and alumel to connect to the thermocouple. Samples are held in place using friction from two additional molybdenum spring clips that apply pressure to either side of the sample plate. The manipulator head is attached to a cold finger

that can be filled with liquid nitrogen to bring the sample temperature down to 150 K.

2.2 Iron oxide thin films

$Fe_3O_4(111)$ and FeO(111) thin films were grown upon a platinum single crystal cut such that the (111) surface was exposed, following a recipe well established in the literature [38, 39]. These surfaces have been used extensively in research projects at the Fritz Haber Institute in the past [40, 41]. First, a monolayer film of FeO was grown by depositing a monolayer equivalent of iron at room temperature followed by heating the sample to 950 K in 1.0×10^{-6} mbar O_2 for 2 minutes. If this was the desired film, preparation stopped at this point and the LEED pattern was checked to ensure that a complete, ordered film had been produced (Figure 2.3 (b)).

To produce an Fe_3O_4 film, iron was then deposited in 8 monolayer (ML) equivalent amounts followed by annealing to 880 K in 1.0×10^{-6} mbar O_2 for 5 minutes until the desired thickness was achieved. At this point there was a final oxidation step at 1000 K (Figure 2.4). In this work all experiments were conducted using films made from depositing an amount equivalent to 33 ML of iron as measured using a quartz microbalance. After deposition the quality and cleanliness of the film was checked using LEED and XPS. Typical LEED images obtained at each step of film preparation can be seen in figure 2.3.

The FeO film wets the surface in a bilayer arrangement with oxygen atoms occupying the three-fold hollow sites between the iron atoms [42]. There is an approximately 10% mismatch in the lattice constants of the Pt(111) and FeO(111) surface, which leads to a Moiré pattern as observed in STM (Figure 2.5). Additional iron grows as Fe_3O_4 islands upon this layer to cover the surface via a Stranski-Krastnov growth mode [39].

The surface structure of bulk $Fe_3O_4(111)$ as determined from LEED and STM measurements can be seen in figure 2.6. The $Fe_3O_4(111)/Pt(111)$ thin film displays the same LEED pattern suggesting the same surface structure exists for the thin film as for a bulk $Fe_3O_4(111)$ single crystal. The surface is terminated with a 1/4 monolayer of iron atoms exposed followed by a layer of oxygen atoms.

These films have already been shown to have excellent stability in aqueous solutions [43] and Fe_3O_4 has previously been studied extensively as a model catalyst substrate [44, 45].
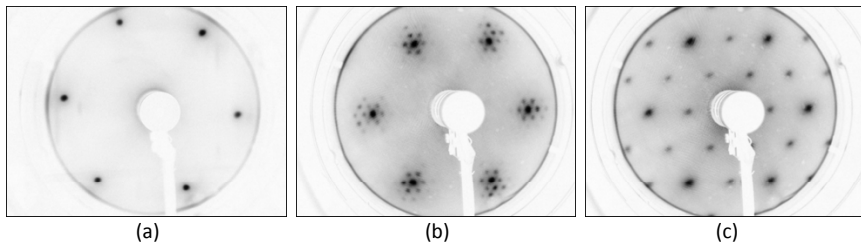

Figure 2.3: Typical LEED patterns observed during iron oxide film preparation. (a) Clean Pt(111), (b) FeO(111) and (c)$Fe_3O_4(111)$.

iron deposition

iron

oxygen

Pt substrate

iron oxidation in 1 x 10^{-6} mbar O$_2$ at 950 K

FeO(111)

After additional iron and iron oxidation in 1 x 10^{-6} mbar O$_2$ at 880-1000 K
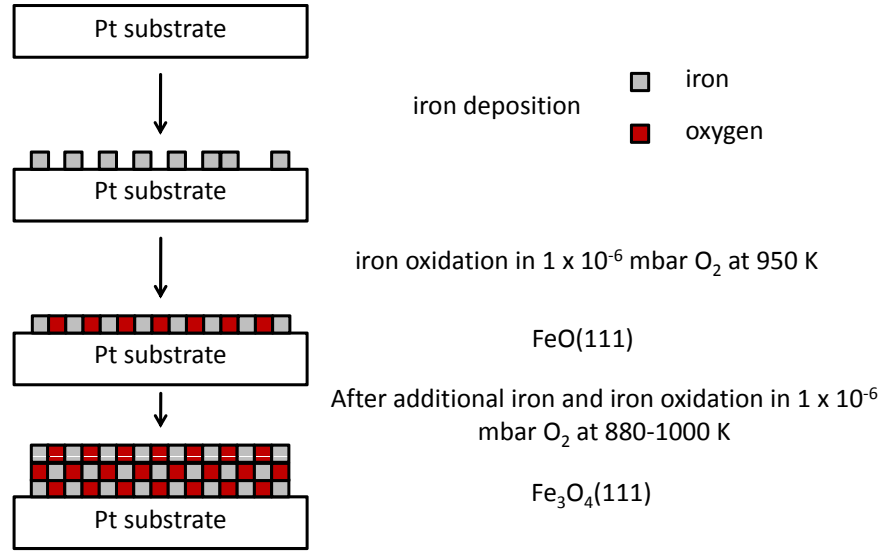
Fe$_3$O$_4$(111)

Figure 2.4: Schematic representation of the preparation of Fe$_3$O$_4$ films reproduced from [39].
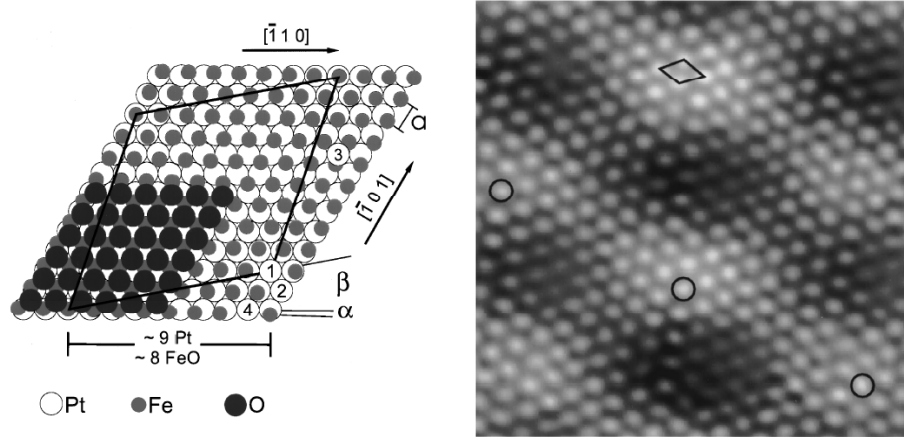

Figure 2.5: Model of the FeO(111)/Pt(111) surface demonstrating the lattice mismatch beside a 55×55 nm^2 STM image of the same surface, demonstrating the Moiré pattern caused by this mismatch. Taken from [42].
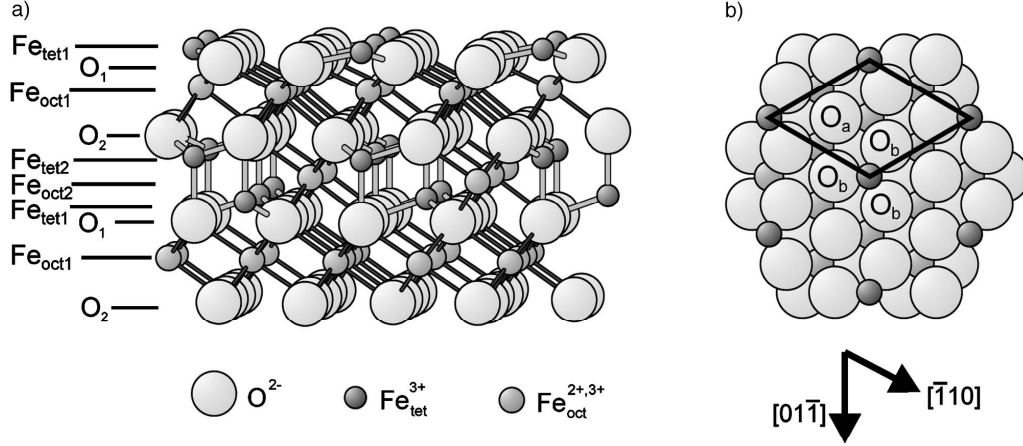
Figure 2.6: (a) Tilted and (b) top down views of the surface structure of bulk Fe_3O_4 of the surface taken from [46].

2.3 Experimental techniques

2.3.1 X-ray photoelectron spectroscopy

This technique utilises x-rays to eject electrons from a sample. Upon ejection, the kinetic energy of these electrons can be measured. Nominally this energy should be equal to the energy of the exciting photon, less the binding energy of the electron in the sample and the work function of the sample. This poses a difficulty as in most cases the work function of the sample is not known. However, this can be overcome by connecting both the sample and the detector to a common ground to align the Fermi energy of the sample and the detector (Figure 2.7). In this arrangement, the kinetic energy of the electron detected, E'_k, is:

$$E'_k = hv - (\phi_d + E_B) \tag{2.1}$$

where hv is the energy of the incident photon, ϕ_d is the work function of the detector and E_B is the binding energy of the electron. From this, it is trivial to determine the binding energy of an ejected electron if the energy of the excitation source and the work function of the detector is known. This binding energy measurement accounts for energy changes from the rearrangement of the electrons to screen the core hole created by this process. As such, it does not exactly correspond with the initial state energy of the electron ejected, but has qualitative agreement with this.

The binding energy may be regarded as the energy difference between the initial state and the final state of the system after an electron has been ejected. The different lines of a spectrum arise from the different possible final states after a single electron has been removed from an atom. The intensity of these lines is determined by the cross-section or probability for each final state.

An example of this is the spin-orbit splitting observed for p, d and f levels. After an electron is ejected from a complete p, d or f core level, there are two possible outcomes for the spin
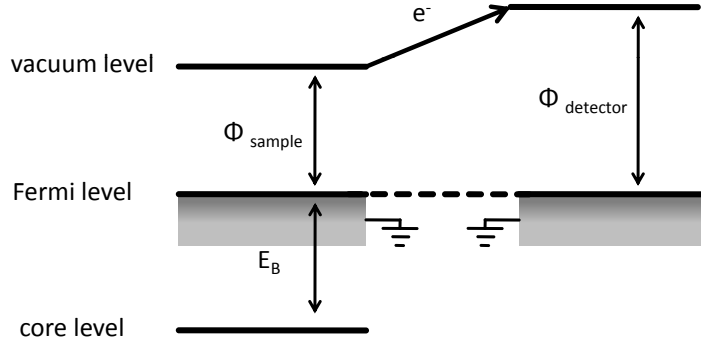
Figure 2.7: Schematic representation of the effect of grounding the sample and detector on the energy levels in the system.

of the unpaired electron interacting with the angular momentum of the orbital. For example, a d level has orbital angular momentum, $l = 2$. When coupled with the spin of an unpaired electron, $s = 1/2$, this results in two possible values for the total angular momentum, $j = 5/2$ and $j = 3/2$. The two states relating to these different values of total angular momentum have slightly different energy, resulting in two distinct lines in XPS. The relative intensity of these two lines is determined by the degeneracy of these two states ($g_j = 2j + 1$), such that the peak area of the $d_{5/2}$ state is larger than the $d_{3/2}$ state by a factor of 1.5.

Shake-up satellites can also occur when the final state of the atom is an ion in its excited state instead of the ground state [47]. This leads to a reduction in the kinetic energy of the emitted electron and an increase in the measured binding energy. This effect results in a second peak with a few electron volts higher binding energy than the main peak.

The intensity, I, of a given peak can be determined by the following equation [48]:

$$I = nf\sigma\theta y\lambda AT \tag{2.2}$$

where n is the concentration of the element from which the peak is derived, f is the x-ray flux incident on the surface, σ is the Scofield factor, a measure of the cross-section for photoemission, θ is the angular efficiency factor for the instrumental arrangement, y is the efficiency of the photoelectron process for generating electrons in the primary peak, λ is the inelastic mean free path of the emitted photoelectron, A is the area from which photoelectrons are detected and T is the efficiency of the detector. The Scofield cross-section factor is the primary factor responsible for the different intensity of peaks corresponding to different final states and represents the overlap between the initial and final states under the influence of the electric field of the incoming x-rays.

Scofield cross-section factors have been calculated from scattering theory for each element [49] and the inelastic mean free path can either be estimated from a so-called universal curve or calculated [50]. This becomes more complicated for heterogeneous systems with more than one component, but this technique can still be applied with reasonable accuracy by averaging these values based upon the composition of the material. f, θ, A and T should be constant within a

13

given experiment, but will vary between experimental setups. The x-ray flux in particular may vary over time, even for a given setup.

Measured spectra are directly comparable with the density of states of a sample and often plotted as electron counts or counts per second versus binding energy, with binding energy decreasing from left to right. There is always a high background of secondary electrons present caused by inelastic scattering events, with the background being higher on the high binding energy side of any peak due to the inelastic scattering of the electrons being emitted from the related core level. Each element has a characteristic distribution of peaks within the spectrum which can be used to identify the chemical components of a sample.

The binding energy of a particular energy state in an atom can also change with the oxidation state or the local chemical or physical environment of the atom. Core-level binding energies are determined by the electrostatic interaction of the electron with the nucleus. This can be reduced by the electrostatic shielding of other electrons surrounding the nucleus which can be altered by removing charge or adding charge through bonding. This means that qualitatively removing electron density from the valence band results in an increase in binding energy and adding electron density to the valence band results in a decrease in binding energy. This effect is usually thought of as an initial state effect and is what can be used to determine the chemical state of an element within a material.

From this point of view the binding energy shifts in a system are often considered to be purely initial state effects and used to assign the oxidation state of elements in a material, but care must be taken as this may not always be the case. Changes in the final state energy of the system can also have a marked effect on the measured binding energy through changes in polarisability leading to greater or lesser screening of the electron hole left behind by the emission process. Other effects can also affect the measured binding energy, such as size effects when dealing with small metal clusters [51]. For small enough metal particles the binding energy shifts to higher binding energy. As the particle size increases, the measured binding energy converges to the value measured for bulk metal. This change arises from both initial and final state effects. The initial state changes due to lattice strain, that exists because bond lengths are shorter in smaller particles [52], and the final state changes with the particle size as the electrons in larger particles can more easily screen the electron hole left behind.

The technique is inherently surface sensitive as, despite the x-rays penetrating up to 10 micrometers into the surface, the inelastic mean free path of photoelectrons inside a solid is typically less than 10 nanometers. The surface sensitivity of the technique can be further enhanced by tuning the energy of the excitation source, and therefore the kinetic energy of electrons emitted, to reduce the escape depth or by rotating the sample with respect to the detector.

Experimental implementation of this technique requires an x-ray source and a detector to collect the photoelectrons. The x-ray source is typically a Mg/Al dual-anode laboratory source or a synchrotron. In the case of the laboratory sources a monochromator can be used to ensure that only the Kα line of the x-ray source reaches the sample. The energy of the electrons detected needs to be determined by using a detector such as a hemispherical electron analyser with an electrostatic lens system [53]. The energy of electrons entering the detector is retarded

by the lens system and the hemispherical analyser ensures that only electrons of a certain energy reach the detector. By varying the retardation potential, the entire spectrum can be captured. In order for the inelastic mean free path of electrons to be long enough to reach the detector without further interaction, UHV conditions are usually required.

XPS was used to gain information about the chemical state of the systems studied. Before every wet chemical XPS experiment a spectrum of clean Pt(111) was acquired to act as an external reference to account for variations in signal intensity over time. Each XPS spectrum has been normalised to the intensity of the Pt 4f peak from this reference spectrum to ensure that XPS intensities could be meaningfully compared between experiments.

2.3.2   Sum frequency generation spectroscopy

Sum frequency generation is a second order nonlinear optical effect, the generation of which can be utilised to gain vibrational information about a system. In this technique, two laser beams are directed on to a sample surface, one in the visible region of the spectrum (frequency ω_{vis}), the other in the infrared region (frequency ω_{ir}). When pulsed on to a surface at the same time a third beam is generated with frequency equal to the sum of the two frequencies of the incident laser pulses.

$$\omega_{sfg} = \omega_{vis} + \omega_{ir} \tag{2.3}$$

This sum frequency generation signal is dependent upon the second order polarisation, $P^{(2)}$ [54],

$$P^{(2)}(\omega_{sfg} = \omega_{vis} + \omega_{ir}) = \varepsilon_0 \chi^{(2)} E_{vis} E_{ir} \tag{2.4}$$

where ε_0 is the vacuum permittivity, $\chi^{(2)}$ is the second order susceptibility and E_{vis} E_{ir} are the local electric fields. When using the electric dipole approximation, a medium with a centre of inversion will have $\chi^{(2)}$ equal to zero and as such this third beam can only be generated at the interface between two phases where this symmetry is broken. As such, SFG is an inherently surface sensitive technique and the majority of any signal observed arises from the surface. The effect of $\chi^{(2)}$ only becomes significant when the applied electromagnetic field is comparable with the field experienced by the electrons in a molecule. This normally requires high energy pulsed lasers to be realised experimentally [55].

To work as a spectroscopic technique, ω_{ir} is varied and the intensity of the SFG signal measured. The intensity of this signal depends on $|\chi^{(2)}|^2$ [56] with the relationship,

$$I_{sfg} \propto |\chi^{(2)}|^2 = |\chi^{(2)}_{NR}| + |\chi^{(2)}_{R}| + 2|\chi^{(2)}_{NR}||\chi^{(2)}_{R}|cos(\epsilon - \delta) \tag{2.5}$$

where $\chi^{(2)}_{NR}$ is a non-resonant component that arises from truncation of bulk phases, which varies only slowly with ω_{ir}, and $\chi^{(2)}_{R}$ is a resonant component which comes from vibrational modes at the surface. $\chi^{(2)}_{R}$ is significantly enhanced when ω_{ir} is equal to the energy of a vibrational mode of a molecule on the surface that is both Raman and IR active. In this manner a vibrational spectrum of molecules on the surface can be obtained by varying ω_{ir} and recording the intensity of the SFG signal. The selection rules for this technique not only
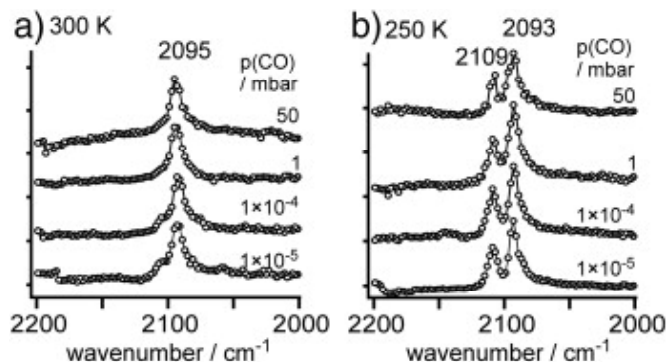
Figure 2.8: SFG spectra of CO adsorbed on Pt(111) at a) 300 K and b) 250 K under continuous CO exposure at the indicated pressures. Taken from [23].

require that there is no centre of inversion, but there must also be a net polar orientation of the molecules at the surface. As such, no SFG signal is observed from molecules arranged in an equal number of opposite orientations on the surface or from a completely disordered surface structure [55].

An example spectrum can be seen in figure 2.8. At 300 K only one peak is observed from the C-O stretch on top of platinum, but at 250 K two distinct vibrational peaks can be seen caused by a CO adlayer at coverages over 0.5. This spectrum has no non-resonant component, with only resonant peaks visible, slightly broadened toward the high frequency side at low pressures [23].

In systems containing a non-resonant component, information can be gained about the orientation of molecules on the surface from the spectral lineshape of the SFG signal [55]. Further information about the orientation of molecules on the surface can be gained by recording spectra with different incident beam polarisations [57, 58]. As the SFG signal generated is coherent, the magnitude, direction and phase are specifically related to the incident laser beams and varying the incident beam polarisations can yield information about the average tilt angle of interfacial molecules [59].

$\chi^{(2)}$ has 27 components of the form $\chi^{(2)}_{ijk}$. In a centrosymmetric medium all of these components are equal to zero, but in a case where this symmetry is broken, such as at the interface, some of these components are non-zero. When describing light incident on a surface, it is often useful to describe the components of the light with polarisation parallel (p) and perpendicular (s) to the plane of incidence. The polarisation of the IR and visible beams incident on the surface can be controlled using optical components, leading to only certain components of $\chi^{(2)}_{ijk}$ being relevant to the generation of an SFG signal. In the case of a gold surface where over 97% of the infrared beam is reflected, this means that only the two orientations of the incoming beams which result in resonant suceptibilities with a z infrared component generate a substantial SFG signal. This means that $\chi^{(2)}_{yyz}$ can be probed by using s polarised visible light and p polarised IR light or $\chi^{(2)}_{zzz}$ and $\chi^{(2)}_{xxz}$ can be probed by using p polarised IR and visible light.

This information can be used to work out the average orientation of molecules adsorbed on

16

to a surface. By determining the hyperpolarisability of a particular vibrational mode for an individual $\chi^{(2)}_{R,ijk}$ component, a dependence of the angle of the molecular axis to the surface normal can be found. This dependence is different for each $\chi^{(2)}_{R,ijk}$ component, but depends on the ratio of two components of the molecular hyperpolarisability, which can be obtained experimentally from the Raman depolarisation ratio. However, determining this ratio in this manner leads to a large error, which can lead to large uncertainties in the calculated tilt angles [55].

Information about the polar orientation of specific groups of atoms in the molecules adsorbed on the surface can be obtained from the phase of the SFG signal [60, 61]. This requires absolute measurement of the phase [60], which is obtained by taking additional measurements using a quartz crystal as a reference. This is technically challenging and is not implemented in most experimental SFG setups.

This technique has sub-monolayer sensitivity [62] and, due to its inherent surface sensitivity, can be used to probe surfaces both in vacuum and under high pressure conditions [20, 31, 32] as well as at solid-liquid interfaces [56, 61].

SFG spectroscopy was selected for its inherent surface sensitivity, which allowed measurements to be taken through liquid layers. In this work all spectra were obtained using p polarised visible and infrared light.

2.3.3   Scanning tunnelling microscopy

Scanning tunnelling microscopy was the first technique that allowed atomic resolution real space images to be captured [63]. It was the first of many scanning probe techniques to be developed and is still widely used today in the study of surfaces [64, 65].

STM operation depends upon the tunnelling of electrons from filled electron states in a sharp metallic tip to empty states within a sample surface or vice versa, depending upon the relative tip-sample bias which is applied [66]. The most common method of operation involves keeping the tunnelling current constant by varying the distance between the tip and the surface via a feedback loop while the tip is scanned over the surface. This tip height control is achieved using piezoelectric components and the voltage applied to these components is recorded as the signal. This signal is a convolution of the topography of the surface with the local density of electronic states at the chosen tip-sample bias.

Perturbation theory was initially used to describe the tunnelling currents observed in STM [67]. Using the perturbation approach Fermi's golden rule is commonly used to describe electron transitions. This states that the rate of transition between two states is equal to the absolute square of the matrix element corresponding to those two states multiplied by the density of final states at the energy of the initial state,

$$T_{i \to f} = \frac{2\pi}{\hbar} |\langle f | H' | i \rangle|^2 \rho \qquad (2.6)$$

where $\langle f |$ is the final state, $|i\rangle$ is the initial state, ρ is the density of states in the final state and H' is the perturbation Hamiltonian, which may or may not have a time dependency.

In the Tersoff-Hamann approximation [68, 69], the tip states are replaced with a single

spherical s-type wave-function. This is a reasonable approximation for metal surfaces at large separations due to the rapid decay of energetically deeper occupied states, meaning that the charge density projected in the vacuum barrier is dominated by the charge density at the Fermi level. This is not always the case for semi-metals and semi-conductors but is a reasonable assumption for metals. Using this approximation and assuming that the charge density is suitably described by the superposition of atomic charge densities the corrugation Δz can be estimated. If spherical charge densities of the form $(C/r)exp(-2\kappa r)$ are used the result is

$$\Delta z \approx \frac{2}{\kappa}exp\left[-2\left(\sqrt{\kappa^2 + \frac{\pi^2}{a^2}} - \kappa\right)z\right] \tag{2.7}$$

with $\kappa = \hbar^{-1}[2m_0(V - E_f)]^{1/2}$, a, the distance between two adjacent atoms along the scanning trajectory, z the tip-sample separation, V, the height of the potential in the barrier and E_f, the tunnelling energy. This is a rough estimate of the corrugation which gives results around the experimentally observable limit of 10^{-2} Å at larger sample separations. This is in most cases much smaller than the observed corrugation [70] and does not predict the tendency toward saturation, reduction or sign reversal at smaller separations, all of which have been observed experimentally.

While the above methods explain some of the features of STM, they still fail to predict atomically resolved images which are routinely obtained, especially on metal surfaces. Dynamic theory can explain the high resolution obtained, but requires the problem to be approached as an excited state problem involving many-particle physics.

The physical implementation of an STM usually entails a small, compact rigid system to try to minimise the effects of vibration. A conducting tip is held within a scanner tube made of piezoelectric material which allows the tip-sample distance to be manipulated as well as the position of the tip above the surface. A separate coarse approach mechanism is usually necessary as the piezoelectric component controlling the tip height needs picometer scale sensitivity for imaging and is not appropriate for moving the tip over large distances. Additional vibrational damping such as an active damping unit may be used to further reduce the effect of any vibrations on imaging. The effect of thermal drift can be minimised by creating a system with axial symmetry such that only drift in the vertical direction is significant. With such a setup atomic resolution can be routinely achieved.

The tip itself is also an important component of any STM. The tunnelling current measured is averaged over the surface area of the tip within tunnelling distance of the sample. Single atom tips located at the end of a sharp shank are ideal, but are difficult to achieve in practice with a cluster of multiple atoms at the end of a round protrusion being the more likely outcome of tip preparation. After a tip has been formed, it can be further refined by processes such as pulsing the tip with high voltages or intentionally crashing the tip into the surface in a controlled manner and in the process of retracting the tip from the surface some material may be left behind on the surface or picked up by the tip from the surface resulting in a new tip.

In this work tips were fabricated using electrochemical etching of Pt/Ir wire using a KOH/KSCN etching solution suspended in a gold loop which were then left to break under their own weight. This consistently led to high quality, sharp tips. STM was selected to add real-space, local

structural information to the information gained from spectroscopic techniques.

2.4   Liquid deposition

Liquid deposition was performed using glassware that had been chemically cleaned prior to experimentation. Glassware was cleaned using a multiple step process taken from electrochemistry practices. Step one involved submerging all surfaces to be exposed to liquid in a dilute $KMnO_4$ and KOH solution for at least 24 hours. Step two consisted of rinsing all the glassware before submerging it in a solution of dilute H_2O_2 and H_2SO_4. This was then followed by several rinsing steps using distilled water with optional boiling of the glassware between rinses depending on the fragility of the glassware.

During deposition, crystal samples were suspended above the solution in a hanging meniscus configuration to ensure that only the single crystal surface was exposed to solution. The solution and sample were then left undisturbed for the duration of the deposition.

2.4.1   Palladium deposition

Solutions of $PdCl_2$ with added HCl and NaOH to control the pH were chosen as the precursor solution for palladium deposition. This combination allowed the pH of the precursor solution to be adjusted without adding additional anions to the reaction mixture. Sodium salts tend to be highly soluble, which allowed any salt residues arising from using NaOH to be easily removed during rinsing steps. The $PdCl_2$ precursor solution was made using solid $PdCl_2$(Alfa Aesar, 99.9%) dissolved in 0.15 M HCl (Merck, Suprapur) to aid in dissolution of the solid. From this a stock solution of 50 mM $PdCl_2$ was produced and diluted to make the lower concentration solutions of varying pH required for experiments.

2.4.2   Gold deposition

To allow for easy comparison between the results obtained using gold and palladium, $AuCl_3$ precursor solution was used, with the pH once again being controlled using HCl and NaOH. A 30% by weight solution of $AuCl_3$ in dilute HCl (Sigma Aldrich, 99.99%) was used to make the precursor solution using 0.15 M HCl as before.

2.4.3   Magnesium phthalocyanine self assembled monolayers

Magnesium phthalocyanine (Fluka, greater than or equal to 90% Mg) was dissolved in either toluene or ethanol, then contacted with the crystal surface overnight inside the STM cell. Before ex-situ measurements the solution was poured off, the sample rinsed with the solvent, then dried using helium.

Chapter 3

In-situ surface science on single-crystalline substrates

Many relevant processes occur at the interface between solids and liquids. Understanding these processes as they happen requires techniques which can be applied in-situ. Many surface science techniques have been modified for use at the solid-liquid interface and these techniques have been reviewed by Zaera [71, 72].

In-situ surface science methods have been used extensively in the field of surface electrochemistry, for example to gain atomic level information about adsorption processes on single-crystalline metal electrodes [73] and to investigate the sites of corrosion in steel [74] using electrochemical scanning tunnelling microscopy (STM). Other in-situ methods such as infrared (IR) vibrational spectroscopy have also been used to investigate adsorption at the electrode/electrolyte interface [75]. Surface electrochemistry research has concerned itself mainly with metallic samples as electrode materials need to be conducting.

Another field where the solid-liquid interface is of interest is the field of geochemistry, as many important processes take place at the interface between an aqueous phase and a mineral surface, such as mineral formation, weathering and the transport of nutrients. X-ray scattering techniques have been applied to determine the surface structure and vertical ordering of water above the interface between water and mineral surfaces [76]. Atomic force microscopy (AFM) has also been applied to studying solid-liquid interfaces to investigate structures such as the (1014) cleavage plane of calcite in water [77].

In order to prepare clean samples and retain this cleanliness upon transfer into liquid environments several different approaches have been developed. Clavilier [78] developed a method for preparing well ordered metallic single crystals without the need for a vacuum chamber using flame annealing in air, followed by quenching or cooling the sample in an inert gas environment. By covering the surface in a drop of liquid, the surface can be protected from any interaction with air before measurement. Such an approach cannot be used in conjunction for oxide thin films which require an ultra-high vacuum (UHV) environment for their preparation.

To mitigate the effects of air, gloves boxes were used initially [79], but trace contaminants from the outgassing of the materials used in the glove box housing still had an effect on the experiment. In order to utilise the full range of preparation techniques available using UHV

technology and prevent contamination, a system that allows transfer between liquid and UHV environments is required. Such systems have been developed in the past for surface electrochemical measurements with great success [80, 81]. The UHV portion of the chamber can be separated from a liquid cell by way of a gate valve, preventing the UHV environment from becoming contaminated during in-situ measurement.

Using such techniques allows UHV prepared samples to be used with in-situ techniques. An example of this is the work conducted by Wandelt using IR spectroscopy [82, 83]. After preparation the sample was transferred into a liquid cell, where it was pressed up against a prism such that a thin layer of liquid formed between the sample and the prism.

In-situ surface science techniques have also recently been applied in catalysis research. For example, IR spectroscopy has been used to investigate the selective oxidation of alcohol over supported metal particle catalysts [84] and in-situ STM was applied to study porphyrin catalysts adsorbed onto a gold surface [85]. There has also been some research conducted on catalyst preparation using in-situ x-ray measurements to investigate the interaction of platinum complexes with an oxide surface [86]. The processes occurring during catalyst preparation can have a dramatic effect on catalyst activity [3], but relatively little information is available about the processes occuring at the solid-liquid interface during catalyst preparation.

For this reason, this work aims to create equipment which can be used to investigate processes occurring at solid-liquid interfaces, in particular during the catalyst preparation process both ex-situ and in-situ. To achieve this an experimental setup was designed that allowed transfer between liquid and UHV environments, without any exposure to air. This setup was then tested on metallic single-crystalline samples and metal oxide thin films as a proof of concept.

This chapter describes in the first section the testing of an existing scanning tunnelling microscope, both ex-situ and in-situ, in an attempt to image individual molecules which have been deposited from liquid on single-crystalline metal oxide thin films using this equipment. The second section describes the design, building and testing of an experimental setup for conducting in-situ SFG spectroscopy measurements at the solid-liquid interface and presents some preliminary results.

3.1   In-situ scanning tunnelling microscopy

Previously within the workgroup efforts have been made to image small catalyst precursors, such as $PdCl_2$, using STM on thin film metal oxide substrates, such as Fe_3O_4, by taking in-situ measurements in aqueous solution during the deposition process. These molecules were definitely present on the surface as evidenced by the imaging of particles after rinsing and annealing the surface [87, 43], but individual molecules could not be resolved during deposition or immediately after. This suggests that these molecules were simply too small or mobile to be resolved under the imaging conditions used.

In order to test the function of the in-situ measurement of the STM on oxide thin films, an attempt to image larger molecules was made. Magnesium phthalocyanine (MgPc) was chosen as a probe molecule due to its large size (1-1.5 nm) and the fact that it has already been studied in vacuo on the Au(111) [88] and the FeO(111)/Pt(111) [89] surfaces, two surfaces already studied

within the workgroup.

As a first step, MgPc was deposited upon a flame annealed Au(111) single crystal from a 1 mM solution in toluene for 20 hours before being rinsed with fresh toluene and removed to air. These ex-situ measurements served as a basis to which later measurements could be compared and demonstrated that the STM was capable of imaging MgPc (Figure 3.1). Small bright features of approximately 2 nm diameter are clearly visible on the surface, arranged in long, stretched out, curved lines.
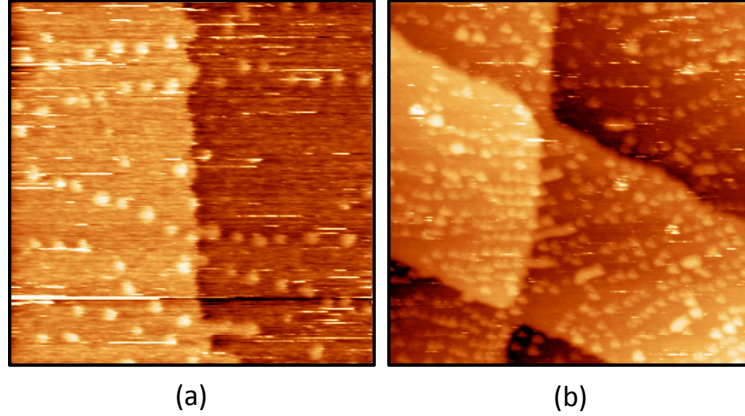

(a)   (b)

Figure 3.1: Ex-situ STM images of an Au(111) surface after deposition of MgPc from 1 mM toluene solution after rinsing the surface with toluene. All images were taken with a bias of 0.1 V and a tunnelling current of 0.1 nA. Image (a) is 70×70 nm^2 and image (b) is 180×180 nm^2.

Further measurements were then made in-situ in toluene. As toluene is non-conducting, no effort was made to isolate or coat the tip in any way. First, measurements were made to ensure that the toluene itself was not being imaged and that the observed features arose from MgPc. As can be seen in figure 3.2 (a), no features can be observed when the surface is contacted with pure toluene.

After deposition, the same long, curved lines can be seen as were seen in the ex-situ measurements (Figure 3.2 (d)). This suggests that the presence of toluene does not significantly affect the imaging of the surface after MgPc has been deposited. The images were actually clearer than in the ex-situ situation, but this could be related to the condition of the tip during the two different experiments.

A model describing a possible reason for the distribution of the MgPc molecules can be seen in figure 3.3 (c). The unit cell of the Au(111) surface contains 44 atoms in the bulk, but 46 atoms at the surface. The top layer is compressed, leading to a slight buckling of the top Au layer as the top layer varies between face centered cubic-like (fcc) stacking and hexagonal close packed-like (hcp) stacking between the first and second layer in a so-called herringbone reconstruction [90].

When bright features are placed along the rows formed by the different stacking regions of the herringbone reconstruction (separated by approximately 10 nm in air [91]), very similar patterns emerge as to what was observed experimentally. This is likely the cause of the ordered
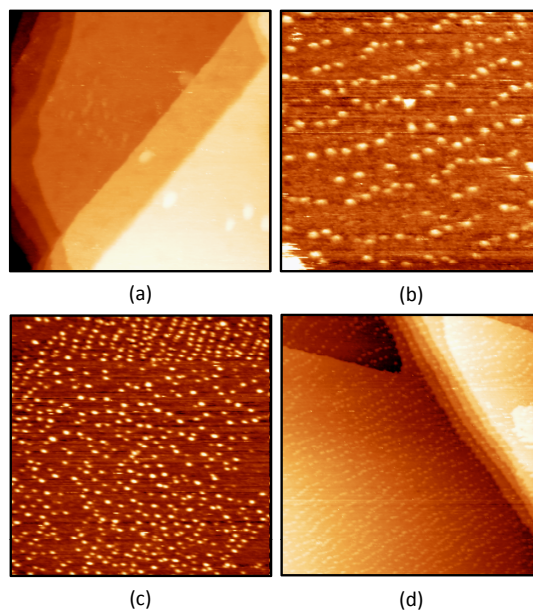
Figure 3.2: In-situ STM images of an Au(111) surface (a) in pure toluene and after deposition of MgPc from 1 mM toluene solution ((b), (c) and (d)). All images were taken with a bias of 0.1 V and a tunnelling current of 0.1 nA. Image (a) is 150×150 nm^2, image (b) is 60×60 nm^2 and images (c) and (d) are 180×180 nm^2.
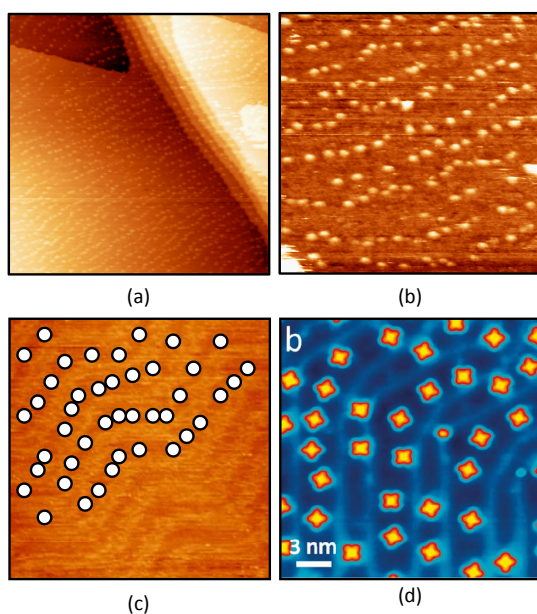

Figure 3.3: In-situ STM images of an Au(111) surface in toluene after deposition of MgPc from 1 mM toluene solution ((a) and (b)) and (c) proposed model for recreating the pattern of MgPc molecules observed, superimposed over an image of the Au(111) herringbone reconstruction imaged in air. All images were taken with a bias of 0.1 V and a tunnelling current of 0.1 nA. Image (a) is 180×180 nm^2 and images (b) and (c) are 60×60 nm^2. Image (d) shows an Au(111) surface with manganese phthalocyanine molecules deposited on the surface under UHV conditions taken from [88]

distribution of these molecules, as they preferentially adsorb on the different regions caused by this reconstruction. Under UHV conditions, manganese phthalocyanine has also been observed to adsorb within both the fcc and hcp regions on the Au(111) herringbone reconstruction with no particular preference for elbow sites [88]. The similarities can be seen clearly in figure 3.3 (d), although the molecules on the surface are more closely packed as the different stacking regions are closer together on surfaces prepared under UHV conditions.

(a)   (b)
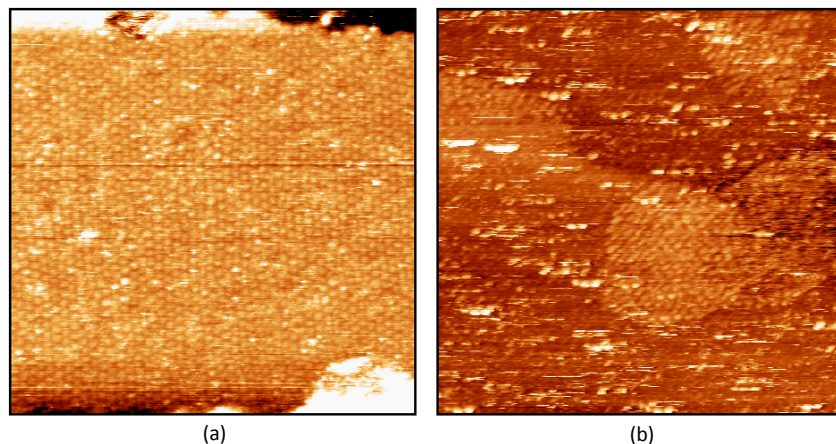
Figure 3.4: STM images of an FeO surface (a) before and (b) after exposure to toluene. All images were taken with a bias of -0.8 V and a tunnelling current of 0.1 nA. Image (a) is 60×60 nm^2 and image (b) is 70×70 nm^2.

After this, an FeO(111)/Pt(111) surface was prepared and exposed to toluene (Figure 3.4). Images were taken before and after exposure. Large terraces could be observed in both cases, but the clear Moiré like pattern became much less ordered and difficult to resolve after exposure. This is in agreement with what was observed previously for FeO films exposed to water [92]. When depositing MgPc no clear images were obtained in-situ, but after rinsing the surface and drying it with a flow of He, molecular scale features, likely relating to adsorbed MgPc could be observed as seen in figure 3.5. The resolution obtained was not high enough to resolve specific adsorption sites, but the images obtained exhibit the same general structure as observed previously from UHV studies where MgPc was evaporated on to the surface (Figure 3.5 (c)).

Further attempts were made using ethanol as the solvent and once again clear imaging in-situ was difficult, but some differences were seen in the ex-situ measurements. Instead of some individual molecules being imaged, continuous bright features were seen decorating step edges (Figure 3.6). This may be explained by the polar nature of ethanol, which therefore interacts more strongly with the polar FeO surface than in the case of toluene, which is non-polar.

The difficulties with in-situ measurement on this surface may be related to a weaker interaction of MgPc with the FeO surface in solution than with gold. The images were full of streaks, likely related to the tip interacting with molecules on the surface. A high mobility of molecules would also make it impossible to image individual molecules. Future attempts should proceed with a molecule that binds more strongly to the surface.
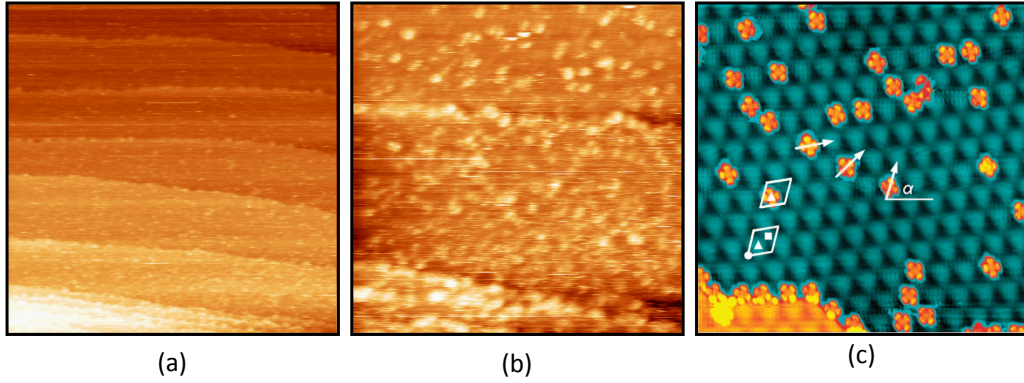
Figure 3.5: STM images of an FeO surface after depositing MgPc from a 1 mM toluene solution for 20 hours, rinsing the surface with toluene and drying it in a stream of helium. All images were taken with a bias of -0.8 V and a tunnelling current of 0.1 nA. Image (a) is 200×200 nm^2 and image (b) is 60×60 nm^2. Image (c) is a 33×33 nm^2 topographic image of MgPc deposited on an FeO(111)/Pt(111) surface under UHV conditions taken from [89].
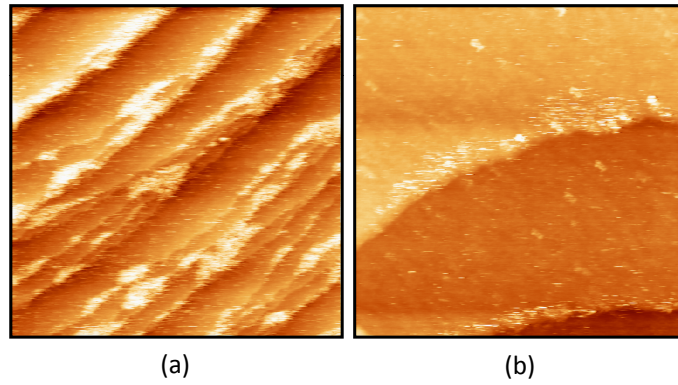

Figure 3.6: STM images of an FeO surface after depositing MgPc from a 1 mM ethanol solution for 20 hours, rinsing the surface with ethanol and drying it in a stream of helium. All images were taken with a bias of -0.8 V and a tunnelling current of 0.1 nA. Image (a) is 350×350 nm^2, image (b) is 180×180 nm^2 and image (c) is 550×550 nm^2.

3.2 In-situ sum frequency generation

This section is divided into three subsections. The first describes the design and construction of a new experimental setup for conducting in-situ SFG spectroscopy at the solid liquid interface. The second subsection describes the testing of the load lock transfer system for retaining clean samples upon transfer into the liquid cell. The final subsection describes the testing of the SFG spectrometer and presents some preliminary results from measurements taken at the solid-liquid interface.

3.2.1 Chamber design and construction

To realise the concept of an experimental setup that could perform in-situ SFG spectroscopy measurements, a new experimental setup had to be designed and built. The concept for the new experimental setup was to construct equipment that could act as a bridge between classical surface science studies performed under UHV conditions and work conducted under ambient conditions and at the solid-liquid interface in order to better understand the processes occuring during catalyst preparation.

To effect this, the idea was to build a setup that was separated into chambers that could be isolated from one another, one of which would remain under UHV conditions at all times for sample preparation and characterisation, another containing a liquid cell where experiments could be conducted at the solid-liquid interface and a third chamber to act as a transfer chamber between the other two that could be pumped down to UHV or backfilled with an inert gas to allow transfer into the liquid cell or removal of samples into ambient conditions (Figure 3.7). Such a design gives access to the liquid environments required for experiments at the solid-liquid interface, while retaining the high level of cleanliness and UHV conditions required for sample preparation and ex-situ characterisation.
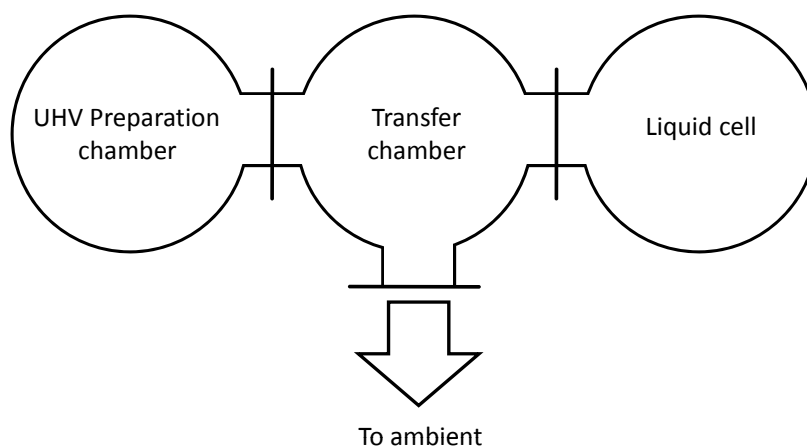

Figure 3.7: Schematic concept of the setup to be built and designed for surface science experiments at the solid-liquid interface.

Sum frequency generation (SFG) spectroscopy was chosen as an ideal technique to implement

for in-situ surface science measurements. This technique is inherently surface sensitive due to the selection rules requiring no centre of inversion, a condition that is always met at the surface. SFG spectroscopy has already been used to great effect within this workgroup to study model catalysts both under UHV and high pressure conditions [20, 31, 32]. IR spectroscopy has already been shown to be effective when using a thin layer configuration [83, 93], so this arrangement was chosen for the SFG system. As the detection of the signal occured outside the experimental setup and the beams were directed through air, simple flippable mirrors were also used to direct the beams to different locations allowing spectra to be taken both within the UHV chamber and the liquid cell.
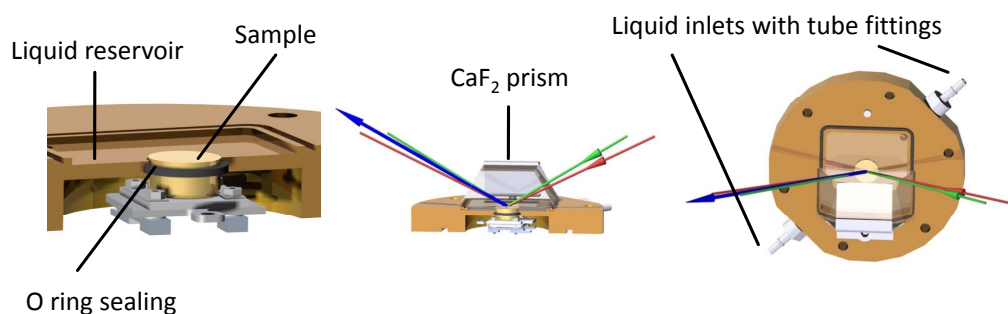
Figure 3.8: Specialised liquid cell designed for in-situ SFG.

A purpose designed liquid cell was designed in order to allow in-situ solid-liquid SFG measurements to be conducted (Figure 3.8). The cell consisted of a polyether ether ketone (PEEK) body with a hole in the centre containing an o-ring, through which the sample could be inserted to seal the sample surface from the rest of the experimental setup. The other side of the cell was sealed using a CaF_2 prism, isolating the cell volume from the environment. The laser beams could pass freely through this prism to interact at the sample surface. Once liquid was introduced into the cell, the sample could be pushed gently up against the CaF_2 prism to form a thin film of liquid between the sample and the prism. A liquid outlet and inlet allowed liquid to be continuously flowed through the system. This prism was set up with geometry such that the incoming laser beams were totally internally reflected, with the evanescent beam probing the sample surface. The sample holder used was the same as that used for a similar setup already used within the workgroup for in-situ STM, which allowed samples to be seamlessly transferred between the two systems.

To allow samples to be transferred between different chambers, two manipulators were used in combination with a magnetic transfer rod. Samples could be transferred between the two manipulators using the magnetic transfer rod. The first manipulator was inside the preparation chamber, while the second was located in the transfer chamber, but could be extended into the liquid chamber to press the sample through the o-ring and against the prism inside the liquid cell (Figure 3.9). The three independent chambers were separated from each other using gate valves and all had their own connections to pumps, which allowed them to be pumped separately. The transfer chamber also had a gate valve leading to the atmosphere, which allowed samples to be removed for STM measurement or samples to be changed without requiring the preparation
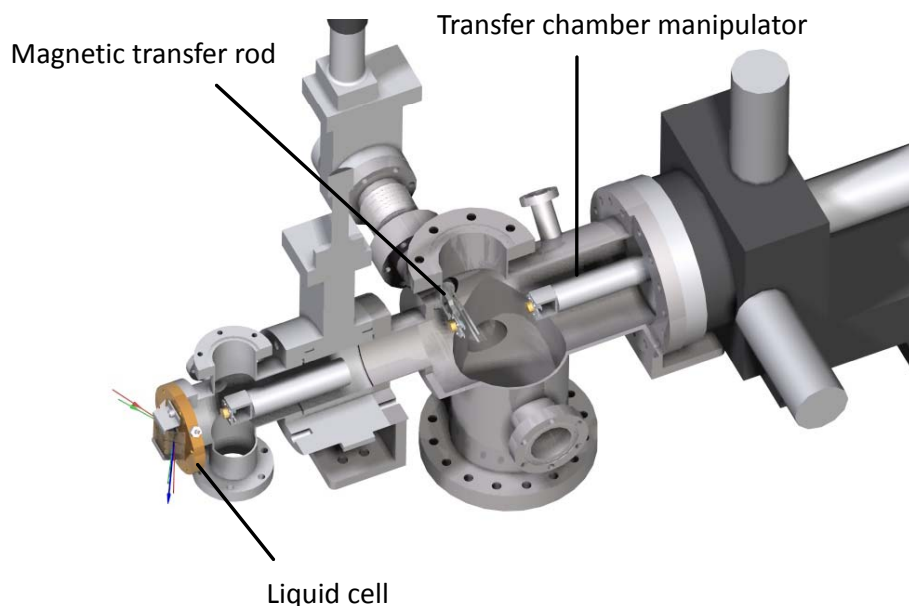
chamber to be vented.

Figure 3.9: Render of transfer chamber demonstrating how samples can be transferred from the preparation chamber, through the transfer chamber and into the liquid cell.

The preparation chamber was designed to be an effective unit for surface science experiments in its own right. It had to have all the necessary elements to produce model catalyst samples, but in addition it was built to contain other UHV based analytical techniques. For sample preparation, in addition to the heating filament on the sample holder, the preparation chamber housed a sputter gun ion source, a triple evaporator situated opposite a quartz microbalance, a single evaporator and leak valves for backfilling the chamber with gas. For analysis, the chamber was equipped with low energy electron diffraction (LEED) optics, a quadrapole mass spectrometer which could be used for temperature programmed desorption (TPD) measurements and a hemispherical electron analyser, which was set up adjacent to the sputter gun and a dual anode x-ray source which could be used for ion scattering spectroscopy (ISS) and x-ray photoelectron spectroscopy (XPS). The chamber was also fitted with two CaF_2 windows to allow laser light to be directed into UHV to perform SFG spectroscopy measurements. A schematic representation of the setup can be seen in figure 3.10.

The experimental setup was situated next to an optical bench which contained the necessary optics for SFG spectroscopy. The general layout of the optics on this table can be seen in figure 3.11. Two mirrors could be flipped in and out of the beam path to switch between the two laser beams converging on the sample in UHV or the liquid cell. An adjustable beam delay stage ensured that the two pulses were temporally aligned upon reaching the sample. The reflected infrared beam was collected to be used as a reference to account for the wavelength dependent variations in the IR power during spectrum acquisition. The reflected visible beam and generated SFG signal were spatially separated, such that the reflected visible light could be blocked from reaching the photomultiplier where the SFG signal was recorded.
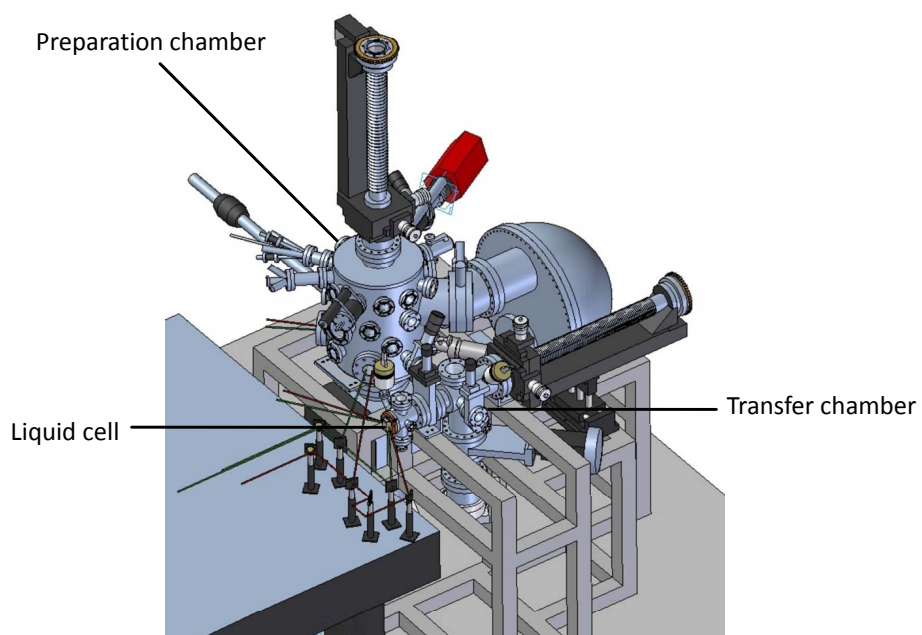
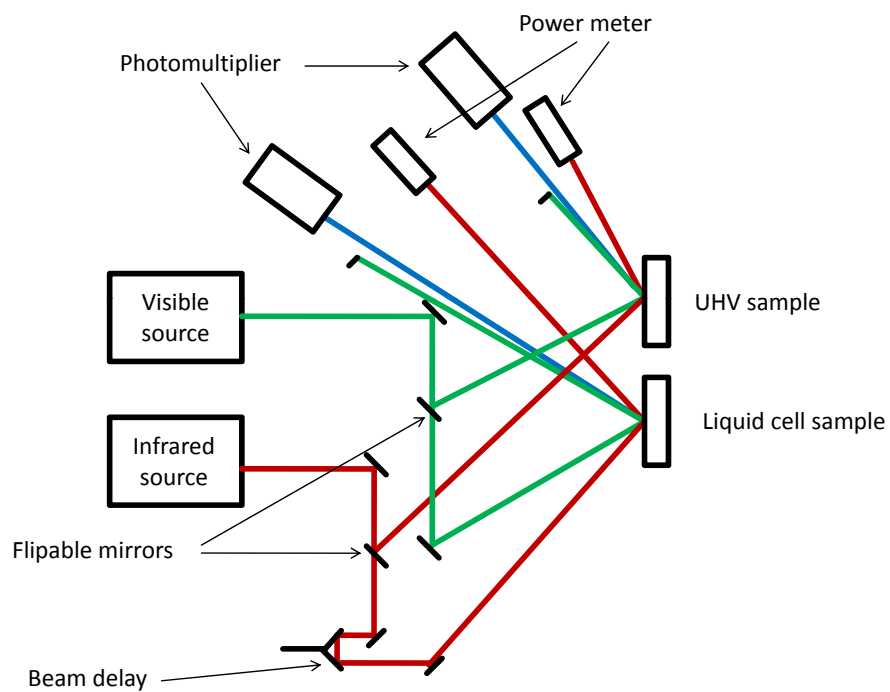Figure 3.10: Render of complete setup as designed.

Figure 3.11: Representation of laser path allowing SFG both in UHV and at the liquid cell using mirrors which can flip in and out of the beam path.

This setup meets all the criteria of the design and allows experiments to be conducted both ex-situ in UHV and in-situ at the solid-liquid interface. The following sections will outline experimental work conducted using this experimental setup.
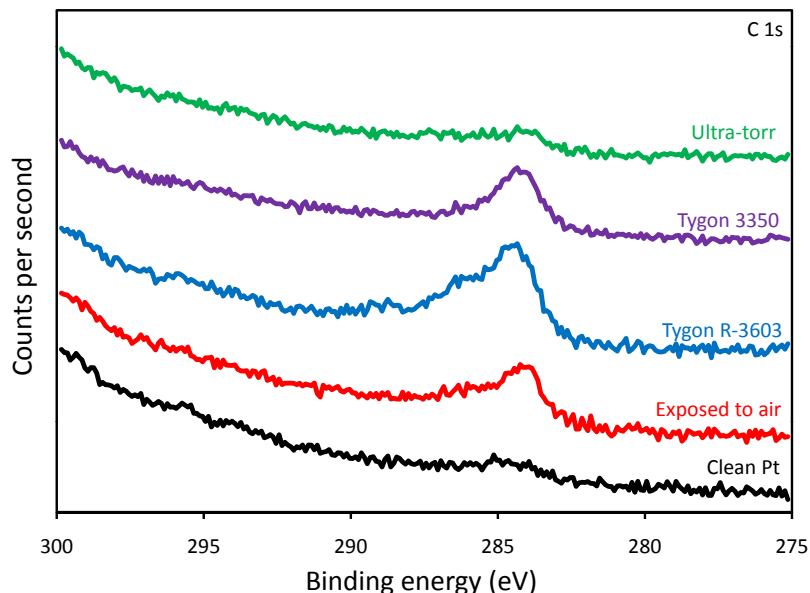
3.2.2 Transfer cleanliness

Figure 3.12: C 1s XPS spectra showing the amount of carbon contamination present on a freshly cleaned platinum single crystal and after exposure to air or the liquid cell which has been sealed using various methods and materials.

The goal of using an isolated transfer system was to ensure the cleanliness of samples prepared in UHV before contacting them with liquid to directly measure the effects of contact with solutions of interest without influence from any contaminants from the atmosphere. In order to determine the effectiveness of the transfer chamber in meeting this goal, XPS data was collected before and after transferring a sample into the SFG liquid cell to see if any contaminants had been introduced. A clean Pt(111) crystal was prepared, its spectrum measured, then the sample was placed into the liquid cell. After this exposure the sample was removed into the transfer chamber and the gate valve to the turbopump opened for thirty minutes before being returned to the preparation chamber for further measurement.

Initial testing showed a large C 1s peak upon transferring the sample into the liquid cell, with a similar sized carbon peak whether or not the sample was exposed to water (Figure 3.12 blue trace). This amount of carbon was larger than what was observed upon exposing a sample to water outside the liquid cell after exposure to air (Figure 3.12 red trace). Through a process of elimination it was determined that it was the Tygon R-3603 tubing used to connect the water tubes to the liquid cell that was the source of the contamination. This tubing was replaced by Tygon 3350 platinum-cured silicone tubing, which significantly reduced the level of carbon contamination upon insertion into the cell (Figure 3.12 purple trace), but the amount of carbon contamination was not significantly different to using no transfer chamber at all.

In order to solve this problem the Tygon tubing was replaced by glass tubes in combination with Swagelock Ultra-torr fittings. After baking out the transfer and liquid chambers, this led to a C 1s as small as that observed for a freshly cleaned sample (Figure 3.12 green trace). Clean lines, reservoirs and valves for liquid delivery are still required to complete the system, but the current setup allows samples to be as clean as possible before being exposed to liquid.

3.2.3 Testing of the sum frequency generation spectrometer

With the experimental setup complete, the first step was to ensure that everything was working as expected using a well characterised system. The adsorption of CO on Pt(111) was studied previously using the same laser system in combination with an SFG compatible UHV chamber [23]. This experiment was used as a basis for comparison to ensure that the SFG spectrometer was still working as intended under UHV conditions.

CO was dosed upon clean Pt(111) at room temperature with a continuous background pressure of 1.0×10^{-6} mbar and the SFG spectra recorded (Figure 3.13 black trace). This spectrum compares favourably with spectra taken previously using the old setup (Figure 3.13 red trace) where the CO stretching frequency for the on top position was also found to be 2095 cm^{-1} after dosing CO at room temperature with a constant background of 1.0×10^{-5} mbar [23].
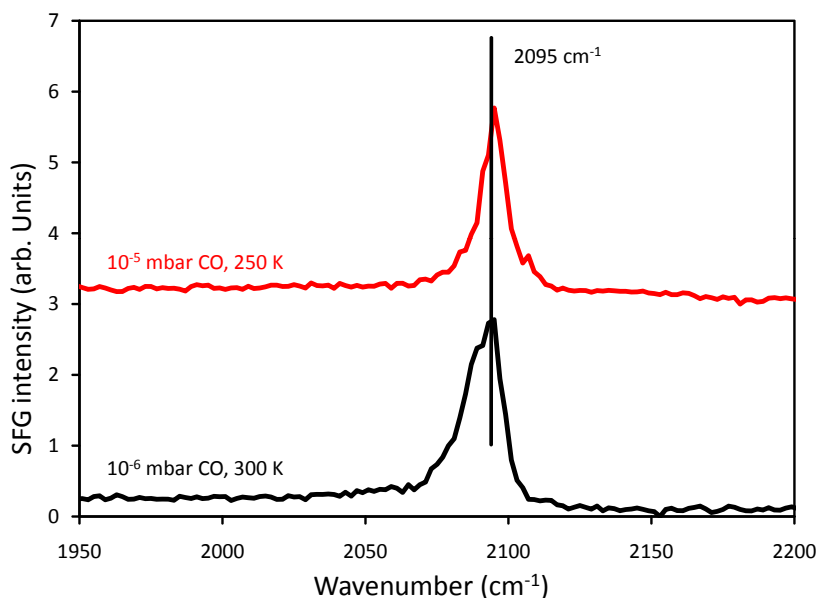

Figure 3.13: SFG spectrum obtained at room temperature from dosing a continuous background of 1.0×10^{-6} mbar CO on clean Pt(111) from the current setup. For comparison a spectrum previously obtained using the same laser system with a continuous background of 1.0×10^{-5} mbar at 250 K is also presented.

Moving on to more complicated systems, Pd on $Fe_3O_4(111)/Pt(111)$ was chosen as it has been studied previously as a model oxide supported metal particle catalyst at the Fritz Haber institute [44, 94]. A nominal thickness of 4 Å of palladium was deposited at room temperature on a freshly prepared Fe_3O_4 film using PVD, then annealed to 450 K. CO was then dosed with

a constant background pressure of 1.0×10^{-6} mbar at 90 K. Two peaks could be observed as seen in figure 3.14, which are assigned as CO bound linearly on top of Pd sites (2107 cm^{-1}) and in a bridging configuration (1977 cm^{-1}) on the Pd particles. These values are in reasonable agreement with previous studies on supported Pd particles [95, 96]. With those two measurements it was shown that the system still works in principle along the UHV path and further testing was required to see its performance along the liquid path.
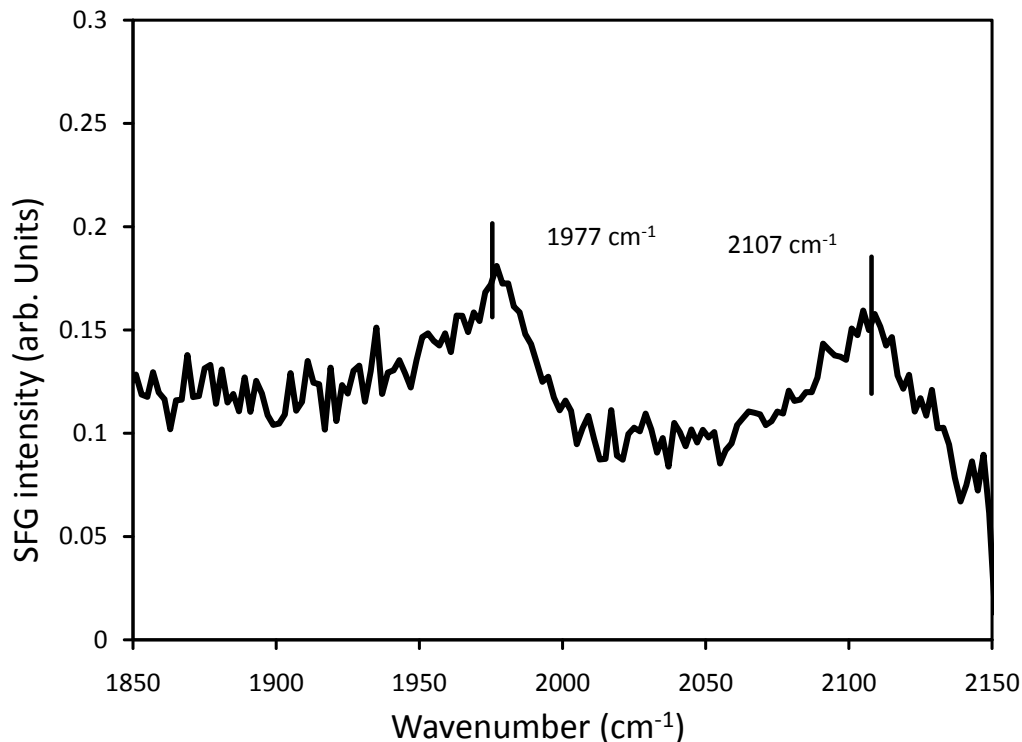
Figure 3.14: SFG spectrum obtained from dosing a continuous background of 1.0×10^{-6} mbar CO at 90 K vacuum deposited Pd particles on a thin Fe_3O_4 after annealing the sample to 450 K.

The initial testing along the liquid path was conducted using an Ag(100) crystal under ambient conditions. Silver has a rather high non-resonant background, which allowed an SFG signal to be detected at all wavelengths. This significantly simplified the alignment process.

The first measurement was conducted without the CaF_2 prism with the crystal surface exposed to air to test that the laser power along the second path was sufficient to generate an SFG signal. This proved to be the case and a small non-resonant background spectrum was recorded (Figure 3.15 black trace). The CaF_2 prism had become cracked during cleaning before this measurement and could not be used, but a small CaF_2 window was available for testing purposes.

The non-resonant background was still present with largely the same features after this window was inserted into the beam path (Figure 3.15 red trace). Upon filling the cell with water, an SFG signal was still detected, although most of the features previously observed had disappeared (Figure 3.15 blue). There was also an appreciable depression in the spectrum centered around 3500 cm^{-1} and as this coincided with a similarly shaped hole in infrared

spectrum reflected from the sample (Figure 3.15 purple) it is clear that this is simply due to the infrared light being absorbed by the water layer, reducing the size of the SFG signal. However, there is a good signal intensity from 2500 cm^{-1} to 3100 cm^{-1} that could be used for SFG experiments measuring C-H vibrational modes.
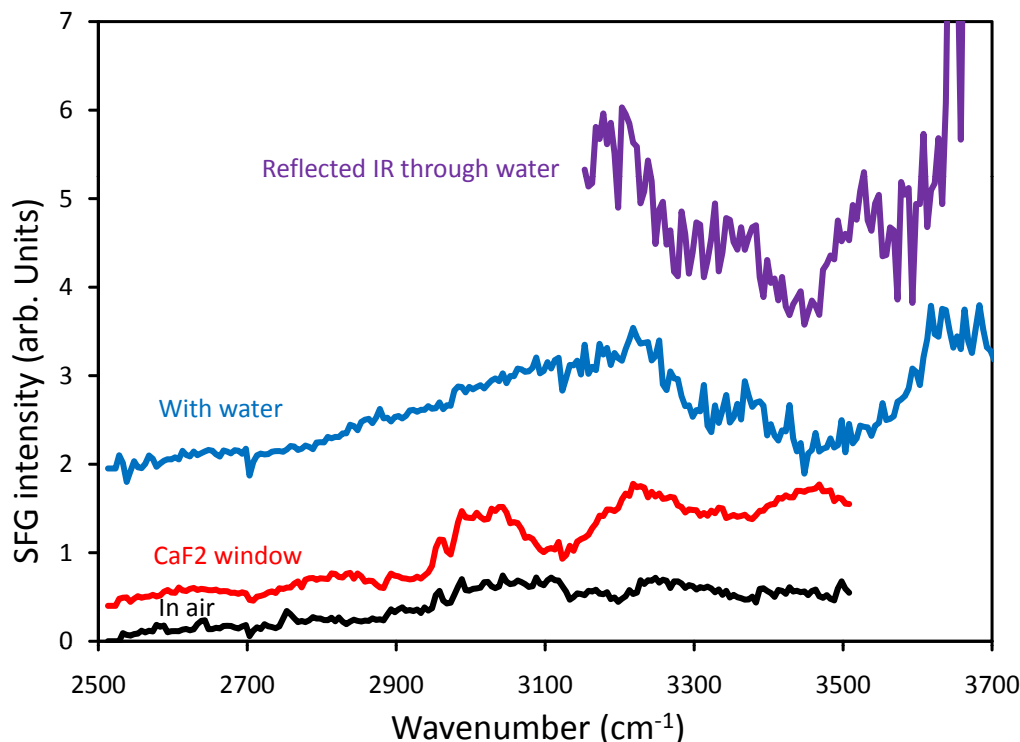

Figure 3.15: SFG spectrum obtained from an Ag(100) single crystal in air, pressed up against a CaF$_2$ window and when the liquid cell was filled with water. Part of the IR spectrum recorded for the water measurement is also displayed, demonstrating the adsorption of IR by water.

After initial testing of the liquid SFG beam path, Au(111) with a self-assembled monolayer (SAM) of octadecanethiol (ODT) was chosen as a system which could generate a signal in the C-H stretch region [54]. The CaF$_2$ prism had also been replaced at this time and was available for experiment. As for silver, the first step was to take a background measurement of the non-resonant background of the gold sample. This would ensure that any features observed later were from adsorbed molecules and not simply features of the non-resonant background. The spectrum was taken in air without the prism and no significant features could be seen in the non-resonant background (Figure 3.16).

The gold crystal was exposed to a 1 mM ODT solution in ethanol for 15 hours and the spectrum was taken again in air without the prism in place (Figure 3.17 black trace). This spectrum displayed three principle C-H modes, namely the symmetric CH$_3$ stretch at 2878 cm^{-1}, the Fermi resonance at 2938 cm^{-1} and the antisymmetric stretch at 2962 cm^{-1}. These values are in good agreement with previously measured spectra for ODT SAMs [54], proving that the system is operational.

The CaF$_2$ prism was then inserted into the beam path, the cell filled with ethanol and the
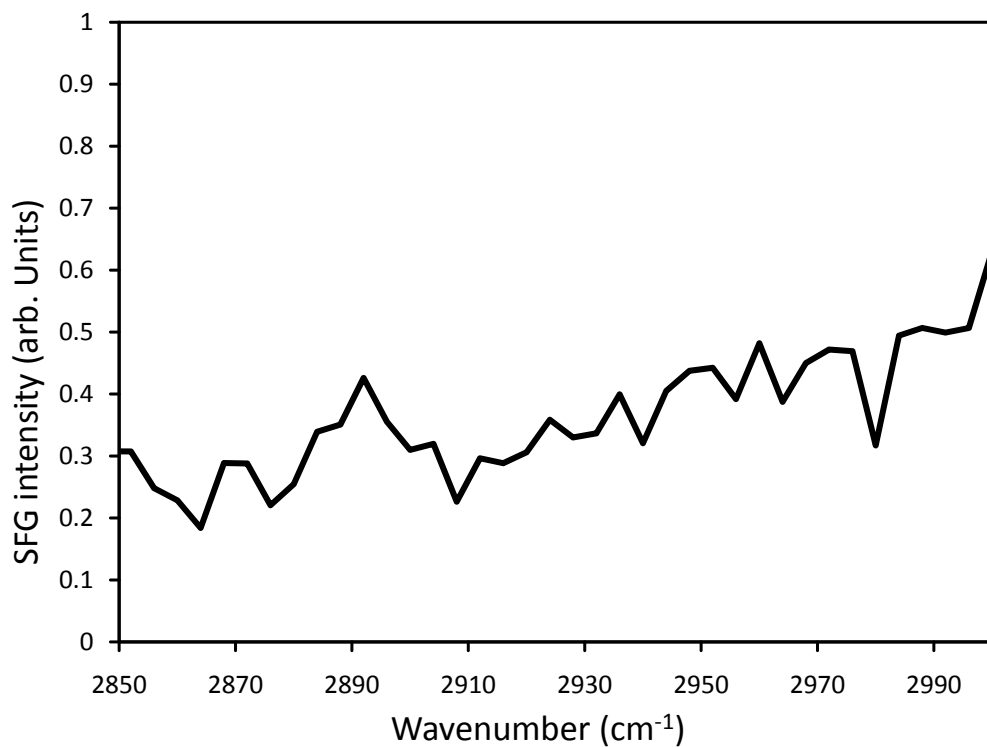
Figure 3.16: SFG spectrum obtained from an Au(111) single crystal in air.
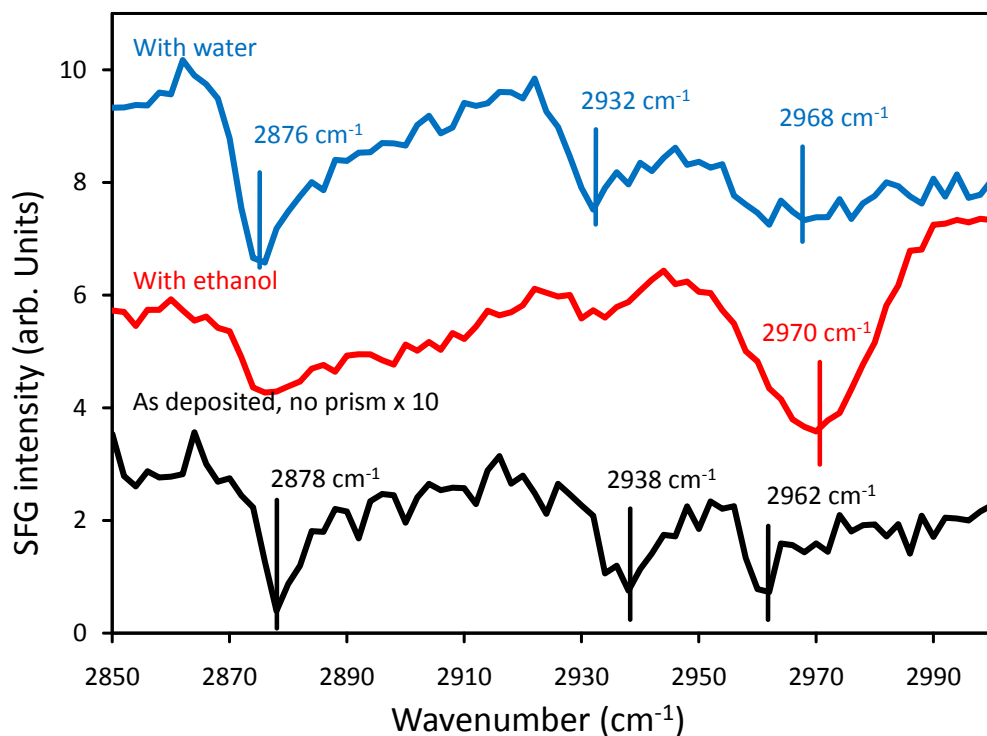

Figure 3.17: SFG spectrum obtained from an Au(111) single crystal after being exposed to a 1 mM ODT solution for 15 hours in air, then sealed with the CaF$_2$ prism and the liquid cell filled with ethanol and after rinsing the cell, then filling it with water.
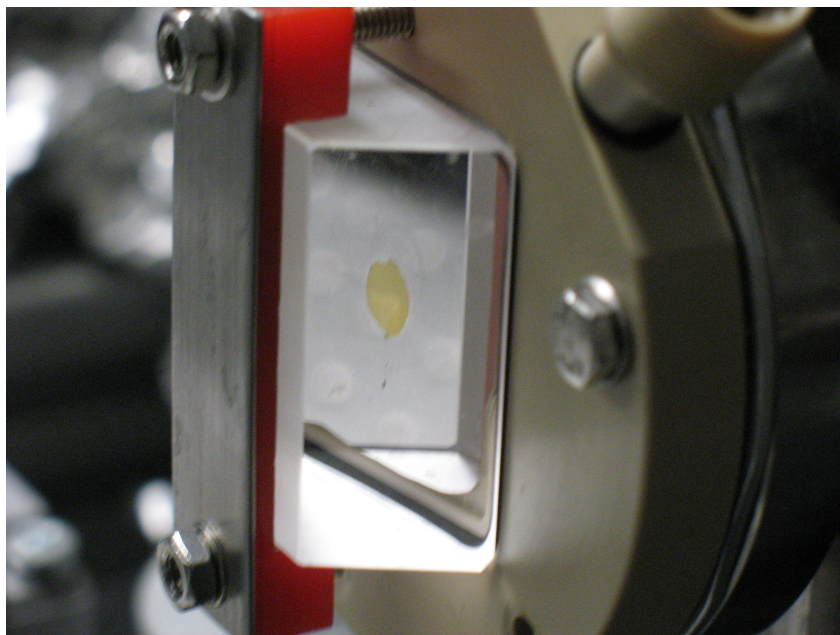
Figure 3.18: Photograph of a gold sample inside the liquid SFG cell when filled with ethanol.

sample gently pressed against the prism to form a thin layer of ethanol between the sample and the prism as seen in figure 3.18. The spectrum was then measured again as shown in the red trace in figure 3.17. The strong signal at 2970 cm^{-1} arises from the C-H anti-symmetric stretch of ethanol indicating that the ethanol molecules are ordering themselves at the interface above the ODT monolayer. As the C-H modes of ethanol overlap with the C-H modes in ODT, nothing concrete can be said about any changes in the ODT monolayer. In order to investigate any possible changes the cell was disassembled and rinsed with water before being reassembled and the cell filled with water for measurement (Figure 3.17, blue trace). The three principle C-H modes can once again be observed with only slight shifts suggesting there has been no significant change in the structure of the ODT monolayer from its interaction with water. As such, the operation of the SFG system has been demonstrated in vacuum, ambient conditions and at the solid-liquid interface.

Now that the new experimental setup had been proven to work under vacuum and ambient conditions as well as at the solid liquid interface, the next step to complete the demonstration of the concept as designed would be to take an oxide sample prepared in UHV, transfer it into the liquid cell and contact it to water without any contact to air in order to acquire an SFG spectrum. After the measurements detailed in this chapter the electronic circuitry for the Nd:YAG laser failed and further measurement was not possible. Clean transfer and measurement of SFG spectra through liquid layers have already been demonstrated separately, but a complete experiment incorporating both will be conducted at a later date using a new laser system which is currently being set up for experimentation.

Due to the time required to set up and configure the new laser system, further research focused upon ex-situ studies of catalyst preparation in order to provide a basis of knowledge to understand in-situ experiments conducted in the future using the experimental setup built

during this work.

3.3   Summary

Testing was conducted using an existing electrochemical STM to image MgPc as a model molecule. It was imaged successfully both in-situ and ex-situ on an Au(111) single crystal and ex-situ on an FeO(111)/Pt(111) thin film. On the Au(111) surface the MgPc molecules were found to lie within the troughs of the herringbone reconstruction of this surface. On the oxide surface the ex-situ measurements demonstrated that the solvent used has an effect on the distribution of the particles on the surface. This work demonstrated that molecular resolution was achievable, even under in-situ conditions, using this equipment.

An experimental setup was designed and built to take sum frequency generation spectroscopy measurements both on samples under UHV conditions and at the solid-liquid interface. This was achieved by connecting a liquid cell to a standard UHV chamber via a transfer chamber to allow for clean transfer between UHV and liquid environments without compromising the quality of the vacuum. Initial in-situ measurements were obtained of the spectrum of a self assembled monolayer of octadecanethiol on the Au(111) surface in air, ethanol and water. This measurement demonstrated the successful operation of the experimental setup at the solid-liquid interface to allow future in-situ investigations of the process occuring during catalyst preparation to be conducted.

With the construction of this new experimental setup complete, this setup was then used for ex-situ studies of the processes occuring during wet chemical catalyst preparation. The details and results of these experiments can be found in the following chapter.

Chapter 4

Wet chemical model catalyst preparation

The previous chapter outlined the design and construction of a chamber which could be used for in-situ measurements of the processes occuring during catalyst preparation at the solid liquid interface. This chamber was also designed to allow samples to be transferred in between ambient, liquid and UHV environments, such that ex-situ measurements could also be made using classical surface science techniques.

This chapter describes experiments using well-established ex-situ surface science techniques to follow and understand the processes occuring on single-crystalline iron oxide thin films prepared under UHV conditions during wet chemical catalyst preparation.

4.1   Introduction and motivation

The material properties of a given catalyst are a critical component of the overall effectiveness and efficiency of a given catalytic process. These in turn depend upon the preparation conditions used to make the catalyst in the first place [97] and any subsequent treatments to create an active catalyst [98]. Oxide supported metal particles have been extensively studied by surface scientists and catalysis researchers alike, but using markedly different approaches in the preparation of their samples.

Surface scientists conducting their investigations under UHV conditions typically use methods such as physical or chemical vapour deposition to deposit metallic particles directly on to single-crystalline oxide substrates [16, 99]. Catalysis researchers on the other hand typically use wet chemical methods such as co-precipitation, deposition-precipitation or incipient wetness/wet impregnation, followed by processes such as calcination, oxidation and reduction resulting in dispersed metal particles over polycrystalline substrates [100]. Such methods are used in the preparation of industrial catalysts as they can be scaled up to produce large volumes of catalyst material.

Using supported metal particles in ultra-high vacuum (UHV) goes some way to closing the materials gap between single crystals and real world catalysts, but this does not take into account any changes that may arise from the different preparation techniques used under UHV

conditions. To address this problem and investigate what effect these different catalyst preparation methods can have upon catalysts this work attempts to explore an intermediate area, where liquid deposition techniques are used upon single-crystalline substrates. Certain preparation techniques, such as co-precipitation are obviously not appropriate to such a study as this can only ever result in polycrystalline supports, and a lack of pores makes incipient wetness impregnation impractical. This leaves only wet impregnation and deposition-precipitation as likely candidates.

Deposition-precipitation has been extensively studied in the past [100, 101, 102]. The method works by adjusting the pH of a solution slowly such that a metal containing compound precipitates slowly on to a support instead of in solution. This is achieved by using systems where the supersolubility curve of the system is shifted to lower concentrations in the presence of the support.

A modified deposition-precipitation procedure can be used for the deposition of noble metal particles. The case of gold deposited upon titanium dioxide [103, 104] and other substrates [98, 105] has been extensively investigated by multiple investigators as it is one of the few methods available for preparing dispersed gold particles on an oxide substrate. It has also been used for other metal particles such as palladium [106].

Due to the low surface area and limited liquid volumes available in our experimental setup, the standard deposition-precipitation method could not be utilised and a modified version was instead implemented where the pH of an acidic solution was rapidly changed to alkaline pH by the addition of NaOH before contacting the surface with the catalyst precursor solution. Such procedures have been shown to be effective for gold on TiO_2 and other substrates [107].

Wet impregnation is conceptually simpler as it involves contacting an excess of the precursor solution with the substrate and allowing the precursor molecules to interact with the substrate. Under appropriate conditions the charge of the surface will be opposite to the charge of the metal containing precursor species in solution, resulting in an electrostatic attraction between the two. Over time the ionic precursor species adsorb on to the surface.

Using both methods the species deposited on to the surface are not metallic and further treatment is required, such as rinsing the surface to remove any undesirable residues, annealing the surface to decompose the precursor complexes and allow particles to form, and oxidation and reduction steps to clean and activate the metal particles. A thorough understanding of the catalyst preparation process requires that all of these preparation steps be investigated. The transfer system previously described provides the perfect opportunity for ex-situ characterisation of model catalysts prepared using wet chemical methods at every step of the preparation process.

The following sections detail experiments using wet chemical methods to deposit palladium and gold particles on single-crystalline $Fe_3O_4(111)/Pt(111)$ supports. The samples are characterised after each preparation step, such as deposition, rinsing and annealing in vacuum. This approach gives a complete picture of the chemical and physical state of the model catalyst at each preparation step to better understand the processes at work.

4.2 Palladium on iron oxide

The focus of this experiment was to investigate the effect and importance of rinsing upon palladium deposited from aqueous solutions. The deposition of palladium particles upon single-crystalline supports from aqueous solutions [87, 43] and in vacuo [108, 109] has already been extensively studied within the Fritz Haber Institute, but no specific investigation into the effect of rinsing has been made. $PdCl_2$ containing catalyst precursor solution has been used in the past to prepare supported palladium catalysts [110, 111], but chlorides can have a negative effect on the catalytic activity and selectivity of the produced catalyst for various catalytic reactions and therefore need to be eliminated [111, 112].

In order to remove chlorides from catalysts prepared using wet chemical methods, the catalysts undergo several rinsing steps until no further chlorine can be detected in the collected water used to wash the surface using a technique such as precipitation using silver nitrate. This approach gives no information about the amount of chlorine that may be left on the surface, only that no more can be removed via rinsing. Directly measuring the amount of chlorine present before and after rinsing using XPS gives a more direct picture of the effect of rinsing on the amount of chlorine on the surface.
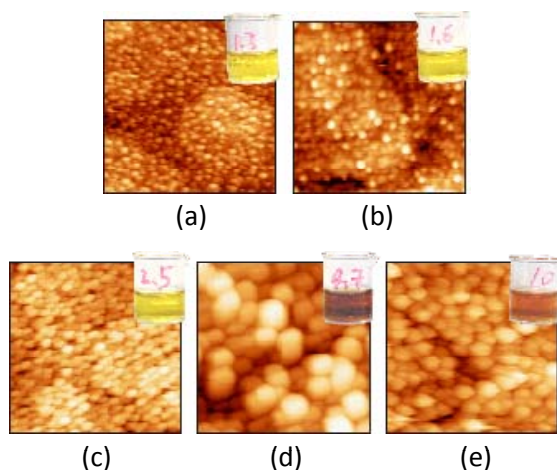

Figure 4.1: STM images of $Fe_3O_4(111)$ surfaces that have been exposed to 5 mM $PdCl_2$ precursor solutions (2 mM in the case of pH 10) for one hour and annealed to 600 K. Each solution can be seen next to the corresponding STM image. The pH of each solution is written on the beaker. Each image is 200×200 nm^2. Images taken from previous research within the workgroup and published as [113, 114].

Previous work within the workgroup already investigated the effect of using $PdCl_2$ solutions with varying pH values [43, 87]. As can be seen in figure 4.1, this resulted in different palladium loadings and particle size distributions. The loading is dependent on the type of interaction which occurs under the conditions used. This is determined by the speciation of the precursor solution and the surface charge. At low pH values only $[Pd(Cl)_4]^{2-}$ and $[Pd(Cl)_3(H_2O)]^-$ ions should be present in solution, while at pH 10 there is a more complex mixture of hydroxide containing ions such as $[Pd(Cl)_2(OH)_2]^{2-}$ and $[PdCl(OH)_3]^{2-}$ [115]. The surface charge of the

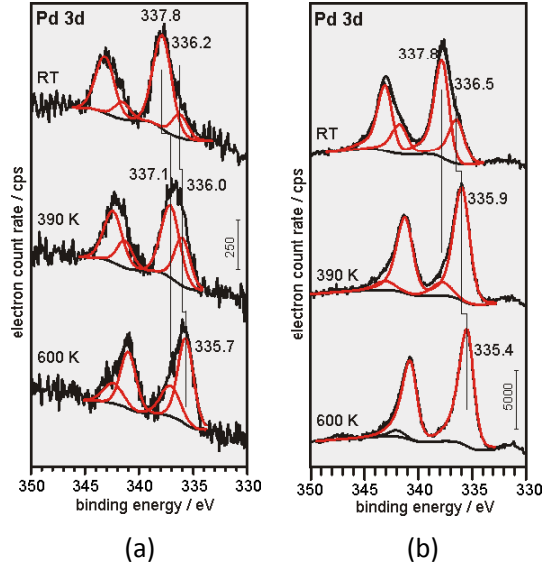Figure 4.2: XPS spectra of $Fe_3O_4(111)$ surfaces that have been exposed to (a) 15 mM $PdCl_2$ precursor solution at pH 1.3 and (b) 2 mM $PdCl_2$ precursor solution at pH 10 after rinsing the surface with water four times, annealing the surface to 400 K in UHV and after annealing the surface to 600 K in UHV. Data published in [43, 87].

system is determined by the point of zero charge of the surface under the given conditions, for example Fe_3O_4 has a point of zero charge of approximately 5.8 [116] in aqueous solutions.

After deposition and a rinsing step, x-ray photoelectron spectroscopy (XPS) measurements were taken, examples of which can be seen in figure 4.2 for deposition at pH 1.3 and pH 10. In both cases two peaks are visible after deposition and rinsing, one at 337.8 eV and one at lower binding energy at 336.2 eV and 336.5 eV for pH 1.3 and pH 10 respectively. The peaks at higher binding energy relate to Pd(II). These Pd(II) peaks were assigned as likely arising from aquochloro complexes of the form $[Pd(H_2O)_xCl_y]^{n+(-)}$ for pH 1.3 and a mixture of Pd chloro-hydroxo complexes and polynuclear Pd_n-hydroxo colloids for pH 10. After annealing to 600 K a peak is observed at 335.7 eV in the case of pH 1.3 and 335.4 eV for pH 10. These peaks were assigned to metallic particles of Pd as they are reasonably close to the binding energy of bulk palladium at 335.1 eV.

In this previous work, the sample was rinsed four times with a fixed amount of water [87], but in some cases chloride could still be measured upon the surface using XPS. With no measurements taken before the rinsing step, important information was still missing about the effect of rinsing upon this system and it could not be determined whether or not rinsing could completely remove chlorine from the surface. This work attempts to investigate these details.

4.2.1 Effect of water rinsing

The first step taken was to characterise the electronic properties of deposited palladium at every step of preparation ex-situ using XPS by taking measurements before deposition, after deposition, after rinsing and after annealing at various pH levels. 5 mM solutions of $PdCl_2$

were prepared from a 50 mM stock solution containing 0.15M HCl, then the pH was set by adding 0.2 M NaOH and making up the volume using distilled water. The sample was then suspended above the solution in a hanging meniscus configuration and left undisturbed for one hour. Using the same palladium concentration and deposition time, varying amounts of palladium were observed upon the surface, with much more deposited at pH 4.7 and the lowest amounts of palladium being deposited at low pH (Figure 4.3).
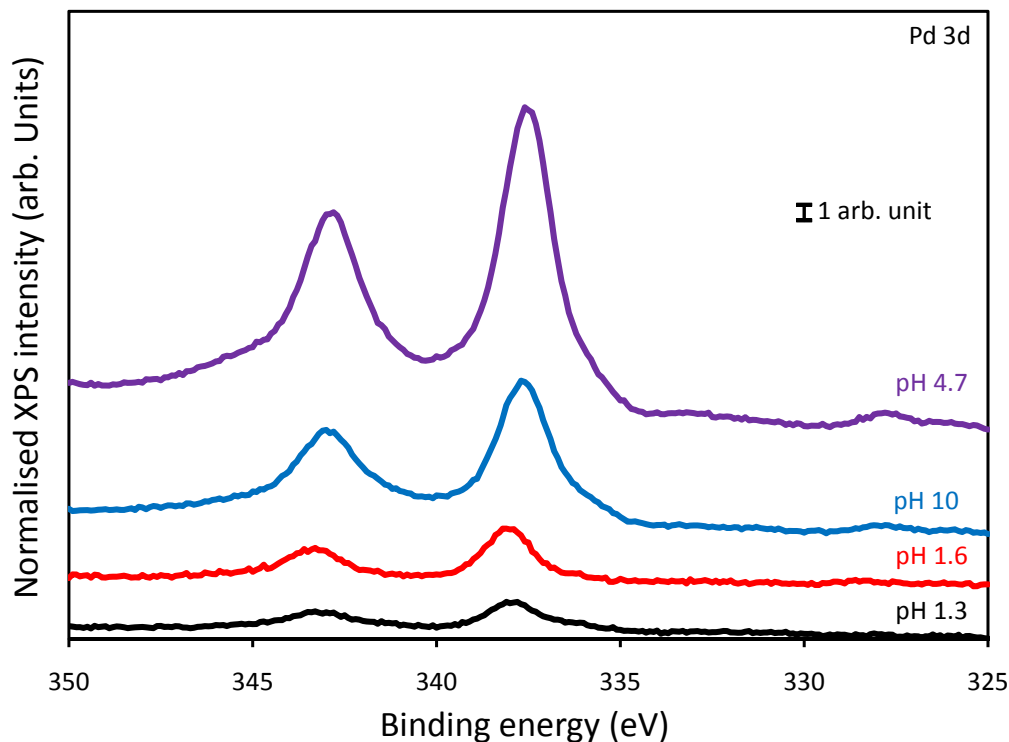

Figure 4.3: Pd 3d XPS spectra demonstrating relative amounts of Pd deposited of Fe_3O_4 films at different pH values.

Upon rinsing, new electronic states were observed. In all cases, some of the palladium was lost, with the most significant losses being observed at pH 1.3 (50%) (Figure 4.4). At this pH, most of the palladium (peak at 337.9 eV) is simply washed away, leaving only a peak at 335.6 eV, shifted from the original 336.1 eV. A small amount of the higher binding energy palladium also seems to have been converted into this lower binding energy species. The palladium deposited at pH 1.6 showed similar behaviour upon rinsing to palladium deposited at pH 1.3 and will not be considered further within this work.

At pH 10 a different behaviour was observed, with the intensity of the peak at 337.6 eV being shifted into the peak at 335.7 eV with minimal palladium losses of about 9% (Figure 4.5). This suggests that the palladium has been reduced by rinsing the surface with water. The palladium deposited at pH 4.7 showed intermediate behaviour between these two cases, with a significant proportion of the palladium being lost during the first rinsing step, followed by a slower shift of intensity from one peak to the other (Figure 4.6).

Similar shifts can be observed in the Pd 3p spectra, but this peak is much smaller and
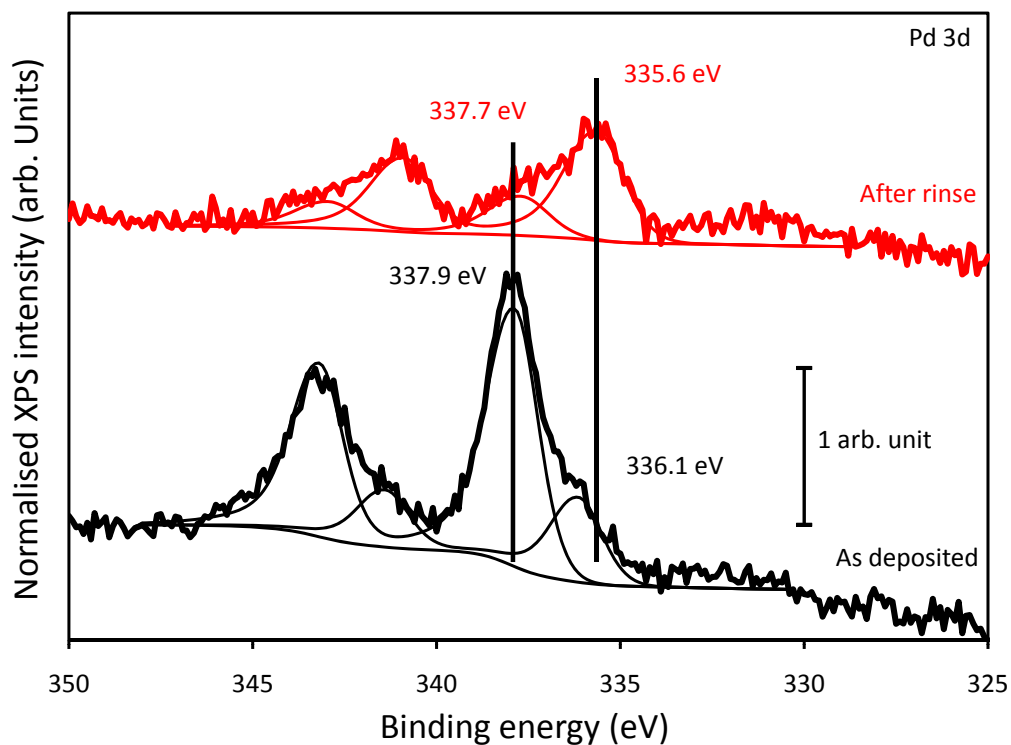
Figure 4.4: Pd 3d XPS spectra showing the state of palladium deposited from 5 mM $PdCl_2$ solution at pH 1.3 before and after water rinsing.
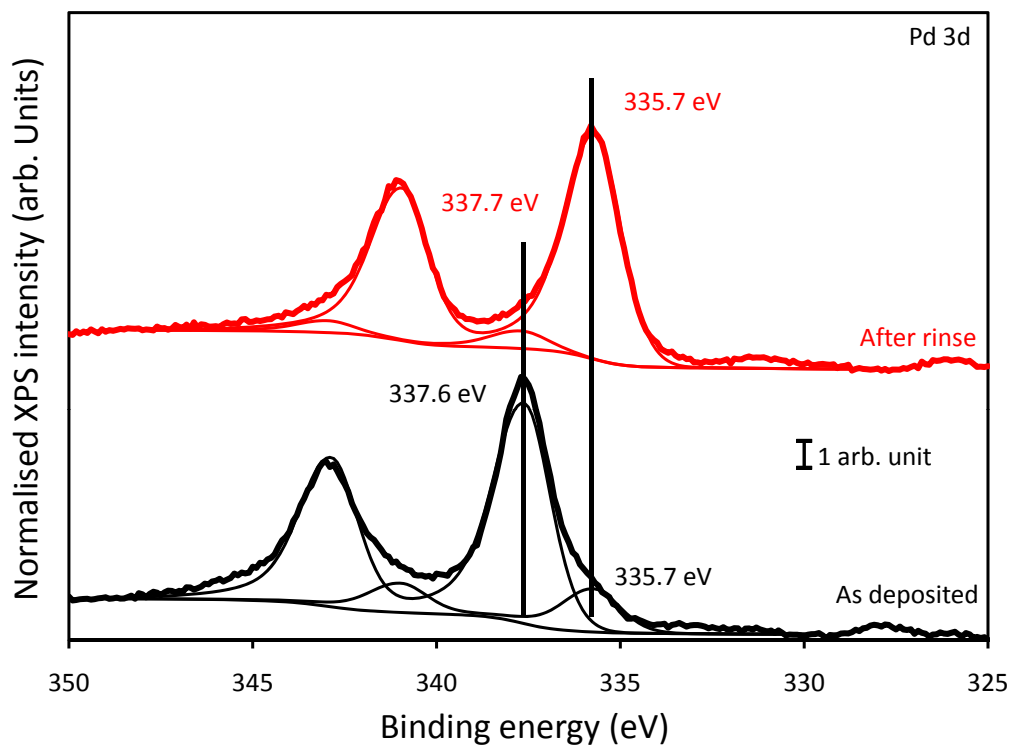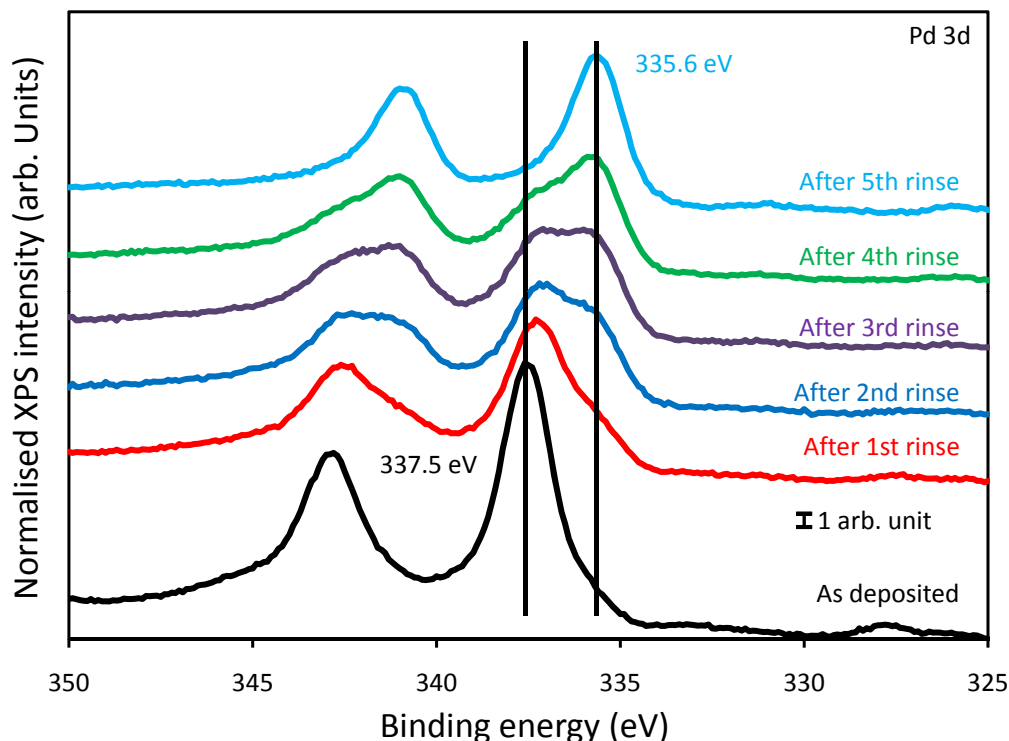

Figure 4.5: Pd 3d XPS spectra showing the state of palladium deposited from 5 mM $PdCl_2$ solution at pH 10 before and after water rinsing.

overlaps with the O 1s peak and as such is only really visible for the palladium deposited at pH 4.7. After palladium is reduced, this peak partially overlaps with the O 1s peak and the two peaks can not be easily deconvoluted (Figure 4.7).

Figure 4.6: Pd 3d XPS spectra showing the state of palladium deposited from 5 mM PdCl$_2$ solution at pH 4.7 before and after water rinsing.

In all cases, samples were rinsed until they reached a steady state, but it was difficult to quantify how much water was required to reach this steady state as it varied from experiment to experiment. This seemed to depend upon the amount of carbon detected on the sample using XPS and is probably related to the cleanliness of the equipment on any given day. Qualitatively, the samples prepared at pH 4.7 seemed to require significantly more water to reach a steady state than those prepared at pH 10 or 1.3. The latter generally reached a steady state after one or two rinses with 100 ml of water when relatively clean in comparison to 5 or 6 rinse cycles using up to 500 ml of water required for the pH 4.7 samples. This is likely due to the higher amount of palladium found upon the surface.

Significant amounts of chlorine could be measured upon the surface after deposition, but in all cases this could be removed and brought below the detection level of our instrumentation by rinsing until the steady state was reached (Figure 4.8). The chemical state of the observed chlorine on the pH 10 deposited samples is significantly different from that of the other samples. To better understand this, measurements were taken using a sample that had been exposed to a blank solution which contained the same concentrations of HCl and NaOH as the solution used to deposit palladium at pH 10, but no PdCl$_2$ (Figure 4.9).

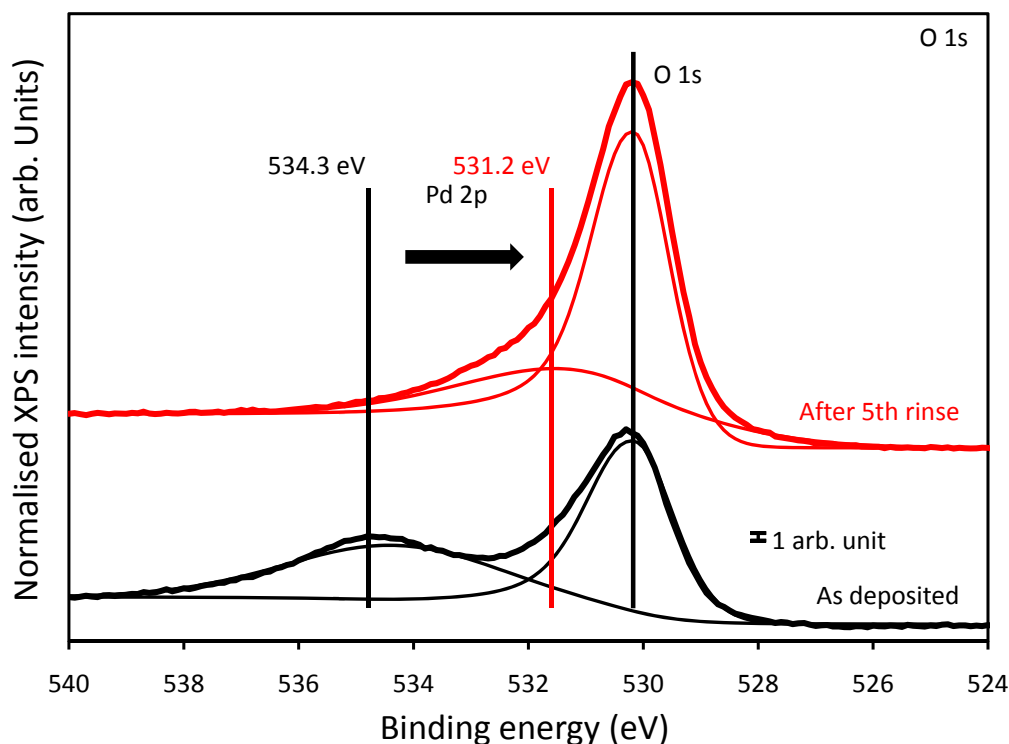The binding energy of the Cl 2p peak from a solution that contained no palladium was

Figure 4.7: O 1s XPS spectra showing the Pd 3p and O 1s peaks after deposition from 5 mM PdCl$_2$ solution at pH 4.7 peak before and after rinsing.

200.2 eV, which was higher than that found for pH 1.3 (198.3 eV) and pH 10 (199.4 eV). This suggests that the chlorine observed upon the surface after palladium deposition is not free Cl$^-$ adsorbed upon Fe$_3$O$_4$, but contained within the palladium containing precursors attached to the surface. The difference observed at various pH levels can be explained by the speciation of the catalyst precursor at different pH levels. At pH 4.7 and 1.3 [Pd(Cl)$_4$]$_2^-$, [Pd(Cl)$_3$(H$_2$O)]$^-$ and [Pd(Cl)$_2$(H$_2$O)$_2$] precursor complexes are present in solution, while at pH 10 there is a mixture of hydroxide containing ions such as [Pd(Cl)$_2$(OH)$_2$]$^{2-}$ and [PdCl(OH)$_3$]$^{2-}$ [115]. This suggests two very different chemical environments for chlorine in the two different situations, explaining the different binding energies observed. This could also explain the different behaviour of the adsorbed palladium and will be revisited later in this chapter.

Sodium could also be observed upon the surface for the samples deposited at pH 4.7 and 10 due to the NaOH used to set the pH of the solution, but was also easily removed by rinsing with water (Figure 4.10).

After rinsing, all samples were annealed to 600 K. This resulted in a single palladium peak at 335.5-335.6 eV(Figure 4.11) in all cases. This is in reasonable agreement with the results observed from previous work [43, 87] (Figure 4.2). The differences observed by Wang in the state of the palladium before annealing can be explained by the much higher volumes of water used during this work as the binding energies of the Pd 3d peaks are closer to the pre-rinsing values observed in this work. The steady state was likely never reached in the previous study as evidenced by the higher binding energies and residual chlorine observed on the surface.
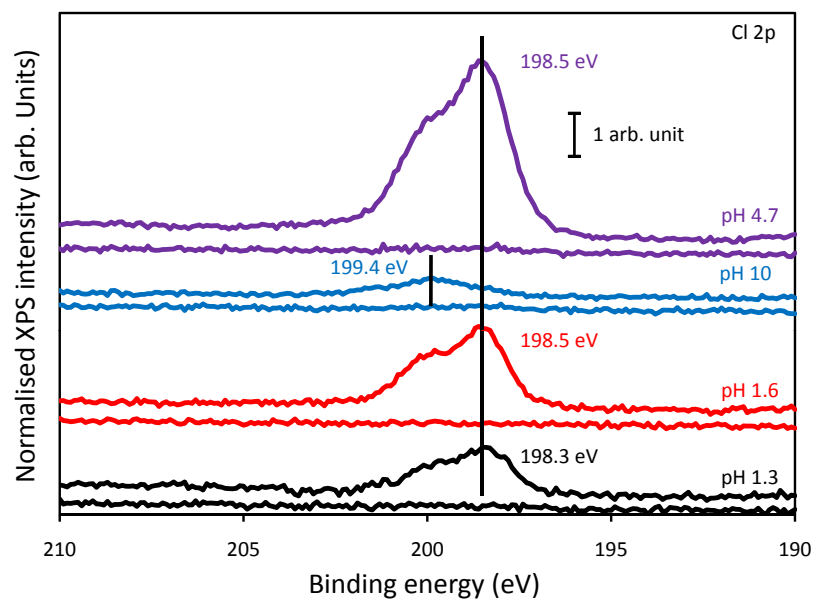
Figure 4.8: Cl 2p XPS spectra showing the amount of chlorine on the surface after deposition from 5 mM PdCl$_2$ solutions at each pH value and the flat traces which arose after rinsing chlorine from the surface using water.
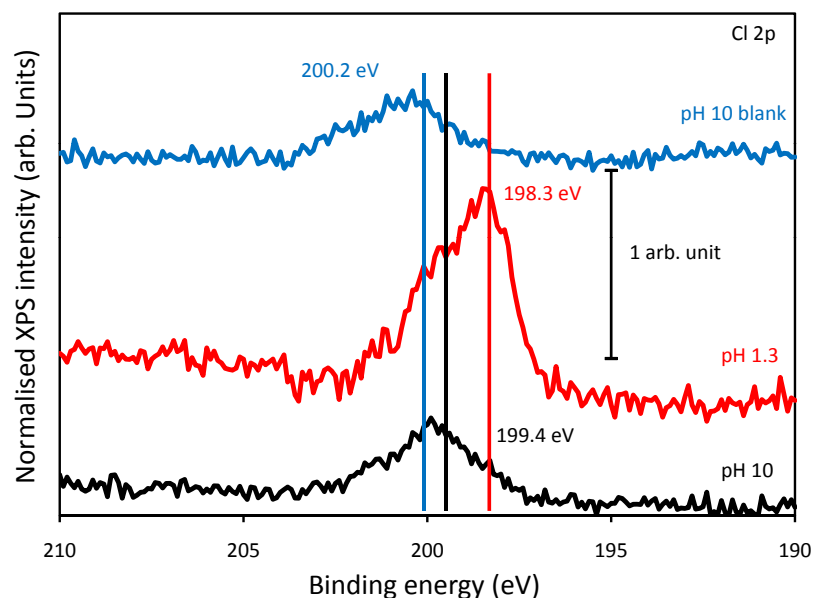

Figure 4.9: Cl 2p XPS spectra showing a comparison between the chlorine found on the surface after deposition of palladium from 5 mM PdCl$_2$ solutions at pH 1.3 and pH 10 with chlorine deposited using a blank solution that contained no palladium.
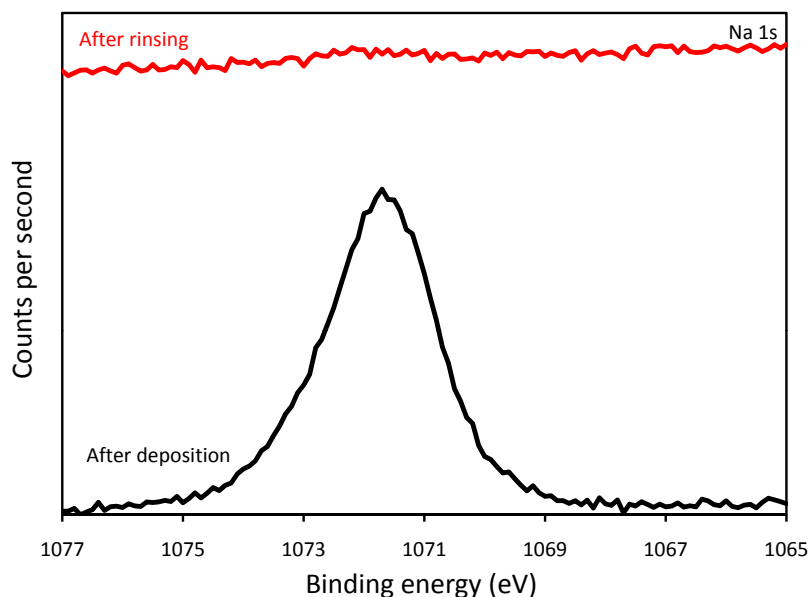
Figure 4.10: Na 1s XPS spectra showing the removal of sodium after a single rinse after deposition using a 5 mM PdCl$_2$, pH 10 solution. This was typical for any sample containing sodium.

This demonstrates the importance of a thorough investigation of the rinsing step as different outcomes occur when the sample is not rinsed until a steady state is reached.

4.2.2 Preparation without rinsing

In order to see how the samples behaved without any influence from rinsing, samples were prepared at pH 1.3 and pH 10 and characterised before and after annealing. These values were chosen as they exhibited the two extremes of the behaviour observed upon rinsing and have further been shown to produce well dispersed metal particles in previous work [114].

Upon annealing, the palladium peaks all ended up lining up at around 335.5-335.6 eV (Figure 4.11), in agreement with previous results observed for liquid deposited palladium [43, 87]. This suggests that the final chemical state of the palladium particles after annealing is not dependent upon the deposition conditions or any post-deposition treatment. After annealing to 600K all palladium particles on the samples prepared appear to be in the same chemical state.

The binding energies observed were consistent with values observed for Pd deposited on to Fe$_3$O$_4$ using PVD in vacuum after annealing to 600 K (335.5 eV). Depositing nominal amounts of 0.5 Å, 2 Å and 4 Å all led to binding energies of 335.5 eV for the Pd 3d peak after annealing to 600 K. Similar results have been observed for Pd particles deposited using PVD on to a thin alumina film [117].

Previously, a detailed study on the oxidation of Pd particles on Fe$_3$O$_4$ found the binding energy of metallic palladium particles to be 335.2 eV after the particles had undergone a stabilising procedure [118]. This results in different particle sizes and metal-support interaction, which may be responsible for the higher binding energy observed in the present case.

This similarity in the chemical states of the particles prepared using different methods will
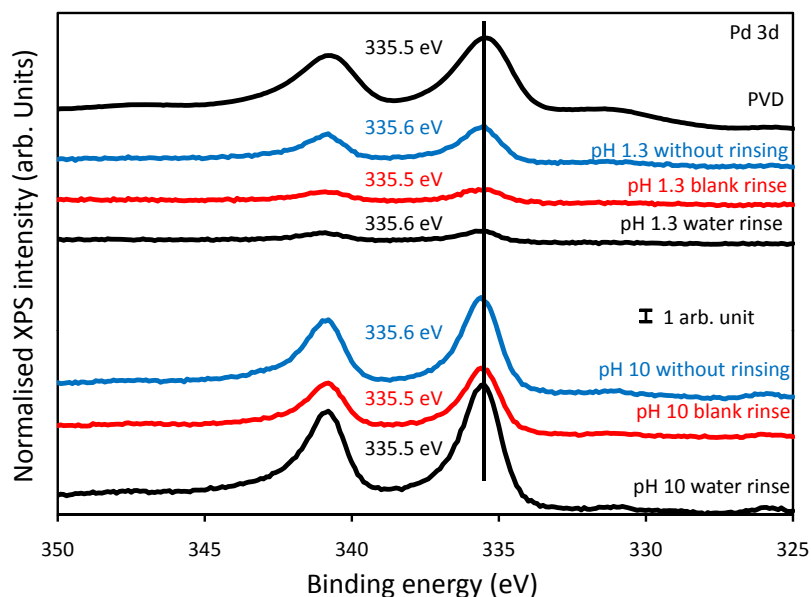
Figure 4.11: Pd 3d XPS spectra showing the final chemical state of palladium on the surface after annealing to 600 K, which have been deposited from 5 mM PdCl$_2$ solutions at pH 1.3 and pH 10 with different post-treatment procedures. The top spectrum was taken from an Fe$_3$O$_4$ on to which a nominal 4 Å of Pd was deposited using PVD after annealing to 600 K. The spectrum was taken using the same setup, but different detector settings, resulting in the wider peaks. This spectrum is not to scale.

be discussed in more detail later in the chapter.

Without rinsing, sodium and chlorine were present after deposition as before. Annealing removed chlorine in the case of palladium deposited at pH 1.3, but most of the chlorine was still present after annealing to 600 K on the sample deposited at pH 10 (Figure 4.12). This chlorine peak only disappeared after annealing to 800 K.

4.2.3 Rinsing with a blank solution

To better understand the processes at work, further experiments were conducted using palladium deposited at pH 1.3 and pH 10. Samples were prepared and characterised in the same manner as before and then rinsed using a blank solution instead of water. This solution contained no palladium, but had the same concentration of HCl and NaOH as had been used to set the pH of the solution previously.

Rinsing the samples using the blank solution produced no significant chemical shifts. As before, some palladium was lost upon rinsing. In the case of the palladium deposited at pH 1.3, a small peak remains at 337.4 eV (Figure 4.13), likely corresponding to the small amount that was converted into the lower binding energy component after rinsing with water. The chemical state of palladium deposited at pH 10 remains largely unchanged upon rinsing with blank solution and the only effect observed is the loss of palladium (Figure 4.14).

When rinsing using a blank solution, the chlorine peak for palladium deposited at pH 10 became smaller upon rinsing, but once again was relatively unaffected by annealing to 600 K
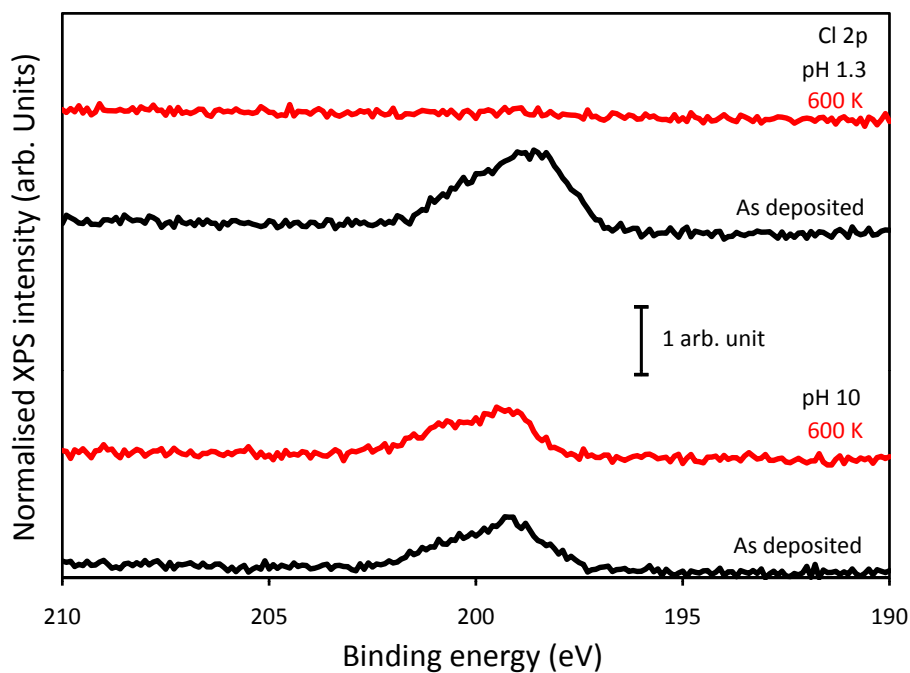
Figure 4.12: Cl 2p XPS spectra showing the state of chlorine on the surface after depositing palladium from 5 mM $PdCl_2$ solution at pH 1.3 and pH 10 and after annealing to 600 K.
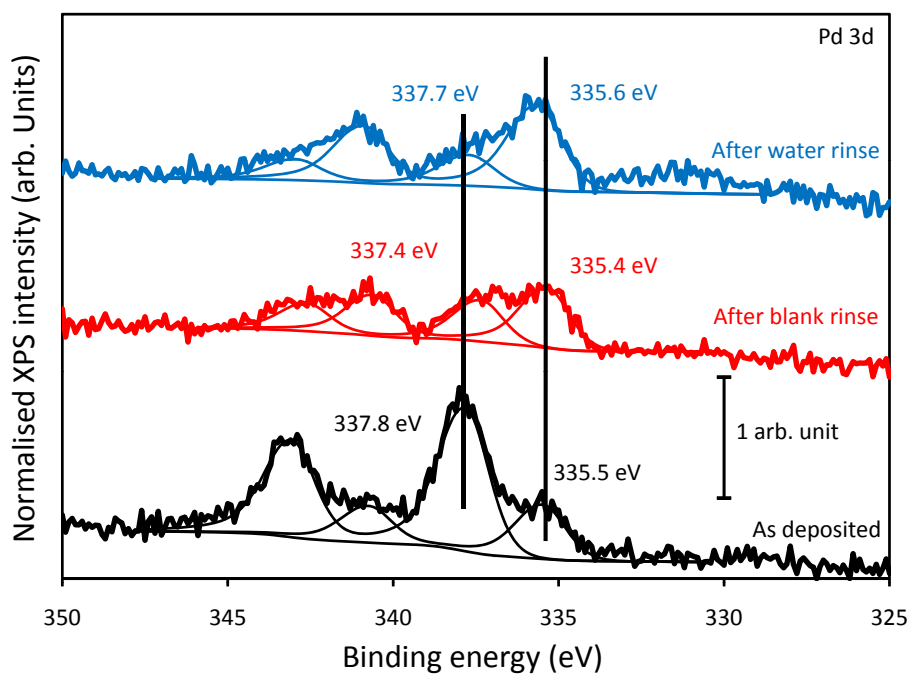

Figure 4.13: Pd 3d XPS spectra comparing the chemical state of palladium on the surface which was deposited from 5 mM $PdCl_2$ solution at pH 1.3 after rinsing with a blank solution in comparison to rinsing with water.
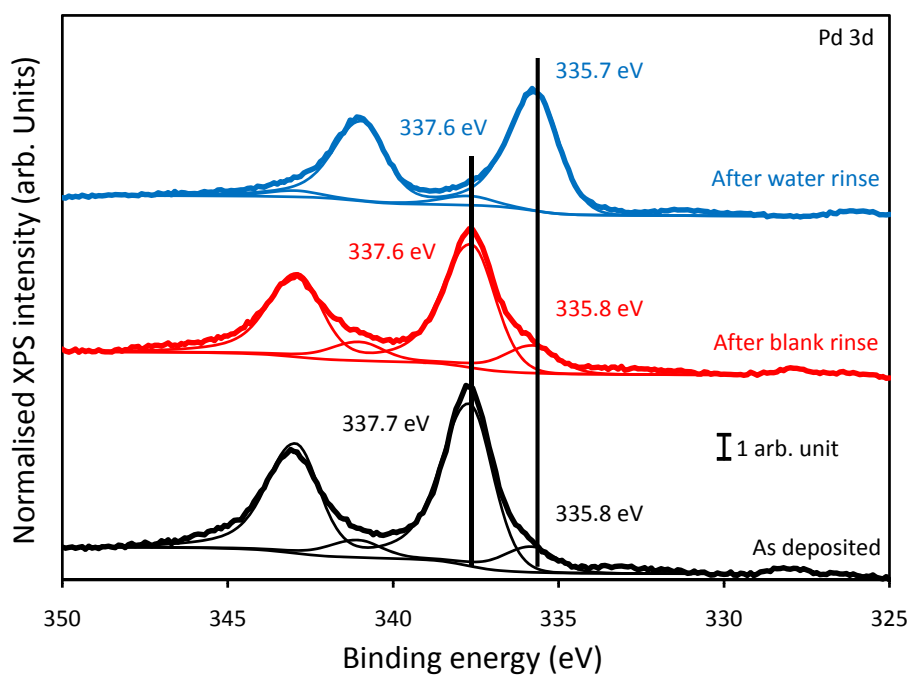
Figure 4.14: Pd 3d XPS spectra comparing the chemical state of palladium on the surface which was deposited from 5 mM $PdCl_2$ solution at pH 10 after rinsing with a blank solution in comparison to rinsing with water.
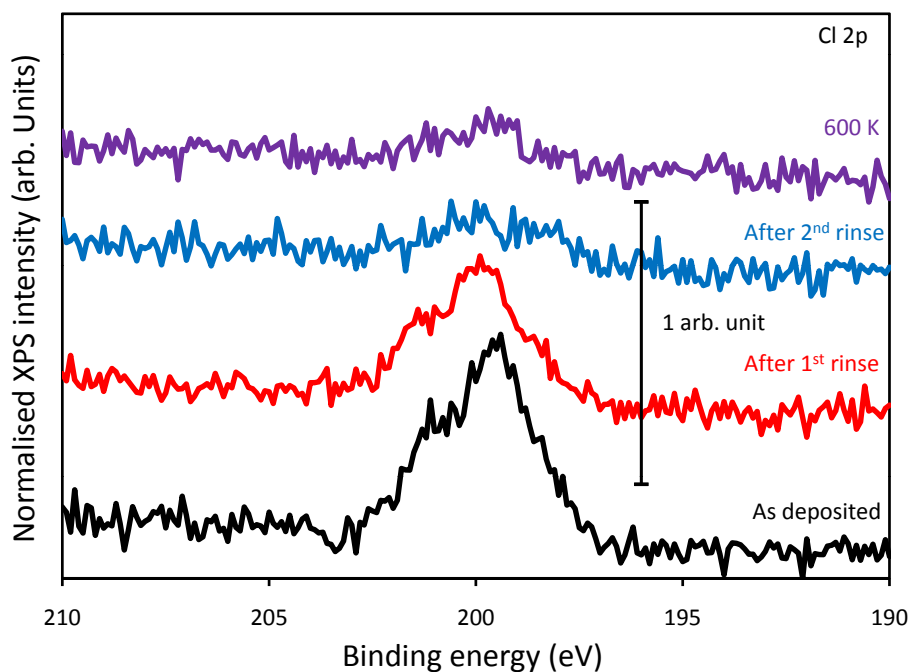

Figure 4.15: Cl 2p XPS spectra showing the state of chlorine on the surface after depositing palladium from 5 mM $PdCl_2$ solution at pH 10, rinsing using blank solutions and after annealing to 600 K.
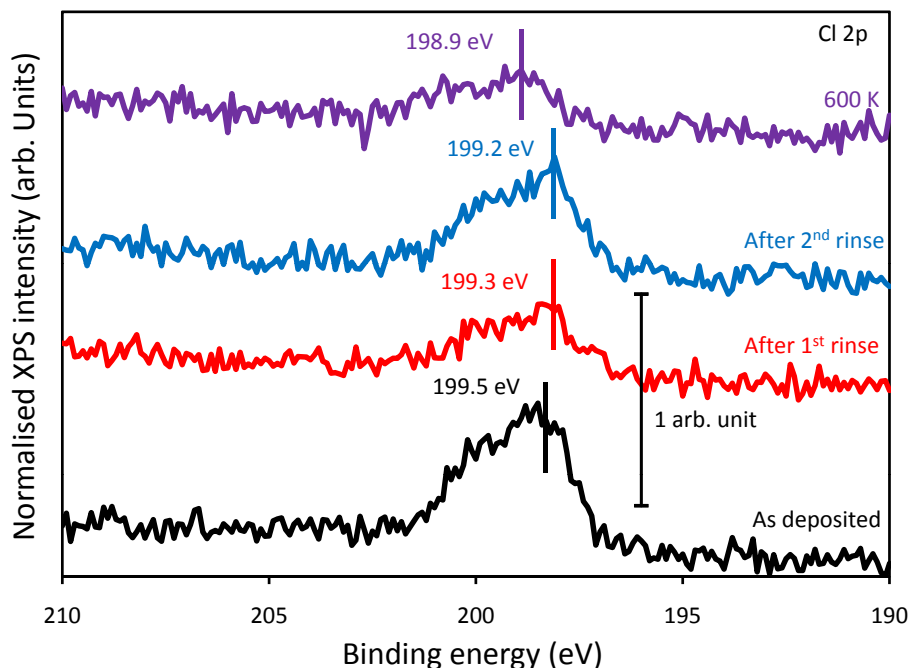
Figure 4.16: Cl 2p XPS spectra showing the state of chlorine on the surface after depositing palladium from 5 mM PdCl$_2$ solution at pH 1.3, rinsing using blank solutions and after annealing to 600 K.

(Figure 4.15). The effect of rinsing using blank solution on the samples deposited at pH 1.3 was less clear with the amount of chlorine varying slightly and either increasing or decreasing with rinsing. Not all chlorine was removed by annealing to 600 K, but the binding energy of the Cl 2p peak shifted slightly to higher binding energy upon annealing, toward the binding energy observed for palladium deposited at pH 10 (Figure 4.16).

4.2.4 Scanning tunnelling microscopy measurements

With the reduction of deposited palladium upon rinsing, an attempt was made to image the surface to see if particles were being formed. Using scanning tunnelling microscopy (STM) it was possible to resolve small particles on the surface of the sample after rinsing with water, as seen in figure 4.17. These small particles are not visible immediately after deposition without rinsing the sample (Figure 4.18). The size of these particles varied between 2.0 and 3.5 nm which is around the size of the smallest features that can be resolved using this system under these conditions.

In order to determine what effect residual chlorine on the surface may have on the size of particles two samples were prepared using pH 1.3 solution. The first was rinsed using water and the second was rinsed with blank solution as described previously. This resulted in two samples with similar levels of palladium measured using XPS, but the sample rinsed with water contained no chlorine that could be detected while the sample rinsed using blank solution still had significant amounts of chlorine present as seen previously.

After annealing to 600 K, STM images were recorded (Figure 4.19). Rinsing the surface
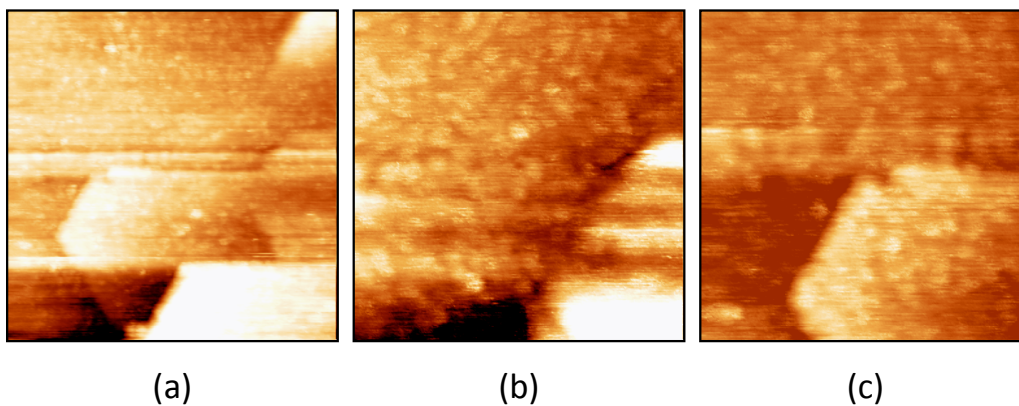
(a)   (b)   (c)

Figure 4.17: STM images of an Fe_3O_4 surface after deposition of palladium from 5 mM $PdCl_2$ solution at pH 10 and rinsing the surface with water. All images were taken with a bias of -0.3 V and a tunnelling current of 0.1 nA. Image (a) is 100×100 nm^2 and images (b) and (c) are 50×50 nm^2.
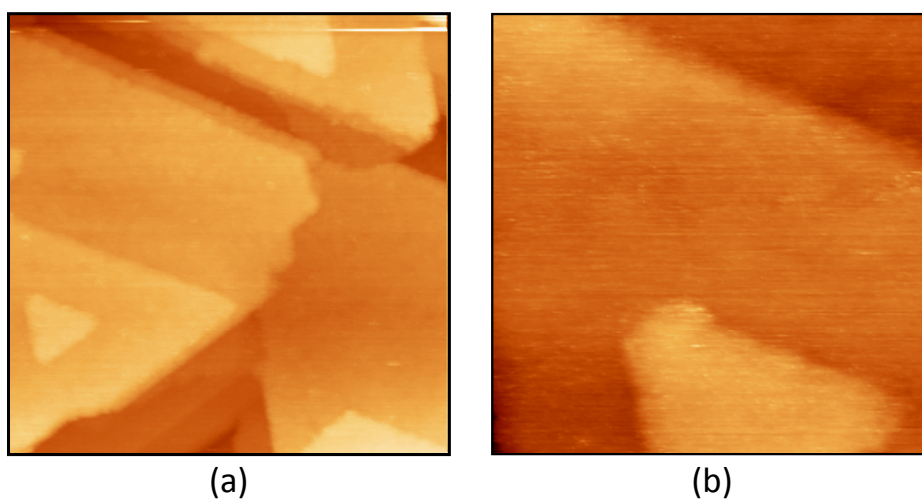

(a)   (b)

Figure 4.18: STM images of an Fe_3O_4 surface after deposition of palladium from 5 mM $PdCl_2$ solution at pH 10 without rinsing the surface with water. All images were taken with a bias of -0.3 V and a tunnelling current of 0.1 nA. Image (a) is 200×200 nm^2 and image (b) is 50×50 nm^2.
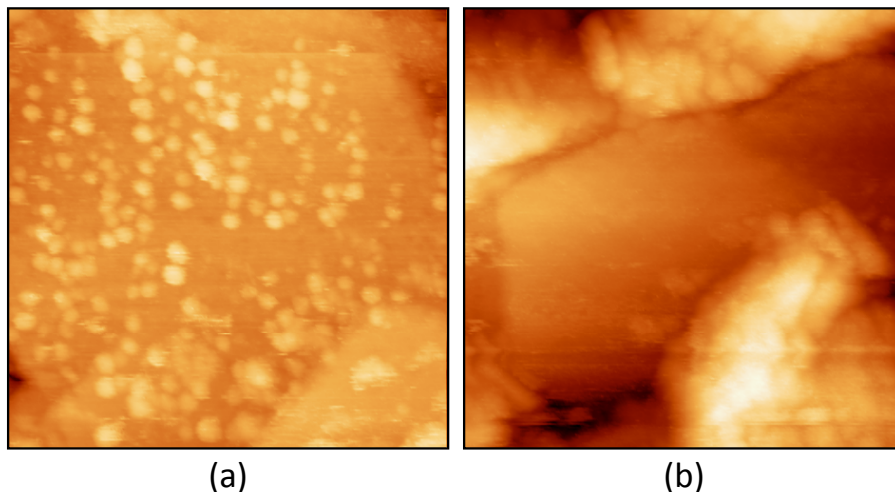
(a)   (b)

Figure 4.19: STM images of an Fe_3O_4 surface after deposition of palladium from 5 mM $PdCl_2$ solution at pH 1.3 after (a) rinsing the surface with water and (b) rinsing the surface with a blank solution, then annealing to 600 K. All images were taken with a bias of -0.3 V and a tunnelling current of 0.1 nA. Both images are 100×100 nm^2.

with water resulted in small particles, which are spread over the surface with some parts of the substrate exposed (Figure 4.19 (a)). These particles range from 2-6 nm in size. In contrast to this, after rinsing the surface with a blank solution individual particles were difficult to resolve, but appear to be much larger, with the smallest being around 8 nm in size (Figure 4.19 (b)). Any material on the substrate seems to have conglomerated together on the surface forming large mounds. This suggests an increased mobility of palladium on the surface in the presence of chlorine, leading to larger collections of palladium on the surface and poor dispersion.

Particle size is not as important for supported palladium catalysts as it is for gold, but research has shown that it can have a marked effect on the chemical properties of a catalyst. Smaller particles have been shown to be more easily oxidised and more active for CO oxidation [95]. This is likely related to changes in the energy of adsorption which have been observed for particles of different sizes using microcalorimetry [119]. This provides additional incentive for removing the chlorine from Pd catalysts independent of the negative effects observed for some catalytic reactions [111, 112].

The importance of the removal of chlorine to retaining small particles sizes will be discussed in the next section.

4.2.5 Discussion

The results of these experiments are summarised in figure 4.20 to give an overview of the data obtained.

The different behaviours observed for the different precursor solutions suggest different deposition mechanisms under high and low pH conditions. After rinsing until a steady state is reached, all palladium peaks exhibit similar binding energies, very close to what is observed for annealed samples. This suggests that the state of the palladium after rinsing is the same in all

Summary of palladium wet deposition data

		Non-rinsed		Water rinsed		Blank rinsed	
		pH 1.3	pH 10	pH 1.3	pH 10	pH 1.3	pH 10
Pd 3d BE (eV)	as deposited	337.9 336.2	337.7 335.7	337.9 336.1	337.6 335.7	337.8 335.5	337.7 335.8
	after rinsing	-	-	337.7 335.6	337.7 335.7	337.4 335.4	337.6 335.8
	after 600 K	335.6	335.6	335.6	335.6	335.5	335.6
Cl detected	after deposition	Yes	Yes	Yes	Yes	Yes	Yes
	after rinsing	-	-	No	No	Yes	Yes
	after 600 K	No	Yes	No	No	Yes	Yes
% Pd lost on rinsing		-	-	50%	9%	49%	18%

Figure 4.20: Table summarising the data collected for wet chemical deposition of palladium on $Fe_3O_4(111)/Pt(111)$.

cases.

The different binding energy of the chlorine peak and its reduced size in samples deposited at pH 10 suggests that the absorbed palladium contains very few chloride containing ligands and is likely of the form of absorbed polynuclear $Pd(OH)_2$ particles as suggested by Wang. As observed previously, these could not be resolved using STM, suggesting densely packed layers of colloids on the surface which are unable to be resolved using our STM under ambient conditions. The small loss of palladium upon rinsing suggests a strong bond to the surface, likely through a chemical bond formed with hydroxyl groups or other defects upon the surface formed during contact with the catalyst precursor solution, leading to the mechanism proposed in figure 4.21(a). This is close to the interactions that occur during deposition-precipitation, but the process used in this work has been modified to meet the requirements of the equipment used.

While it was not possible to image the individual precursor molecules immediately after deposition (Figure 4.18), small particles were observed after rinsing the surface with water (Figure 4.17). These particles were homogeneously distributed over the entire surface with no specific preference for step edges or other sites. This suggests that the precursors deposited from solution are also homogeneously distributed over the surface.

The more significant chlorine peak and speciation of solution at low pH suggests that at pH 1.3, ions such as $[PdCl_3(H_2O)]^-$ adsorb directly to the positively charged surface at this pH. This electrostatic bond should be weaker than a direct chemical bond, explaining the ease with which palladium is removed during any rinsing step. This reduced interaction can also be seen in the particles formed after annealing to 390 K. These particles can be easily moved by an STM tip during imaging as observed in a previous study [87], which is not observed for particles deposited at pH 10, which are significantly more stable. This interaction has been depicted in figure 4.21(b). This is the mechanism by which a standard impregnation deposition occurs.
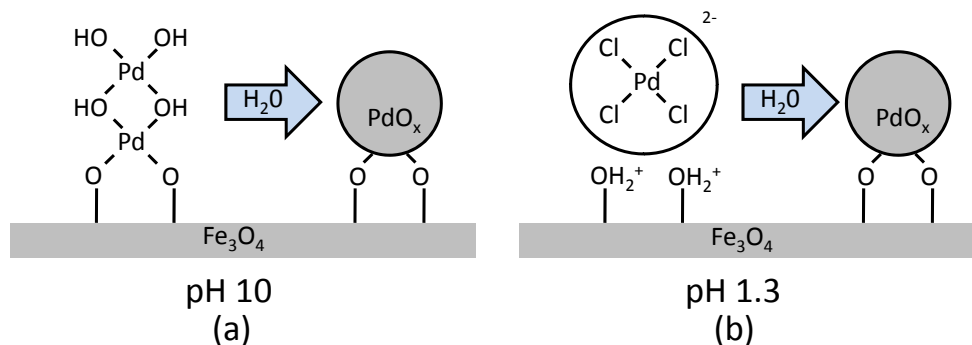
Figure 4.21: Proposed initial adsorption mechanisms and resulting species after rinsing with water for palladium deposited at (a) pH 10 and (b) pH 1.3.

The reasons behind the changes in binding energy upon rinsing could be either due to the change in pH causing a respeciation at the surface or to reduction through ligand exchange with water. In the case of pH 10 deposited palladium, the hydroxo-ligands may be replaced by aquo-ligands due to rinsing with water.

There was some variation in the amount of palladium deposited between experiments as can be seen in figure 4.22. This variation was larger for pH 1.3, where the amount of palladium was smaller, but this palladium was washed away upon rinsing leaving a similar amount bound to the surface. This variation does not seem to correlate with the amount of carbon on the surface, as it can be demonstrated that there is no correlation between the area of the Pd 3d peak and the C 1s (Figure 4.23), which suggests this is not simply an effect of the amount of contamination on the surface blocking the measurement of palladium. When comparing the area of the Cl 2p peak to the area of the Pd 3d peak there appears to be positive correlation at pH 10 and negative correlation at pH 1.3 (Figure 4.24).

This could be related to the two different mechanisms as the palladium deposited at pH 1.3 should be from chlorine containing precursors, so one would expect the amount of chlorine on the surface to increase with the amount of palladium. In the case of palladium deposited at pH 10, it is expected that most of the palladium is anchored to the surface in a grafting type reaction in the form of a palladium hydroxide type species, likely by grafting to hydroxyl groups on the surface as seen for gold deposited on to TiO_2 in a similar manner [120]. Chlorine could act to block these sites, preventing this grafting reaction, in which case higher amounts of chlorine on the surface would imply lower amounts of palladium as is observed. The overall amounts of palladium and chlorine deposited must arise from some as yet unidentified factor, such as the temperature of the ambient environment or the presence of a specific carbon containing contaminant but in any case, the binding energy and therefore the chemical state of the deposited palladium for each pH seems to be consistent.

The results presented here are also consistent with the model proposed above, as the Pd:Cl ratio is approximately 3:1 for Pd deposited at pH 10 and approximately 1:2 for deposition at pH
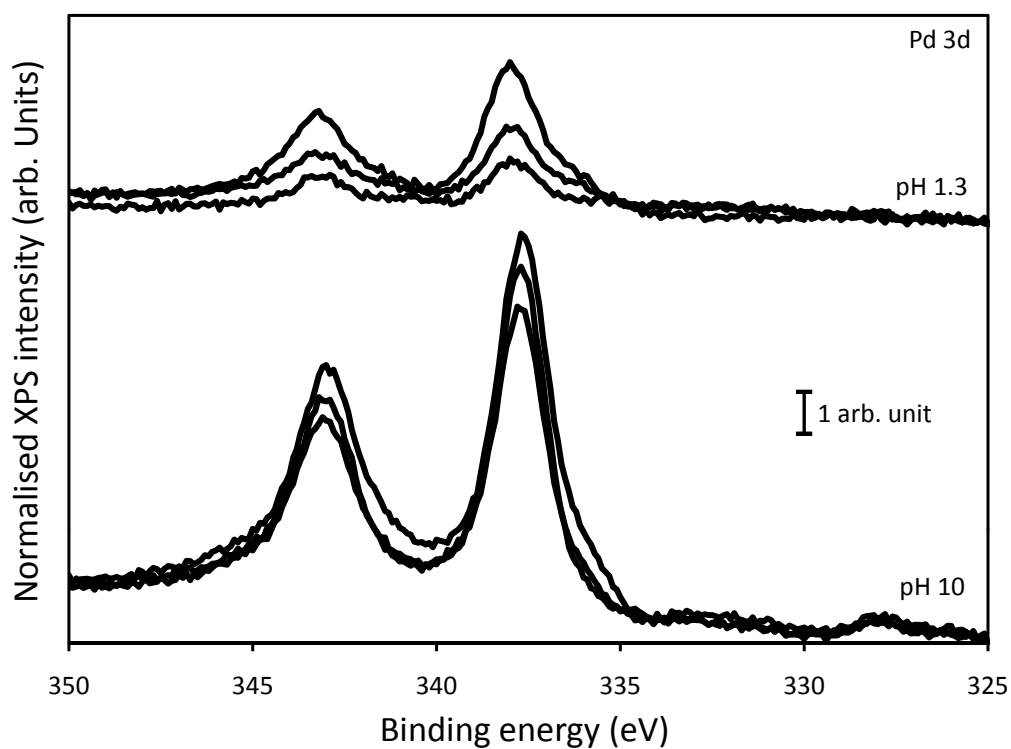
Figure 4.22: Pd 3d XPS spectra demonstrating the variation in the amount of Pd deposited from 5 mM $PdCl_2$ solution under the same conditions at pH 1.3 and 10.
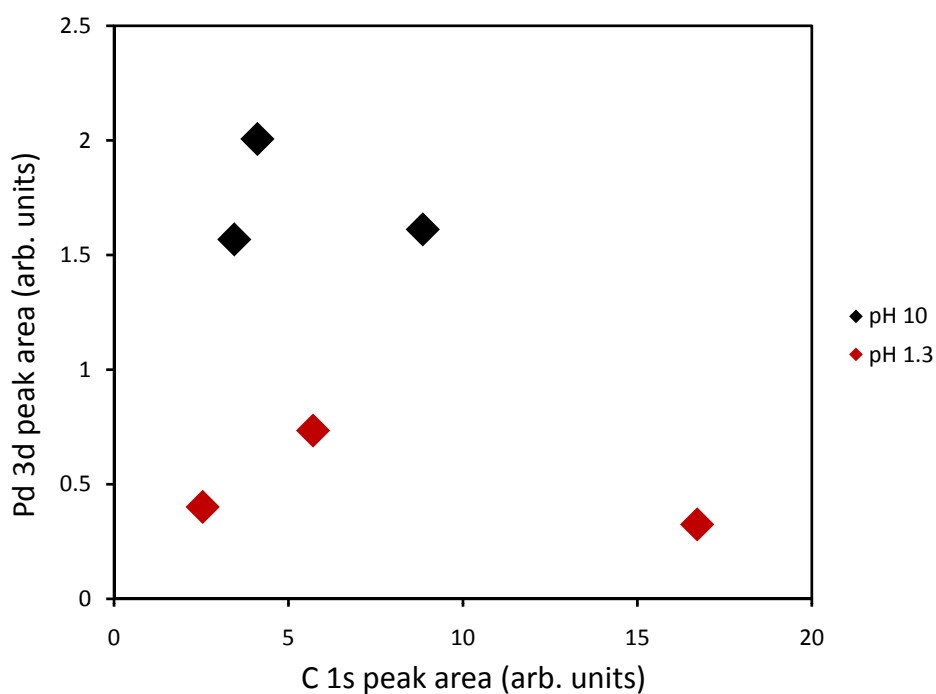

Figure 4.23: Scatter plot showing the area of the Pd 3d peak versus the C 1s peak for multiple depositions at pH 1.3 and 10. The peak areas have been adjusted for the atomic sensitivity factors found in [48].
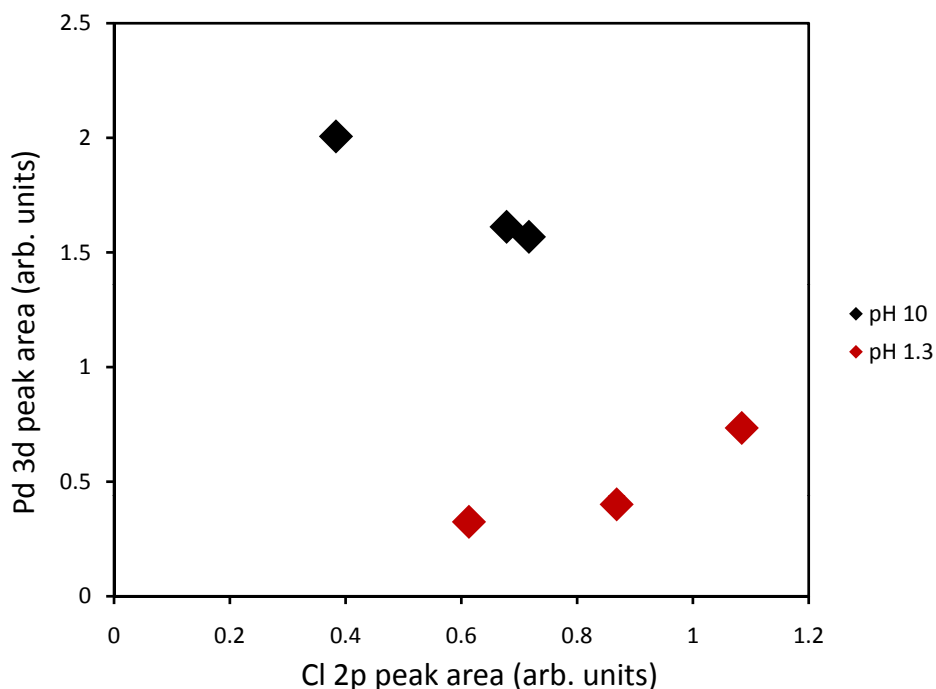
Figure 4.24: Scatter plot showing the area of the Pd 3d peak versus the Cl 2p peak for multiple depositions at pH 1.3 and 10. The peak areas have been adjusted for the atomic sensitivity factors found in [48].

1.3. At pH 10, the concentration of chlorine found on the surface is low, consistent with palladium coming mainly from $Pd(OH)_2$ like species with some chlorine in the mixture. The higher Cl concentration seen at pH 1.3 is consistent with precursors of the form $[PdCl_x(H_2O)_y]^{2-x}$. $[PdCl_2(H_2O)_2]$ complexes deposited on the surface at pH 1.3 would only be weakly bound due to their lack of charge and could be easily rinsed away. A large proportion of the palladium was lost upon rinsing at this pH.

Rinsing the surface is a very effective method for removing chlorine containing contaminants from the surface, as in all cases chlorine levels could be brought below the detection limit of our setup by (< 0.05 ML) rinsing with water, but in the case of the low pH deposited samples it removes a significant proportion of the deposited palladium. Palladium loss results in significant waste of the active part of the catalyst and increased costs for production. The losses in the case of pH 10 deposition are much more modest, but the benefits can be clearly seen with the presence of chlorine having a marked effect on particle mobility and final particle size.

This suggests that rinsing the surface may not be the most appropriate method for dealing with residual chlorine on catalysts prepared using impregnation methods and other methods, such as cycles of oxidation and reduction as attempted by Wang [87] may be more appropriate, but in the case of palladium deposited at pH 10 the smaller losses make this method more acceptable.

This work demonstrates the complete removal of chlorine from the surface by rinsing. This could not be determined by examining the chloride content of water used for rinsing the surface. The removal of chlorine was shown to be important to retaining small particle sizes and such a

result demonstrates the utility of ex-situ surface science techniques in studying processes that occur at the solid-liquid interface.
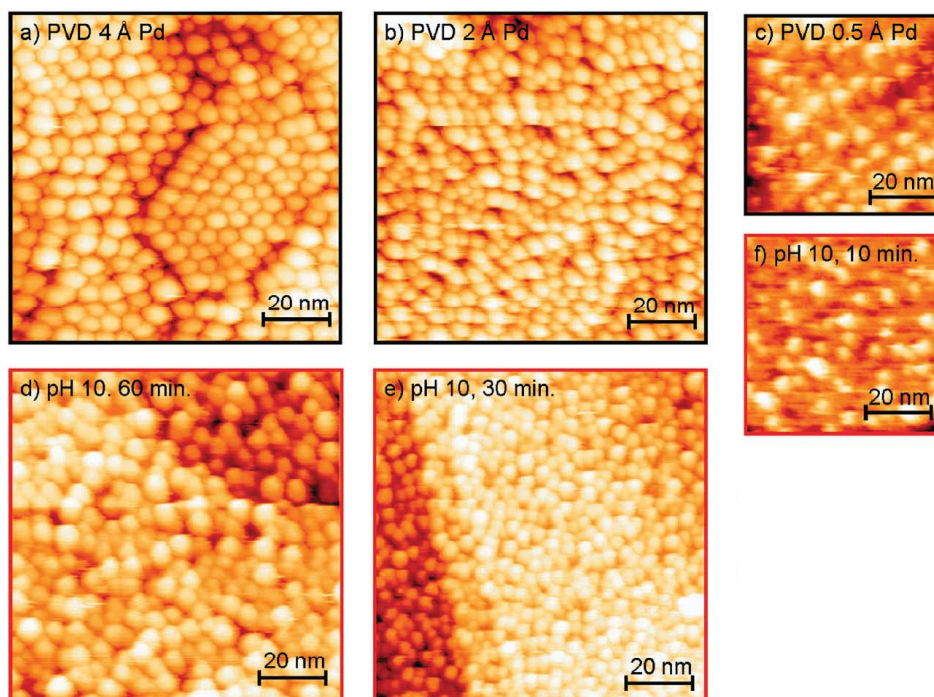

Figure 4.25: STM images comparing Pd particles formed on Fe3O4(111) after deposition of various amounts of Pd by physical vapor deposition (PVD) in UHV (ac), and after interaction with Pd precursor solution for various contact times and rinsing (df). All samples were annealed to 600 K prior to STM imaging. Images (a), (b), (d), (e) are 100×100 nm^2 and images (c), (f) are 60×60 nm^2. Taken from [43]

The binding energy of the Pd 3d XPS peaks for the samples prepared using liquid deposition peaks identical to what was obtained using PVD (refer to figure 4.11) and previously published results demonstrate the similarity in the morphology of samples prepared using PVD and liquid deposition (Figure 4.25) [43]. This demonstrates that after rinsing and annealing the samples prepared using liquid deposition, the resulting model catalysts were very similar to samples prepared using PVD under UHV conditions. This similarity implies that results obtained previously from UHV studies should be valid for the interpretation of experiments using liquid prepared samples and vice versa.

4.3   Gold on iron oxide

Gold is an especially interesting subject for catalysis due to its unique properties as a catalyst [121]. It is more or less inert in the bulk phase, but small distributed gold particles have been shown to be very active in reactions such as CO oxidation as first reported by Haruta [103, 107]. This means that the catalytic properties of small gold particles can be easily separated from

larger particles or bulk gold that might be present in a system as the latter should have no effect on the reactivity of a system.

Ever since Haruta's first report about the high catalytic activity of highly dispersed gold particles a large amount of research has been focused on the preparation of supported gold catalysts on various oxide supports as well as the mechanistic details of gold's catalytic activity. The preparation of dispersed gold nanoparticles has proven to be a significant challenge.

When prepared in the conventional way, by using incipient wetness impregnation with chloroauric acid ($HAuCl_4$) on an oxide support, the resulting gold particles are in the size range of tens of nanometers and are catalytically inactive. The breakthrough which led to nano-sized catalytically active gold particles came with attempts to deposit gold under neutral or alkaline conditions instead of the acidic conditions used in impregnation preparations [107]. Since the precursor under these conditions is present in its hydrolysed form ($Au(OH)_4^-$), this preparation method is considered analogous to deposition-precipitation due to its similarity to other systems [101] prepared in this way.

Haruta further observed that it was possible to produce highly dispersed supported gold particles appropriate for catalysis using $AuCl_3$ catalyst precursor solution contacted with TiO_2. The method originally described by Haruta is not a true deposition-precipitation reaction if the strictest definition of the process is used, as gold hydroxide cannot precipitate at the surface under these conditions [97, 104]. Instead of gradually raising the pH of the system to cause precipitation to occur at the solid-liquid interface, the pH is raised to a set point, then the mixture stirred with mild heating for 1-2 hours to allow the gold in solution to interact with and graft to the the surface.

In an attempt to apply this preparation procedure to a single-crystalline substrate, Haruta used fragments of a $TiO_2(110)$ crystal as a support and analysed the resulting catalyst with scanning electron microscopy and reflection high-energy electron diffraction [122]. The results of this study show that the gold particles are mainly located along the edges of steps or fracture lines on the TiO_2 surface and high dispersion could not be obtained.

To date, there are no reports of highly dispersed gold particles deposited on to a single crystalline substrate using wet chemical methods. The experimental setup designed and described in this work provides the perfect opportunity for investigating the deposition conditions required for producing small, highly dispersed gold particles on UHV prepared single-crystalline substrates.

The mechanism of gold deposition on TiO_2 has been investigated in detail [97, 104]. At the pH levels that result in the smallest particles (pH 7-10), both the gold complexes in solution ($[AuCl(OH)_3]^-$ and $[Au(OH)_4]^-$) and the TiO_2 surface (The point of zero charge for TiO_2 is approximately pH 5 [123]) are negatively charged and as such an electrostatic interaction is not possible. Instead, a surface complex is formed through reactions with surface hydroxyl groups and the complex is strongly bound to the surface through a grafting reaction.

$$TiOH + [AuCl(OH)_3]^- \rightarrow Ti-[O-Au(OH)_3]^- + H^+ + Cl^- \qquad (4.1)$$
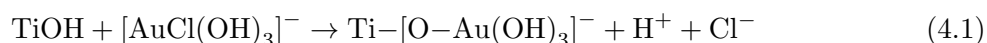
A typical preparation would start with a solution of $HAuCl_4$ having titanium dioxide powder added to it. The pH of this mixture would be gradually raised by addition of NaOH. Once the

desired pH is reached, the mixture is stirred at 70-80 °C for one hour. Washing the prepared sample to remove chlorine has been found to be incredibly important to retaining small particle sizes, so the sample is then washed in water and dried [124]. Afterward, the catalyst is thermally treated to obtain metallic gold particles [125].

Using TiO_2 as a support has resulted in highly active catalysts for CO oxidation, but Fe_2O_3 supported catalysts have also proven to be effective [98, 124, 126]. This chapter describes attempts to create small, dispersed gold particles on an $Fe_3O_4(111)/Pt(111)$ using similar deposition methods, investigates the effect of rinsing on this system and compares gold deposited in this way to gold deposited using PVD under UHV conditions and the results obtained previously on TiO_2.

4.3.1 Investigation of deposition conditions

As a first attempt a stock solution of $AuCl_3$ was made using the same concentration as for $PdCl_2$, diluted to produce a 5 mM $AuCl_3$ solution and contacted with the surface of a freshly prepared Fe_3O_4 film in a hanging meniscus configuration for one hour as for palladium deposition. Such a preparation procedure has shown good results for palladium deposition and Haruta suggested that concentrations in the range of a few mM were ideal for gold deposition [127]. The pH of this solution was measured to be below zero using pH paper.

These preparation parameters resulted in a large amount of gold present on the surface, but the binding energy of the Au 4f peak (84.0 eV) indicated that the gold deposited was in a metallic state (Figure 4.26). Further attempts were made using a solution balanced to pH 10 using NaOH, as alkaline pH values were found to be the most effective for gold deposition on TiO_2 [103], and a shorter interaction time. Less gold was deposited, but once again the XPS data indicated that gold had been deposited in a metallic state.

As metallic gold was being deposited instead of oxidised precursor complexes, it was thought that using the hanging meniscus configuration may have allowed the solution to interact with the sides of the platinum crystal, leading to an electrochemical redox reaction which resulted in metallic gold. Deposition using a pH 10 solution was attempted using the liquid reservoir of the STM cell so that no solution could reach the platinum crystal. This resulted in peak components which were shifted to higher binding energy relative to bulk metallic gold, which indicates that gold was present in an oxidised state (Figure 4.26, blue spectrum). The Au 4f binding energy (87.0 eV) observed from the sample deposited using the STM cell is consistent with the adsorption of a $Au(OH)_3$-like precursor, as is observed from Au deposition on Fe_2O_3 [98].

This difference between the two deposition situations suggests that when using the hanging meniscus configuration, the solution interacts with the sides of the crystal and reduction of gold occurred through an electrochemical redox reaction with the exposed platinum. For this reason it was decided to perform all further experiments on gold deposition using the STM cell, to eliminate the effects from any exposed platinum, using the pH 10 precursor solution. This effect was not seen for palladium deposition where the same XPS spectra are obtained whether the STM cell or the hanging meniscus configuration are used for deposition.

With this preparation procedure established, the sample on which gold was deposited using
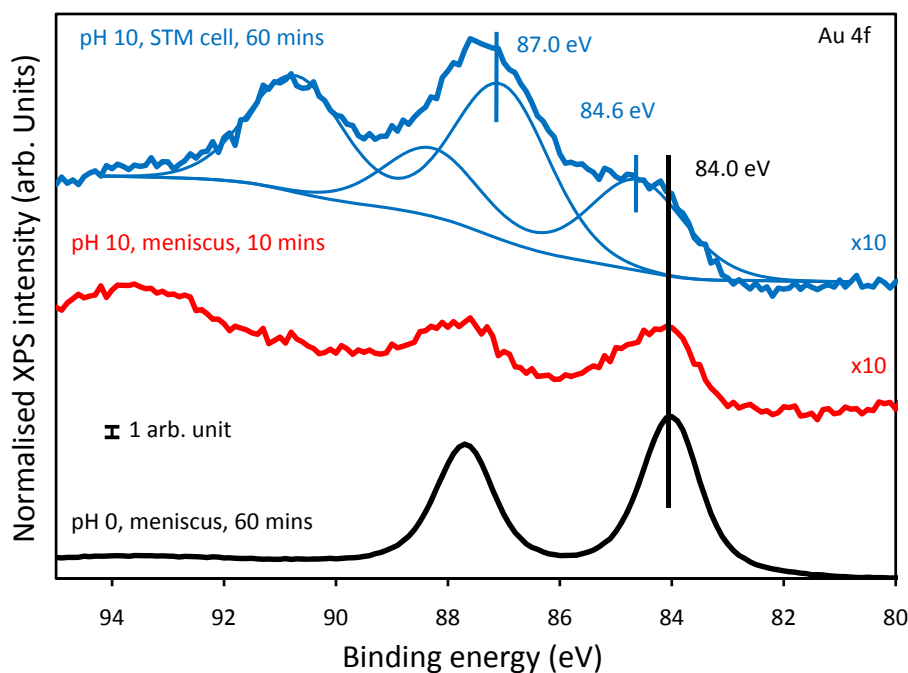
Figure 4.26: Au 4f XPS spectra showing the state and amount of gold deposited on to the surface when exposing an Fe_3O_4 surface to various 5 mM $AuCl_3$ precursor solutions in a hanging meniscus configuration in comparison to gold deposited using the STM cell. The top two spectra have been multiplied by a factor of 10 for the sake of visibility.
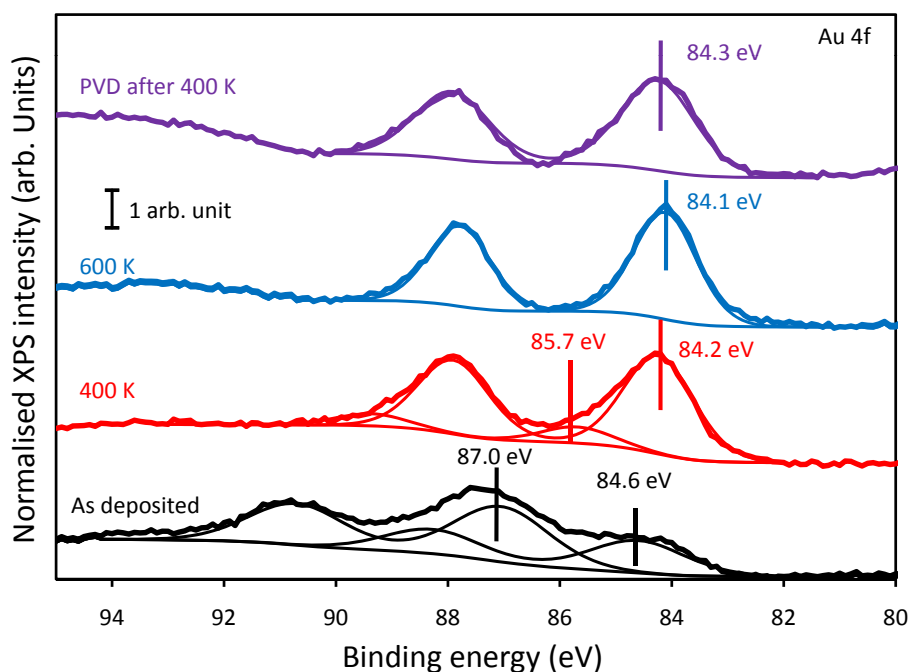

Figure 4.27: Au 4f XPS spectra showing the reduction of gold that has been deposited from 5 mM $AuCl_3$ solution at pH 10 using the STM cell upon annealing. Also shown is a spectrum taken from gold particles prepared using PVD after annealing to 400 K

the STM cell was then annealed to 400 and 600 K. This led to the reduction of the gold, which resulted in the Au 4f peak shifting to a binding energy consistent with what is observed for gold deposited using PVD (Figure 4.27). Similar values (83.8-84.4 eV) have also been seen for gold deposited using PVD on the $Fe_3O_4(001)$ surface [128]. This suggests that after annealing the gold is in a metallic state.

The binding energies observed before and after annealing are in reasonable agreement with experiments conducted using the same precursor solution in deposition-precipitation experiments conducted previously on TiO_2 [104, 129] and Fe_2O_3 [98]. These shifts have been assigned previously as transitions from $Au(OH)_3$ to Au_2O_3 to metallic gold through annealing, with metallic gold coexisting with the oxidised forms at all steps below 600 K [98]. This seems like a probable mechanism in the present case as well. The lower binding energy component observed immediately after deposition (84.6 eV) likely corresponds to small amounts of metallic gold which have been reduced either through interaction with the surface or decomposition due to interaction with light.

There were also notable changes in the O 1s spectrum after deposition. The first, more prominent peak relates to oxygen within the Fe_3O_4 lattice (530.2 eV), but after deposition a second peak appeared at higher binding energy (532.4 eV). This peak was stable and had not been appreciably diminished after annealing to 600 K (Figure 4.28). The energy and conditions of deposition would suggest that this peak could be related to hydroxylation of the surface. The binding energy of this second O 1s XPS peak is consistent with what was observed after exposure of the magnetite surface to water vapour and immersion in water and this peak was shown to be relatively stable up to approximately 1000 K [130]. This shoulder was not observed during PVD experiments and must result from interaction with the solution as opposed to being an effect of gold alone.

4.3.2 Effect of water rinsing

As the presence of chloride has been proven to be detrimental to retaining small particle sizes [125, 131], gold deposition was repeated with an additional rinsing step added to the process to determine what effect rinsing with water may have upon the system. This rinsing step was also performed inside the STM cell to prevent any interaction with platinum during rinsing. The effect of rinsing on gold can be seen in figure 4.29. Upon rinsing, the area of the Au 4f XPS signal reduced by 46%, similar to what was observed for palladium deposited at pH 1.3 after rinsing (See section 4.2.1).

There was a slight variation in the binding energy of the fitted peaks for gold before rinsing in comparison to the previous experiment and this slight variation seems to exist throughout other experiments conducted, but the qualitative form of the peak structure remains the same. This variation may be related to reduction of the precursor during deposition by light as no particular care was taken to prevent this. Ambient light is known to reduce this particular precursor [131], but has been shown not to affect the catalyst after additional steps, such as rinsing and calcination, have been performed [5]. Rinsing the sample with water almost completely reduces the deposited gold to metallic gold. Annealing to 600 K produced a slight additional effect, but the majority of the changes occur already after rinsing. Rinsing had no
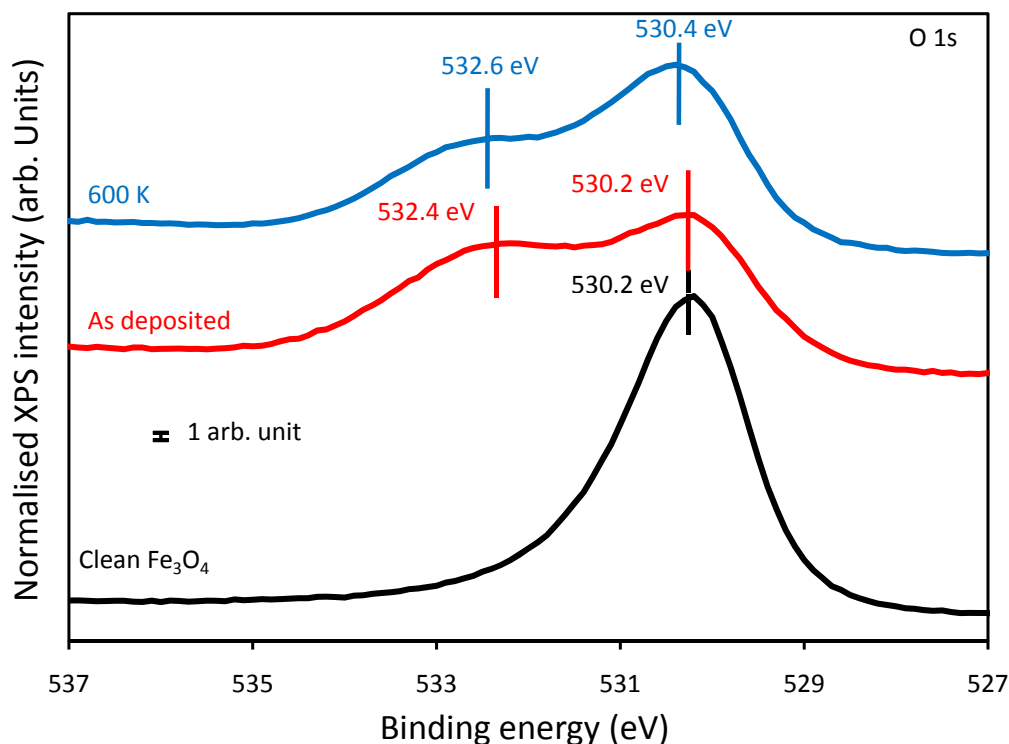
Figure 4.28: O 1s XPS spectra showing the emergence of a new oxygen species after deposition using 5 mM $AuCl_3$ solution at pH 10 and its thermal stability.

appreciable effect on the additional peak observed in the O 1s spectrum.

As for palladium, chlorine was present on the surface immediately after deposition. Annealing had little effect on the amount of chlorine present on the surface on the unrinsed sample (Figure 4.30), but rinsing removed it completely from the surface as was observed for palladium deposition (Figure 4.31). Upon annealing, the Cl 2p peak of the sample that had not been rinsed shifted slightly to lower binding energy, but generally the binding energy of the Cl 2p was very close to the Cl 2p peak from an Fe_3O_4 film exposed to a blank solution (Figure 4.9). This suggests that the chlorine present is likely bound directly to the substrate and any interaction with the gold is minimal.

STM images were also taken at each stage of the preparation process for both samples (Figure 4.32). In all cases the surface was very rough and difficult to image. Fairly large particles can be made out within a size range of 4-10 nm, with the number of larger particles increasing with annealing. It can be seen in figure 4.32 (c) that these particles were already present after rinsing, before any annealing process. These particles were much larger than what can be achieved using PVD on Fe_3O_4 [132] and larger than has been achieved using similar deposition procedures on other supports [125]. As the particle size was large and the amount of gold on the surface seemed to be high, further experiments were conducted using a lower concentration of gold by producing a 2.5 mM $AuCl_3$ solution which also had a pH of 10.
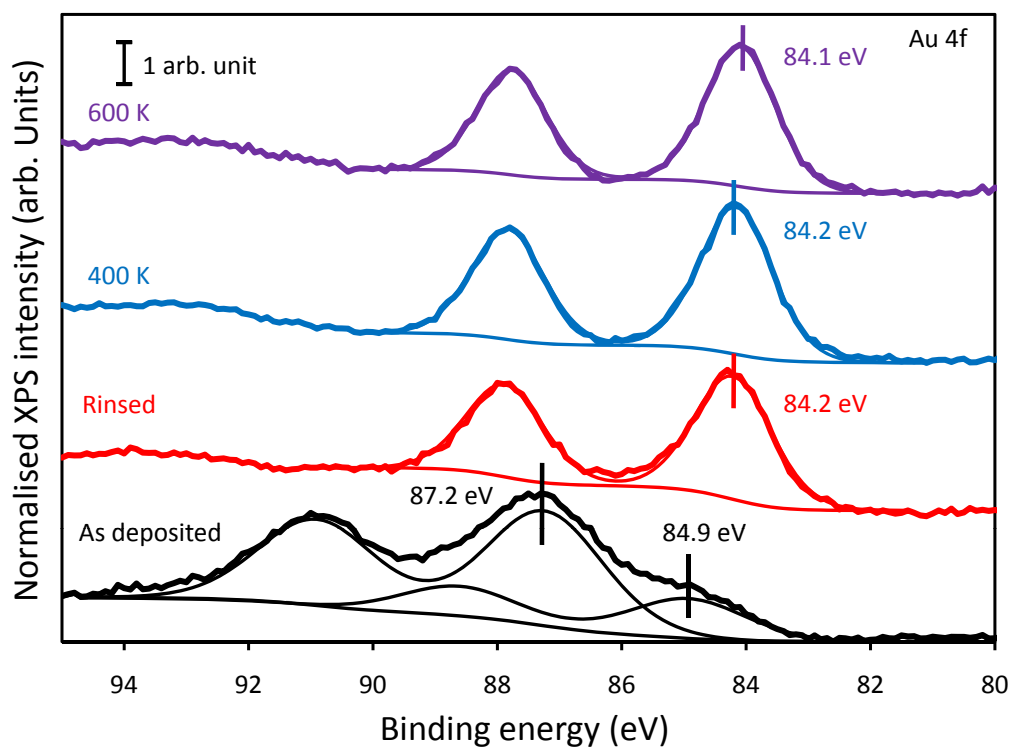
Figure 4.29: Au 4f XPS spectra showing the reduction of gold that has been deposited from 5 mM AuCl$_3$ solution at pH 10 using the STM cell upon rinsing and annealing.
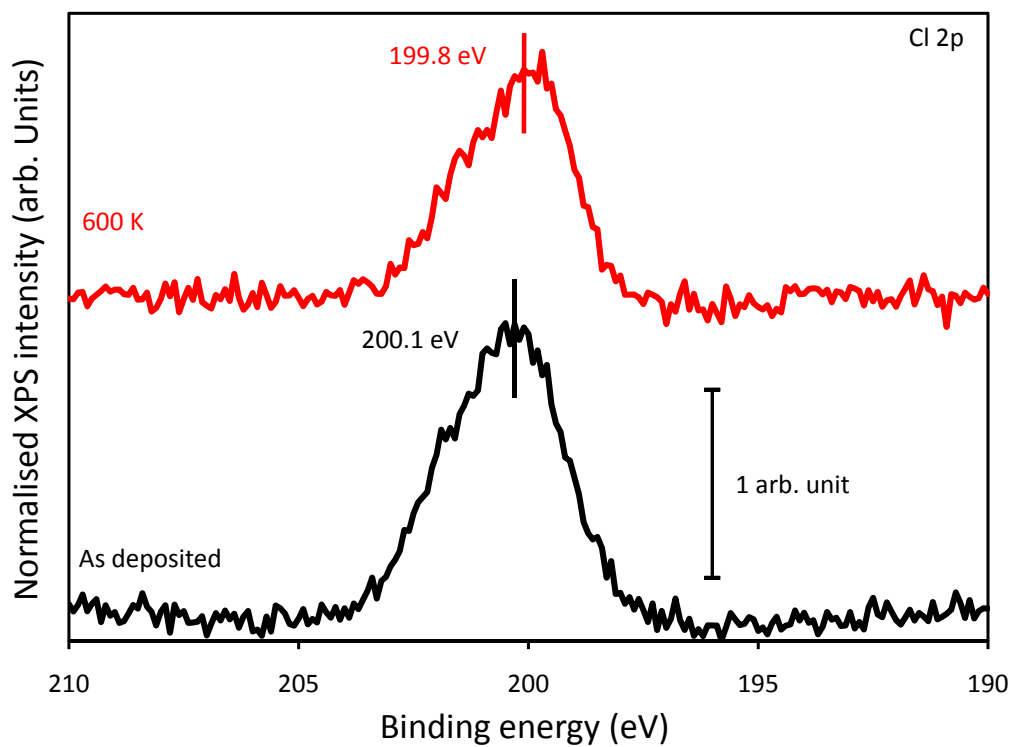

Figure 4.30: Cl 2p XPS spectra showing the chlorine peak after deposition from 5 mM AuCl$_3$ solution at pH 10 and annealing.
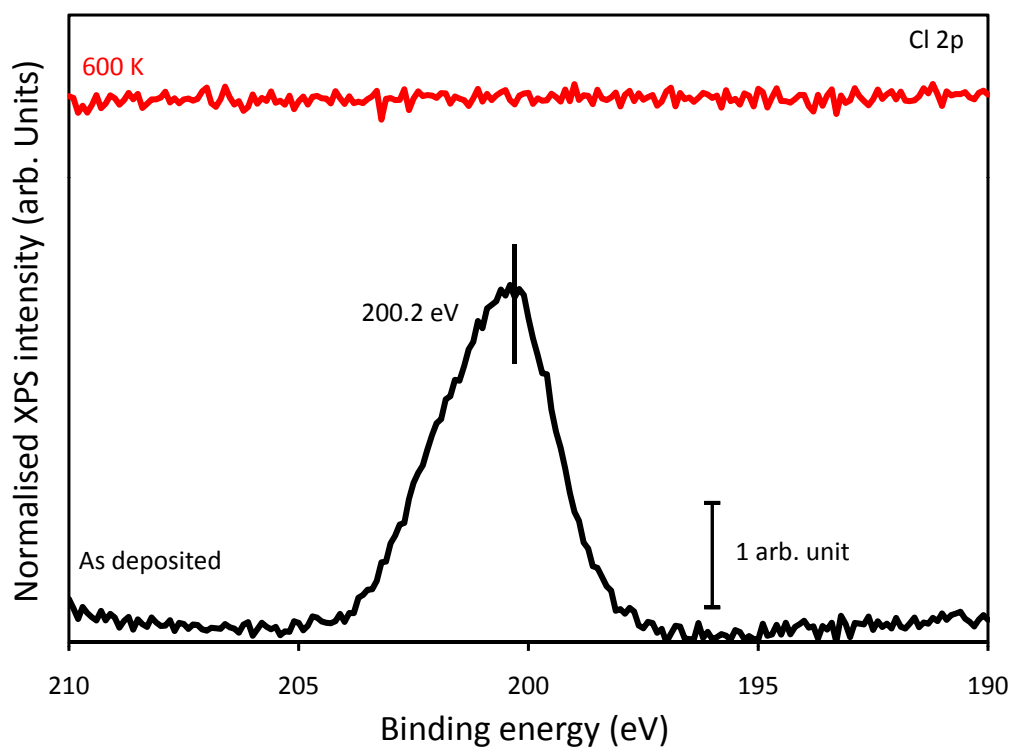
Figure 4.31: Cl 2p XPS spectra showing the chlorine peak after deposition from 5 mM AuCl$_3$ solution at pH 10 and rinsing with water.

Figure 4.32: STM images of an Fe$_3$O$_4$ surface after deposition of gold at pH 10 from a 5mM AuCl$_3$ solution after (a) annealing to 400 K and (b) annealing to 600 K, and another sample after (c) rinsing the surface with water, (d) annealing to 400 K and (e) annealing the surface to 600 K. All images were taken with a bias of -0.3 V and a tunnelling current of 0.1 nA. Images (a), (b) and (c) are 100×100 nm^2 and images (d) and (e) are 200×200 nm^2.
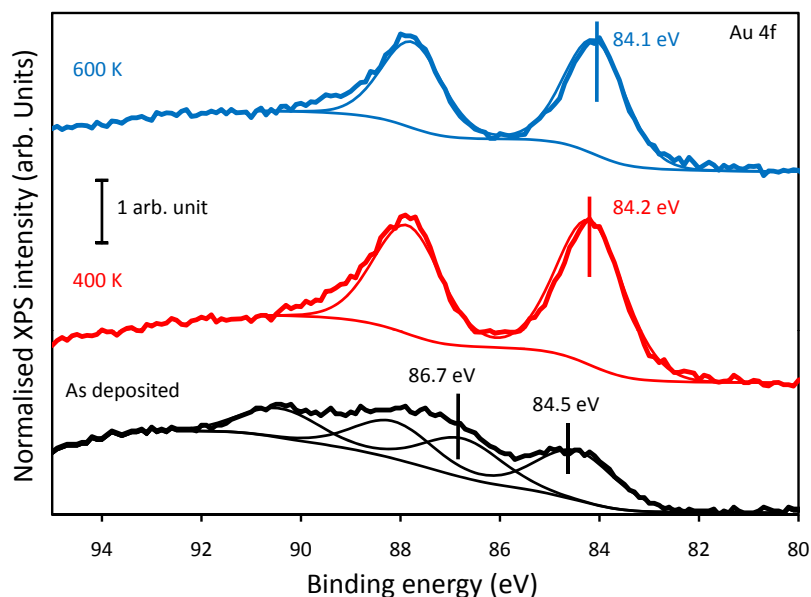
Figure 4.33: Au 4f XPS spectra showing the reduction of gold, that has been deposited from 2.5 mM $AuCl_3$ solution at pH 10 using the STM cell, upon annealing. The background of the film before deposition has been subtracted from this spectrum.

4.3.3   2.5 mM gold deposition

After deposition from the 2.5 mM solution, the binding energy of the gold obtained was in good agreement with that obtained from 5 mM $AuCl_3$ solution, with all the same components still present (Figure 4.33). The size of the signal was smaller, as is to be expected from using a lower concentration, and this made fitting slightly more complicated. In order to properly fit the spectra, the background measurement of the Fe_3O_4 film before gold deposition had to be subtracted due to some features of the film overlapping partially with the Au 4f peak.

Upon annealing, the same behaviour was observed as before, although there seems to be a slight decrease in the size of the signal after annealing to 600 K in comparison to what is observed after annealing to 400 K. This could be explained by larger particles being formed causing part of the gold signal from atoms near the surface to be blocked by other gold atoms on top. This is consistent with what is seen with STM. Smaller particles of about 4-10 nm in size were observed after annealing to 400 K, but upon annealing these increased dramatically in size to the point where the smallest particles were 10 nm in diameter and the largest 25 nm (Figure 4.34). Instead of the large second peak visible in the O 1s spectra seen earlier, a small shoulder appeared at the same energy (Figure 4.35). Once again it was largely unaffected by rinsing or annealing and was stable even up to 800 K. The size of this peak seems to scale with the amount of gold deposited.

Rinsing a freshly prepared sample in water produced similar XPS spectra to before (Figure 4.36, cf. figure 4.29). As for the 5 mM deposition, all chlorine was removed after rinsing the sample with water. From the STM results it is clear that rinsing with water has affected the mobility of gold upon the surface (Figure 4.37). Once again the particles are visible on the surface after rinsing with water, but there does not seem to be an increase in the particle size
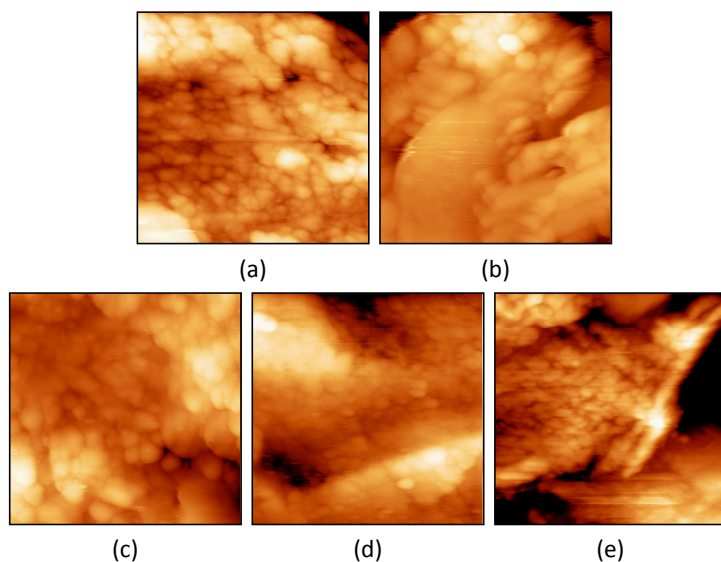
Figure 4.34: STM images of an Fe_3O_4 surface after deposition of gold at pH 10 from a 2.5mM $AuCl_3$ solution after (a) annealing to 400 K and (b) annealing to 600 K. All images were taken with a bias of -0.3 V and a tunnelling current of 0.1 nA are 200×200 nm^2.
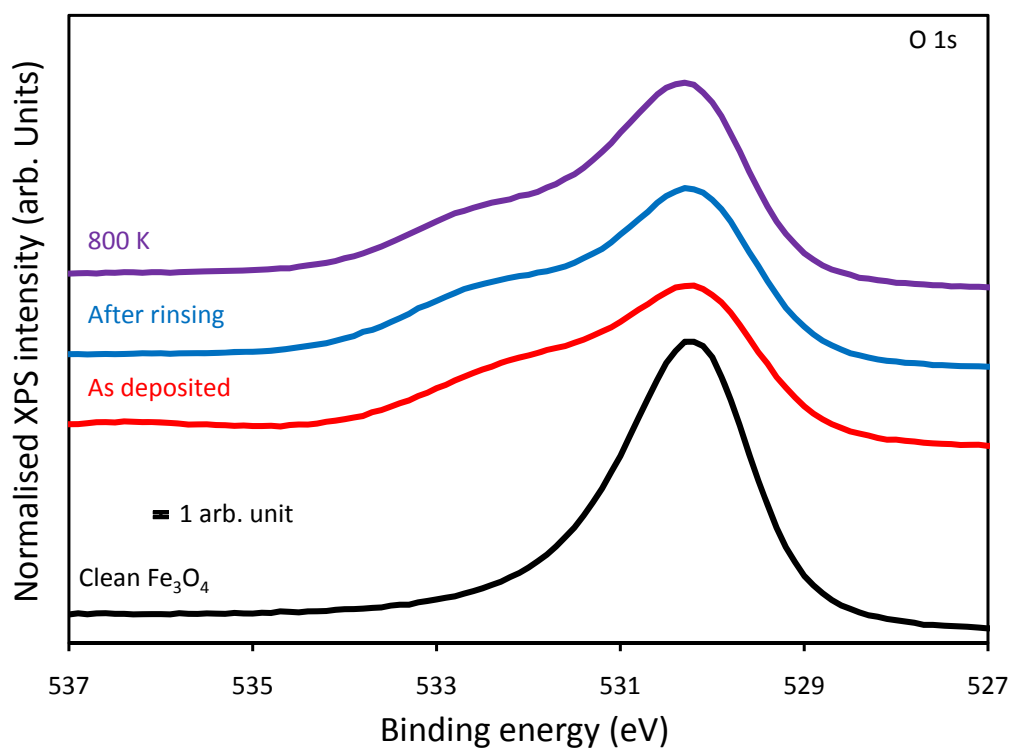
Figure 4.35: O 1s XPS spectra showing the emergence of a new oxygen species after deposition using 2.5 mM $AuCl_3$ at pH 10 and its stability when the sample is rinsed or annealed to 800 K.

after annealing from 400 K to 600 K in contrast to what was seen for the unrinsed sample (Figure 4.34). The particles observed were 6-10 nm in size.
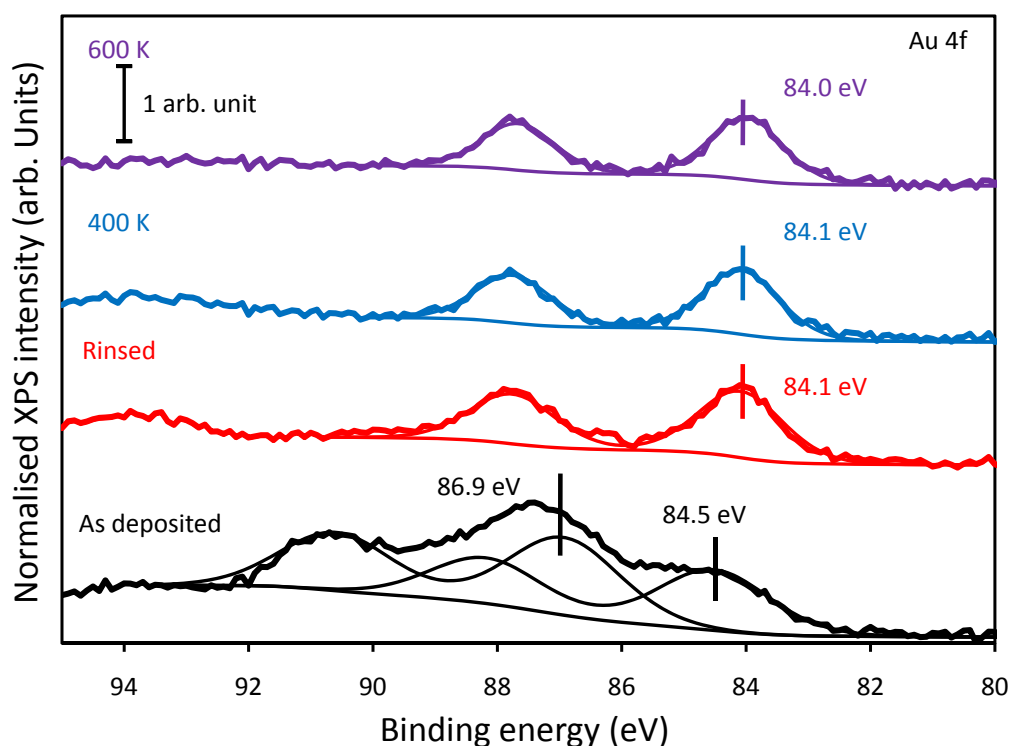
Figure 4.36: Au 4f XPS spectra showing the reduction of gold, that has been deposited from 2.5 mM AuCl$_3$ solution at pH 10 using the STM cell, after rinsing the surface with water and annealing. The background of the film before deposition has been subtracted from this spectrum.

In order to determine whether or not the reduction upon rinsing was due to respeciation on the surface, another sample was prepared and then rinsed using a freshly prepared pH 10 NaOH solution. As for water, this completely removed all chlorine from the surface (Figure 4.38). This also had the same effect on the deposited gold, reducing it as for water (Figure 4.39). This is in contrast to what was observed for palladium, where rinsing a blank solution did not result in the palladium being reduced. This difference is probably related to the relative stabilities of oxidised gold and palladium. Using STM it can be seen that after annealing to 600 K, the smaller 6-10 nm particles are still retained (Figure 4.40 (a) and (b)). This sample was also annealed to 800 K to see if this would have any further effect on particle size. No effect was observed in the XPS spectra and upon annealing to 800 K some larger particles appeared, but the smaller particles in the 6-10 nm range were still present (Figure 4.40 (c) and (d)).

Reducing the concentration of the gold precursor solution from 5 mM to 2.5 mM reduced the gold loading on the surface and resulted in more dispersed, smaller gold particles. These particles were still too large, so attempts were made to reduce the gold loading further.
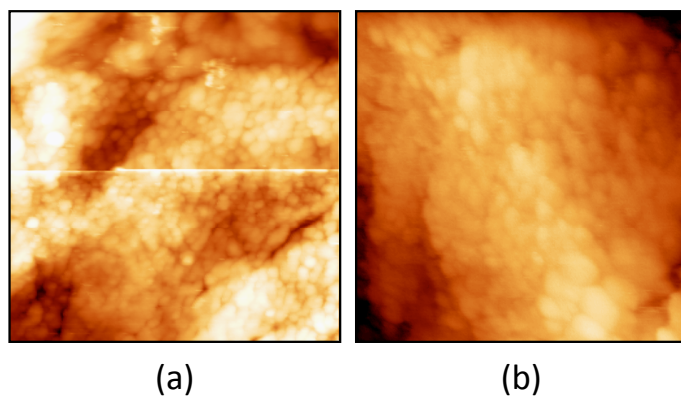
Figure 4.37: STM images of an Fe_3O_4 surface after deposition of gold at pH 10 from a 2.5mM $AuCl_3$ solution after rinsing the sample with water ((a) and (b)), then annealing to 400 K ((c) and (d)) and annealing to 600 K ((e) and (f)). All images were taken with a bias of -0.3 V and a tunnelling current of 0.1 nA. Images (a), (c) and (e) are 200×200 nm^2 and images (b), (d) and (f) are 100×100 nm^2.

Figure 4.38: Cl 2p XPS spectra showing the chlorine peak after deposition from 2.5 mM $AuCl_3$ solution at pH 10 using the STM cell after rinsing the surface with pH 10 NaOH solution.

Figure 4.39: Au 4f XPS spectra showing the reduction of gold that has been deposited from 2.5 mM $AuCl_3$ solution at pH 10 using the STM cell after rinsing the surface with pH 10 NaOH solution and annealing. The background of the film before deposition has been subtracted from this spectrum.
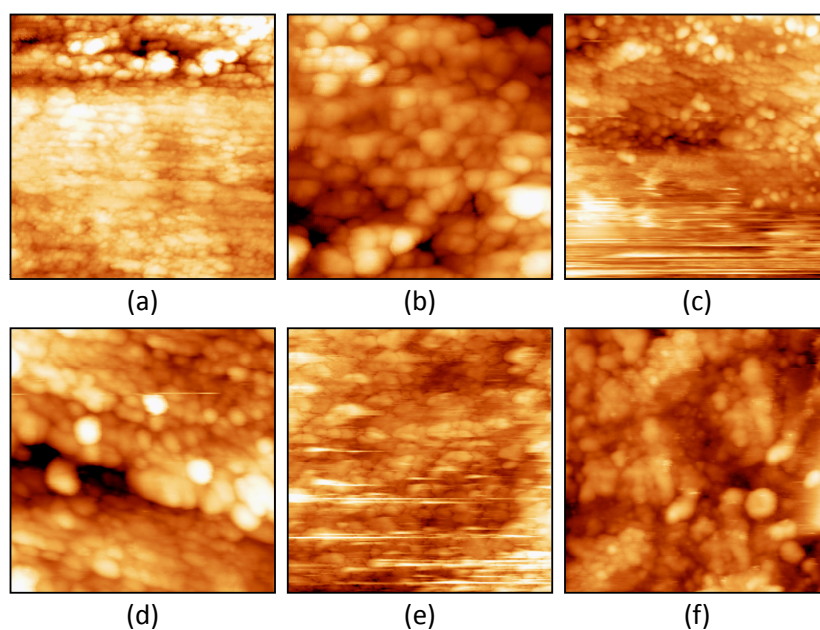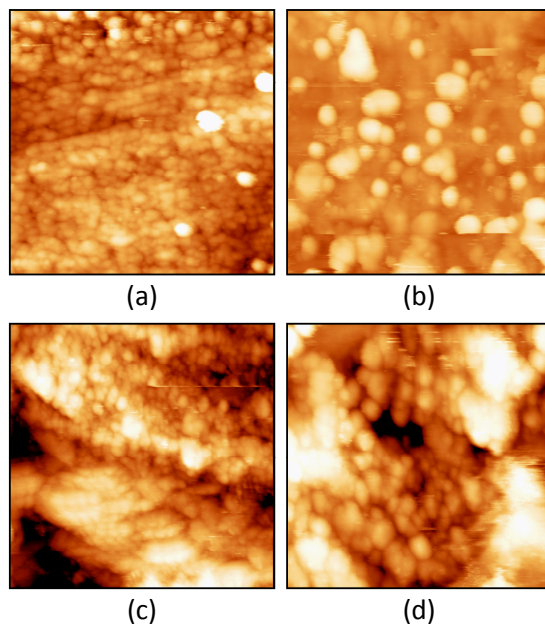

Figure 4.40: STM images of an Fe_3O_4 surface after deposition of gold at pH 10 from a 2.5mM $AuCl_3$ solution after rinsing the sample with pH 10 NaOH, then annealing to 600 K ((a) and (b)) and annealing to 800 K ((c) and (d)). All images were taken with a bias of -0.3 V and a tunnelling current of 0.1 nA. Images (a) and (c) are 200×200 nm^2 and images (b) and (d) are 100×100 nm^2.

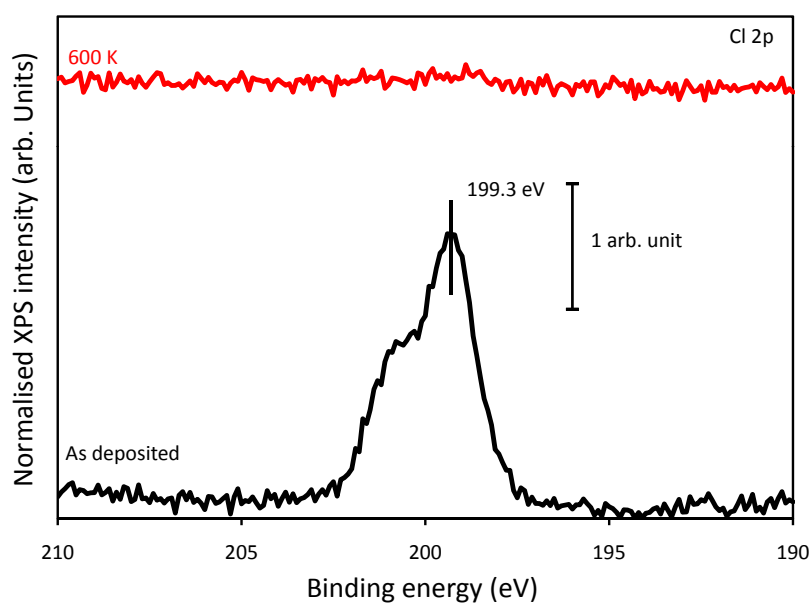Figure 4.41: Au 4f XPS spectra showing the reduction of gold, that has been deposited from 1 mM AuCl$_3$ solution at pH 10 using the STM cell upon annealing. The background of the film before deposition has been subtracted from this spectrum.
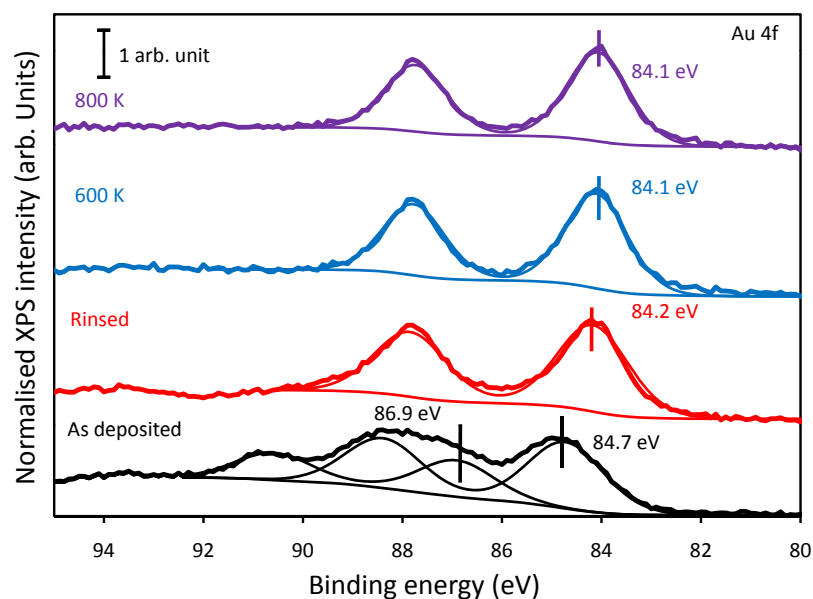

Figure 4.42: Au 4f XPS spectra showing the reduction of gold, that has been deposited from 1 mM AuCl$_3$ solution at pH 10 using the STM cell, after rinsing the surface with water and annealing. The background of the film before deposition has been subtracted from this spectrum.
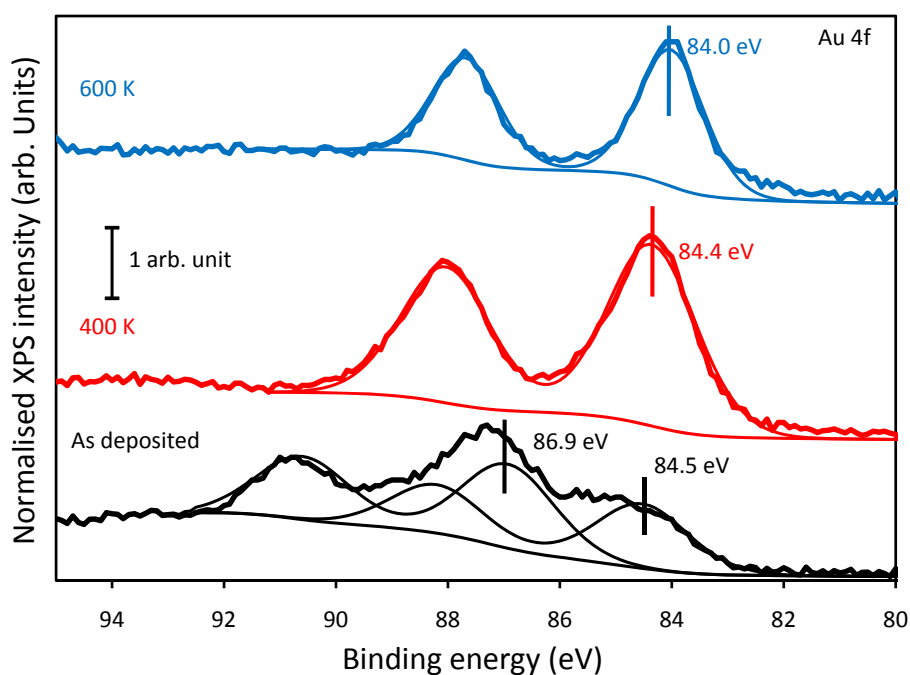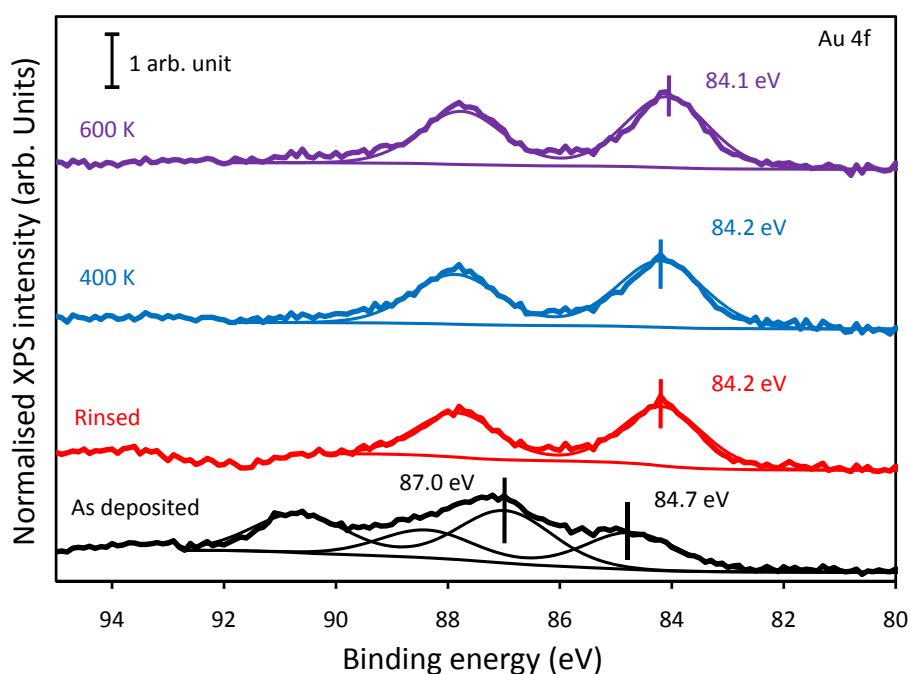
4.3.4   1 mM gold deposition

In order to gain more information about the nucleation and distribution of gold particles and reduce their size, an attempt was made to deposit less gold on to the surface in order to be able to still see the substrate after gold deposition. To this end a less concentrated 1 mM precursor solution at pH 10 was used and it was only contacted to the surface for 5 minutes, instead of the 60 minutes used in previous experiments. The Au 4f spectra obtained for a sample that was not rinsed (Figure 4.41) and a sample that was rinsed using water (Figure 4.42) seemed very similar to that obtained from a one hour deposition using 2.5 mM precursor solution.

Figure 4.43: Cl 2p XPS spectra showing the chlorine peak after deposition from 1 mM AuCl$_3$ solution at pH 10 using the STM cell and after annealing.

As for previous experiments, chlorine could not be removed from the surface by annealing to 600 K(Figure 4.43), but rinsing removed all measurable traces of chlorine (Figure 4.44).

On the basis of the XPS measurements alone it was difficult to say that less gold had been deposited than when using 2.5 mM solution. In fact, the peak area distributions of the Au 4f peak immediately after deposition overlap perfectly. STM measurements showed patches of bare substrate (See figure 4.45 (b) and 4.46 (a)), which had not been previously observed in experiments conducted using 5 mM and 2.5 mM precursor solutions, suggesting that the amount of gold deposited had in fact been reduced. This suggests that the Au 4f peak area may not be the best method for determining gold coverage for this system, likely due to the effect of screening from varying amounts of contamination.

For the sample which had not been rinsed, the particles on the surface seemed to congregate into large collections of smaller particles after annealing to 400 K (Figure 4.45 (a), (b) and (c)). Bare parts of the substrate could also be clearly observed. Upon annealing to 600 K, some much larger particles formed on the surface (Figure 4.45 (d), (e) and (f)), even as large as 100
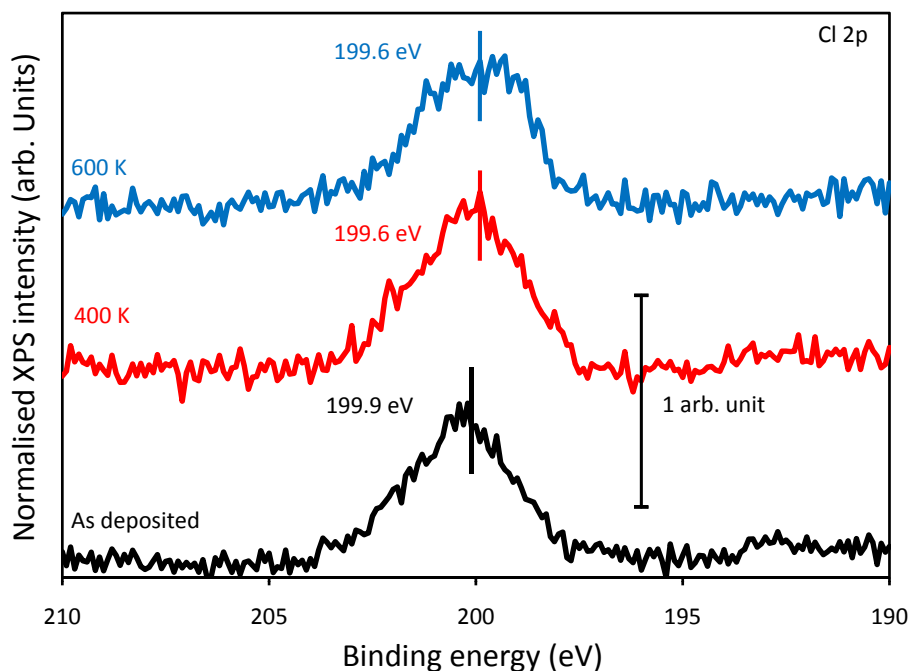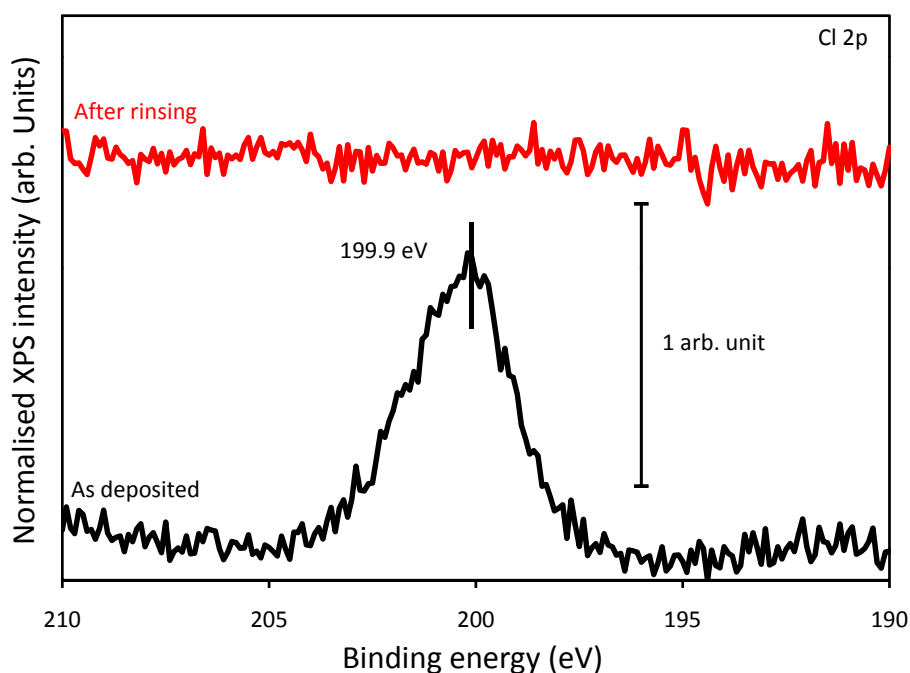
Figure 4.44: Cl 2p XPS spectra showing the chlorine peak after deposition from 1 mM AuCl$_3$ solution at pH 10 using the STM cell and after rinsing the surface with water.
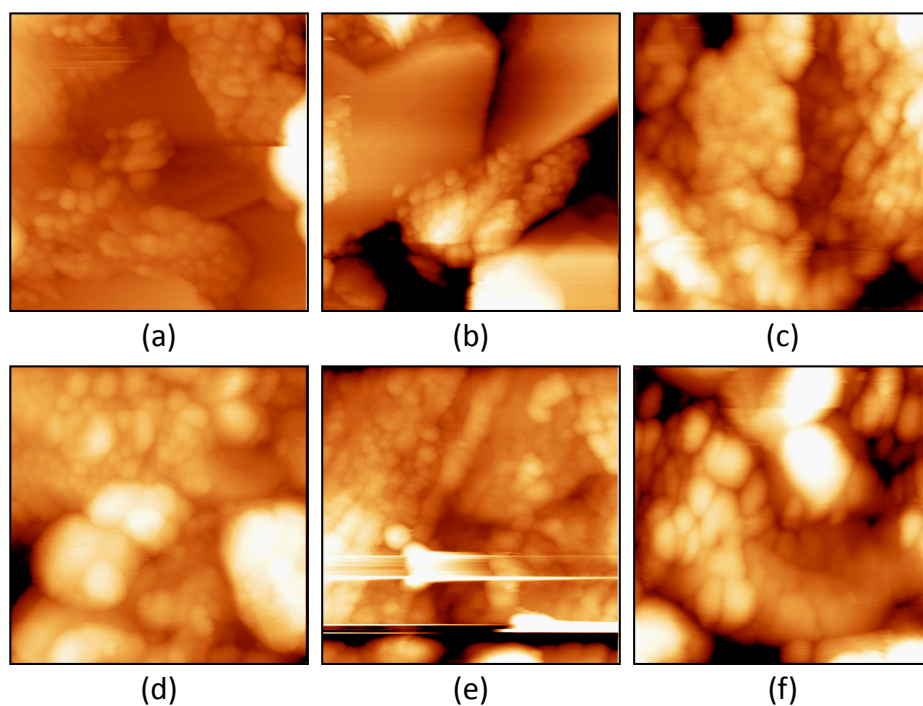
Figure 4.45: STM images of an Fe$_3$O$_4$ surface after deposition of gold at pH 10 from a 1 mM AuCl$_3$ solution after annealing to 400 K ((a), (b) and (c)) and after annealing to 600 K ((d), (e) and (f)). All images were taken with a bias of -0.3 V and a tunnelling current of 0.1 nA. Images (a), (b), (d) and (e) are 200×200 nm^2 and images (c) and (f) are 100×100 nm^2.
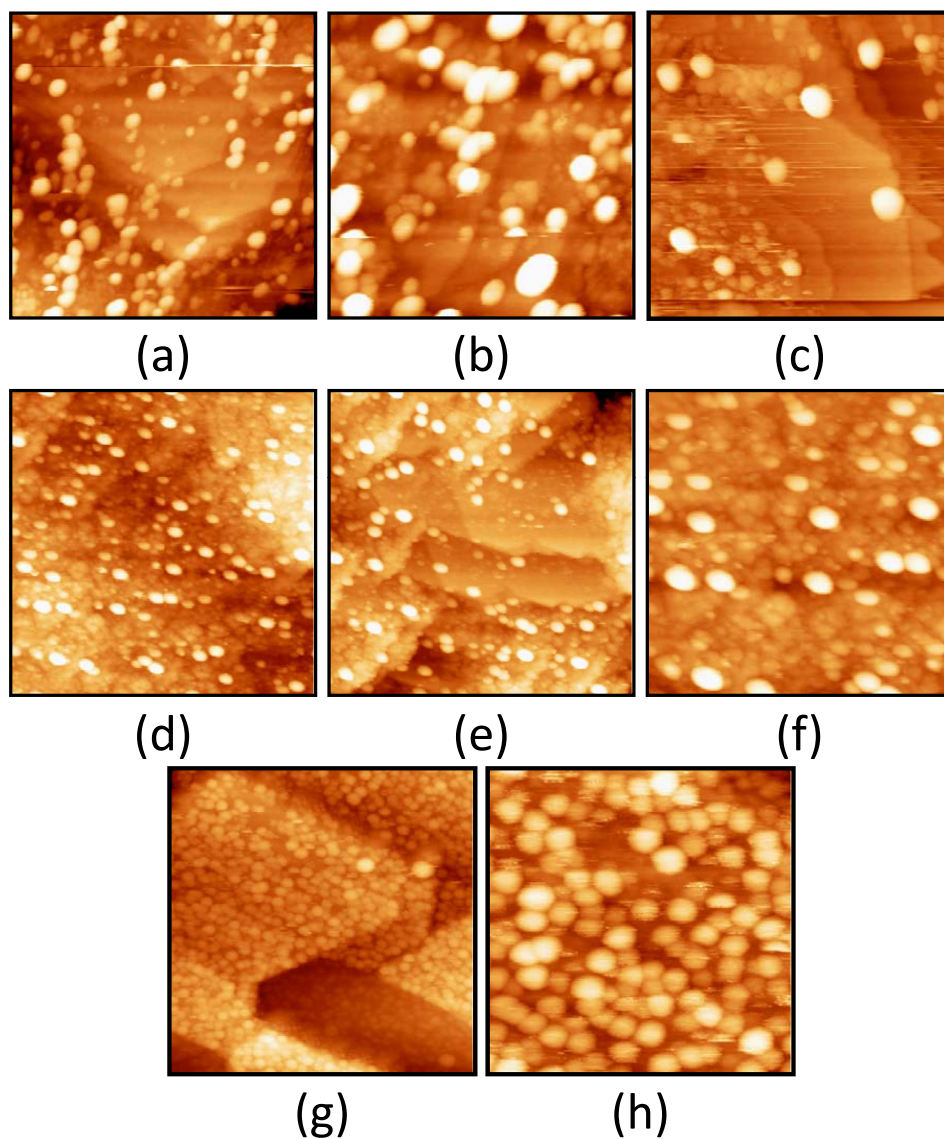
Figure 4.46: STM images of an Fe_3O_4 surface after deposition of gold at pH 10 from a 1 mM $AuCl_3$ solution after rinsing the surface with water, then annealing to 400 K ((a) and (b)) and annealing to 600 K ((d), (e) and (f)). For comparison there are also images of gold deposited using PVD on to a different sample after annealing to 400 K (c) and 600 K ((g) and (h)). All images were taken with a bias of -0.3 V and a tunnelling current of 0.1 nA. Images (a), (d) and (e) are 200×200 nm^2, images (c) and (g) are 150×150 nm^2, images (b) and (f) are 100×100 nm^2 and image (h) is 50×50 nm^2.

nm (Figure 4.45 (d)).

The surface of the rinsed sample has a very different morphology (Figure 4.46). The particles seem to be spread homogeneously over the surface, with no particular preference for step edges. Their distribution seems more uniform and the particle size is much smaller, with particles ranging in size from 4-10 nm, even after annealing to 600 K. This preparation procedure finally led to small, well dispersed gold particles on the $Fe_3O_4(111)/Pt(111)$ surface. After annealing the particles obtained compare favourably with results from depositing a similar amount of gold using PVD (cf. figure 4.46 (a) and (b) with (c) and (d), (e) and (f) with (g) and (h)). The particles obtained were also quite similar to what has been previously observed from gold particles deposited using PVD on $Fe_3O_4(111)/Pt(111)$ under UHV conditions [132].

This demonstrates that gold particles similar to those that are observed from UHV experiments using PVD can be obtained using wet chemical methods on the same substrate. After rinsing and annealing the samples prepared using wet chemical methods, the XPS spectra and STM images obtained are nearly indistinguishable, although the particle distributions obtained under UHV conditions are more uniform.

4.3.5 Discussion

Throughout the various liquid depositions, there is some small variation in the binding energy of the individual Au 4f peaks and the relative intensity of these peaks. There does not seem to be any discernible reason for this as it does not correlate with any measured quantity, such as the intensity of the Cl 2p XPS peak. This may relate to the difficulty of creating exactly the same deposition conditions every time when conducting experiments under ambient conditions or be due to the precursor in solution being reduced by ambient light or at the surface. Conducting these experiments under a more controlled environment such as a glove box and cutting off all sources of light may help to remove these irregularities.

By and large however, this did not appear to materially affect the experimental outcomes, as can be assessed from consideration of the following: All samples seem to be completely reduced to metallic gold after annealing to 600 K, with the major differences between size and conglomeration on the surface being explained by residual chlorine and the amount of gold on the surface. While the chemical state of the gold seems to be the same in each case, the presence of chlorine makes a significant difference to the final particle size, which has been shown to have an adverse effect on any catalytic activity [103].

Further experiments are required to determine whether or not the deposited gold particles are catalytically active and to see if smaller particle sizes can be achieved by using even lower gold loading than is obtained from 1 mM $AuCl_3$ solutions.

Chlorine has previously been found to be detrimental to retaining small particle sizes, both on TiO_2 [120] and Fe_2O_3 [124]. This increase in particle size ultimately decreases the activity of the catalyst. The undesirable nature of chlorine is a large part of the reason why impregnation has fallen out of favour as a preparation method for supported gold particles on metal oxides as large amounts of chlorine are present after deposition due to the speciation of the precursor solution at low pH. This chlorine can only be removed by extensive rinsing which can reduce the amount of gold deposited upon the surface, resulting in expensive catalyst precursor material

being wasted.

This is also in clear agreement with the results presented here, where the presence of chlorine was shown to be a major factor in determining the final particle size. Although the small amount of chlorine present at these higher pH values was trivial to remove, a significant amount of gold was lost during the rinsing process.

The aggregation and larger particles formed on TiO_2 deposited at low pH were previously attributed to two possible factors, the presence of chlorine hindering the formation of Au-O-Ti bonds by blocking potential grafting sites or the weaker electrostatic bonding of the precursor complexes during impregnation [120]. It seems to be confirmed that the presence of chlorine is the major factor accounting for this difference on Fe_3O_4, as in this work the deposition conditions were identical and it was only the rinsing away of chlorine before annealing that can be held accountable for the improved dispersion. Similar experiments would be required on TiO_2 to confirm that the same effects are responsible, but there seems to be no reason why the mechanisms should be drastically different.

It may be worthwhile to further investigate the low pH deposition of gold on Fe_3O_4 with the effects of the platinum crystal removed and using water to remove the chlorine, but the results using palladium (See section 4.2) and previous studies on gold suggest [3, 133] that this is not a fruitful path for efficiently producing dispersed metal particles.

In order to explain the chemical state of deposited gold, the binding energies observed should be compared to the bulk Au 4f binding energies of oxidised gold species, which are in the range of 85-87 eV [134, 135, 136]. The binding energies observed in the present work fall within this range and are assigned as adsorbed precursors (87 eV) and partially oxidised gold (< 87 eV). The low binding energy shoulder (84.5-84.9 eV) from the freshly deposited samples likely includes small particles of metallic gold. Similar shifts from the ideal value for metallic gold of 84.0 eV have been seen with small nanoparticles of gold on TiO_2 previously, where shifts of up to 1 eV were observed purely related to the size of the nanoparticles [136].

This suggests that gold is initially deposited as $Au(OH)_3$, which should be the majority species in solution, along with some metallic gold which likely arises from decomposition of the precursor by light or at the surface. Upon annealing, in a manner similar to what was observed for palladium, the gold is reduced thermally through some partially oxidised species until it finally arrives at metallic gold by 600 K. This is similar to mechanisms which have been proposed for gold deposited on titania and calcined in oxygen containing environments [98].

Thoroughly rinsing the surface with water produces Au 4f peaks at the same binding energy as annealing an unrinsed sample to 600 K, suggesting that this process also leads to metallic gold. This process does not appear to be pH dependent, as rinsing with pH 10 NaOH solution produced the same effect.

In comparison to Haruta's effort to study this deposition method on a single-crystalline substrate [122], the method used in this work has resulted in a higher level of dispersion. In Haruta's work the gold particles formed were aligned along straight lines, likely related to step edges caused by fracturing the single crystal. In contrast the preparation in this work resulted in homogeneously distributed small particles over the entire Fe_3O_4 surface. This is likely due to the increased roughness on the iron oxide surface after exposing it to water [92], which could act

to anchor the precursors more strongly and hence lead to higher dispersion after post deposition treatment steps such as annealing.

Ultimately, after rinsing and annealing, the differences between gold particles prepared using PVD and the wet chemical methods described in this work are negligible. Chlorine has a marked effect on the particle size and distribution, but this could be completely removed by rinsing the surface with water. After annealing this leads to dispersed, metallic gold particles, depending on the coverage.

Chapter 5

Conclusions

This work pursued two primary goals, the development of techniques for the in-situ investigation of processes relevant to catalyst preparation which occur at the solid-liquid interface and the use of existing surface science techniques and an experimental setup from which the samples could be introduced into liquid environments to make ex-situ measurements after each preparation step to gain initial insight into these processes.

In order to test the limits of previously constructed equipment under liquid conditions, testing was conducted using an existing electrochemical STM to image MgPc as a model molecule. Individual molecules were imaged successfully both in-situ and ex-situ on an Au(111) single crystal and ex-situ on an FeO(111)/Pt(111) thin film. On the Au(111) surface the MgPc molecules were found to lie within the troughs of the herringbone reconstruction of this surface. On the oxide surface the ex-situ measurements demonstrated that the solvent used has an effect on the distribution of the particles on the surface. This work demonstrated that molecular resolution was achievable, even under in-situ conditions, using this equipment.

To increase the range of techniques available for surface science catalysis research at the solid-liquid interface, an experimental setup was designed and built to take sum frequency generation spectroscopy measurements both on samples under UHV conditions and at the solid-liquid interface. This was achieved by connecting a liquid cell to a standard UHV chamber via a transfer chamber to allow for clean transfer between UHV and liquid environments without compromising the quality of the vacuum. Initial in-situ measurements were obtained of the spectrum of a self assembled monolayer of octadecanethiol on the Au(111) surface in air, ethanol and water.

Previous work had been conducted using ex-situ surface science techniques to study the use of wet chemical methods to deposit Pd particles on $Fe_3O_4(111)/Pt(111)$, but this work set out to understand the importance of the rinsing step and its effect on Pd deposition. Rinsing with water until a steady state was reached was found to be sufficient to reduce deposited palladium species to metallic palladium in a manner similar to that which is observed when samples are annealed under UHV conditions. After this rinsing step small particles could be seen dispersed over the entire surface, confirming the previous model for homogeneous distribution of palladium from solution. Different mechanisms have been proposed for palladium deposited at low and high pH values, with the deposition at pH 1.3 proceeding through an electrostatic attraction between catalyst precursors in solution and the sample surface and the deposition at

pH 10 occurring through a grafting reaction. Rinsing with water was found to be an effective method for removing chlorine from the surface, although some palladium was lost. In all cases chlorine levels dropped below the detection limit after rinsing until a steady state was achieved, demonstrating that chlorine could be completely removed from the surface by rinsing the samples with water.

Further work was conducted using $AuCl_3$ solutions in an attempt to create well dispersed gold particles on a single-crystalline substrate using wet chemical methods and study these particles using ex-situ surface science techniques. A procedure was found for depositing such particles on an $Fe_3O_4(111)/Pt(111)$ surface. The removal of chlorine through rinsing was found to be critical to maintain dispersion, with significant aggregation observed for unrinsed samples. Gold was deposited on to the surface using a grafting type mechanism similar to that which is observed for palladium deposition on the same surface and gold deposition on TiO_2. The deposited gold species were easily reduced, either through annealing in vacuum or rinsing with water to produce well dispersed metallic gold particles similar to those which can be obtained under UHV conditions.

References

[1] Panel on New Directions in Catalytic Science and Technology. *Catalysis Looks to the Future*. National Academy Press, Washington D.C., 1992.

[2] G Ertl, H Knoezinger, F Schueth, and J Weitkamp, editors. *Handbook of Heterogeneous Catalysis*. John Wiley and Sons, Inc., 2 edition, 1999.

[3] GR Bamwenda, S Tsubota, T Nakamura, and M Haruta. The influence of the preparation methods on the catalytic activity of platinum and gold supported on TiO2 for CO oxidation. *CATALYSIS LETTERS*, 44(1-2):83–87, 1997.

[4] G Marci, V Augugliaro, MJ Lopez-Munoz, C Martin, L Palmisano, V Rives, M Schiavello, RJD Tilley, and AM Venezia. Preparation characterization and photocatalytic activity of polycrystalline ZnO/TiO2 systems. 2. Surface, bulk characterization, and 4-nitrophenol photodegradation in liquid-solid regime. *JOURNAL OF PHYSICAL CHEMISTRY B*, 105(5):1033–1040, 2001.

[5] F Moreau and GC Bond. Gold on titania catalysts, influence of some physicochemical parameters on the activity and stability for the oxidation of carbon monoxide. *APPLIED CATALYSIS A-GENERAL*, 302(1):110–117, 2006.

[6] G Ertl. Reactions at Well-Defined Surfaces. *SURFACE SCIENCE*, 299(1-3):742–754, 1994.

[7] Thomas Risse, Shamil Shaikhutdinov, Niklas Nilius, Martin Sterrer, and Hans-Joachim Freund. Gold supported on thin oxide films: From single atoms to nanoparticles. *ACCOUNTS OF CHEMICAL RESEARCH*, 41(8):949–956, 2008.

[8] Stefania Benedetti, Philipp Myrach, Alessandro di Bona, Sergio Valeri, Niklas Nilius, and Hans-Joachim Freund. Growth and morphology of metal particles on MgO/Mo(001): A comparative STM and diffraction study. *PHYSICAL REVIEW B*, 83(12), 2011.

[9] Xiang Shao, Stefano Prada, Livia Giordano, Gianfranco Pacchioni, Niklas Nilius, and Hans-Joachim Freund. Tailoring the Shape of Metal Ad-Particles by Doping the Oxide Support. *ANGEWANDTE CHEMIE-INTERNATIONAL EDITION*, 50(48):11525–11527, 2011.

[10] PLJ Gunter, JW Niemantsverdriet, FH Ribeiro, and GA Somorjai. Surface science approach to modeling supported catalysts. *CATALYSIS REVIEWS-SCIENCE AND ENGINEERING*, 39(1-2):77–168, 1997.

[11] BC Gates. Supported metal-clusters - synthesis, structure, and catalysis. *CHEMICAL REVIEWS*, 95(3):511–522, 1995.

[12] K Hayek, R Kramer, and Z Paal. Metal-support boundary sites in catalysis. *APPLIED CATALYSIS A-GENERAL*, 162(1-2):1–15, 1997.

[13] PL Gaiboyes. Defects in oxide catalysts - fundamental-studies of catalysis in action. *CATALYSIS REVIEWS-SCIENCE AND ENGINEERING*, 34(1-2):1–54, 1992.

[14] HJ Freund, H Kuhlenbeck, and V Staemmler. Oxide surfaces. *REPORTS ON PROGRESS IN PHYSICS*, 59(3):283–347, 1996.

[15] V. Simic-Milosevic, M. Heyde, N. Nilius, T. Koenig, H. P. Rust, M. Sterrer, T. Risse, H. J. Freund, L. Giordano, and G. Pacchioni. Au dimers on thin MgO(001) films: Flat and charged or upright and neutral? *JOURNAL OF THE AMERICAN CHEMICAL SOCIETY*, 130(25):7814+, 2008.

[16] M Baumer and HJ Freund. Metal deposits on well-ordered oxide films. *PROGRESS IN SURFACE SCIENCE*, 61(7-8):127–198, 1999.

[17] CR Henry. Surface studies of supported model catalysts. *SURFACE SCIENCE REPORTS*, 31(7-8):235–325, 1998.

[18] LW Covert and H Adkins. Nickel by the Raney process as a catalyst of hydrogenation. *JOURNAL OF THE AMERICAN CHEMICAL SOCIETY*, 54:4116–4117, 1932.

[19] O. Beeck. Hydrogenation catalysts. *Discussions of the Faraday Society*, 8:118–127, 1950.

[20] Radoslaw Wlodarczyk, Marek Sierka, Karolina Kwapien, Joachim Sauer, Esther Carrasco, Andreas Aumer, Janaina F. Gomes, Martin Sterrer, and Hans-Joachim Freund. Structures of the Ordered Water Monolayer on MgO(001). *JOURNAL OF PHYSICAL CHEMISTRY C*, 115(14):6764–6774, 2011.

[21] Guenther Rupprechter. Sum Frequency Generation and Polarization-Modulation Infrared Reflection Absorption Spectroscopy of Functioning Model Catalysts from Ultrahigh Vacuum to Ambient Pressure. In Gates, BC and Knozinger, H, editor, *ADVANCES IN CATALYSIS, VOL 51*, volume 51 of *Advances in Catalysis*, pages 133–263. ELSEVIER ACADEMIC PRESS INC, 2007.

[22] PS Cremer, XC Su, YR Shen, and GA Somorjai. Ethylene hydrogenation on Pt(111) monitored in situ at high pressures using sum frequency generation. *JOURNAL OF THE AMERICAN CHEMICAL SOCIETY*, 118(12):2942–2949, 1996.

[23] Esther Carrasco, Andreas Aumer, Matthew A. Brown, Rhys Dowler, Irene Palacio, Sundal Song, and Martin Sterrer. Infrared spectra of high coverage CO adsorption structures on Pt(111). *SURFACE SCIENCE*, 604(15-16):1320–1325, 2010.

[24] Joost Frenken and Bas Hendriksen. The reactor-STM: A real-space probe for Operando nanocatalysis. *MRS BULLETIN*, 32(12):1015–1021, 2007.

[25] BLM Hendriksen, SC Bobaru, and JWM Frenken. Oscillatory CO oxidation on Pd(100) studied with in situ scanning tunneling microscopy. *SURFACE SCIENCE*, 552(1-3):229–242, 2004.

[26] GA Somorjai. New model catalysts (platinum nanoparticles) and new techniques (SFG and STM) for studies of reaction intermediates and surface restructuring at high pressures during catalytic reactions. *APPLIED SURFACE SCIENCE*, 121:1–19, 1997.

[27] O Lev, FR Fan, and AJ Bard. The application of scanning tunneling microscopy to insitu studies of nickel electrodes under potential control. *JOURNAL OF THE ELECTROCHEMICAL SOCIETY*, 135(3):783–784, 1988.

[28] Hendrik Bluhm, Michael Haevecker, Axel Knop-Gericke, Maya Kiskinova, Robert Schloegl, and Miquel Salmeron. In situ x-ray photoelectron spectroscopy studies of gas-solid interfaces at near-ambient conditions. *MRS BULLETIN*, 32(12):1022–1030, 2007.

[29] Knud Gentz and Klaus Wandelt. Electrochemical Scanning Tunneling Microscopy. *CHIMIA*, 66(1-2):44–51, 2012.

[30] Thanh Hai Phan and Klaus Wandelt. Molecular Self-Assembly at Metal-Electrolyte Interfaces. *INTERNATIONAL JOURNAL OF MOLECULAR SCIENCES*, 14(3):4498–4524, 2013.

[31] H Unterhalt, G Rupprechter, and HJ Freund. Vibrational sum frequency spectroscopy on Pd(111) and supported Pd nanoparticles: CO adsorption from ultrahigh vacuum to atmospheric pressure. *JOURNAL OF PHYSICAL CHEMISTRY B*, 106(2):356–367, 2002.

[32] T Dellwig, J Hartmann, J Libuda, I Meusel, G Rupprechter, H Unterhalt, and HJ Freund. Complex model catalysts under UHV and high pressure conditions: CO adsorption and oxidation on alumina-supported Pd particles. *JOURNAL OF MOLECULAR CATALYSIS A-CHEMICAL*, 162(1-2):51–66, 2000.

[33] Huang Zhi and Guo Yuan. Sum Frequency Generation Vibrational Spectroscopy Study of Serial Short Chain Fatty Acids Liquid/Air Interfaces. *CHEMICAL JOURNAL OF CHINESE UNIVERSITIES-CHINESE*, 33(6):1271–1277, 2012.

[34] Takashi Iwahashi, Yasunari Sakai, Kaname Kanai, Doseok Kim, and Yukio Ouchi. Alkyl-chain dividing layer at an alcohol/ionic liquid buried interface studied by sum-frequency generation vibrational spectroscopy. *PHYSICAL CHEMISTRY CHEMICAL PHYSICS*, 12(40):12943–12946, 2010.

[35] S Roke, AW Kleyn, and M Bonn. Femtosecond sum frequency generation at the metal-liquid interface. *SURFACE SCIENCE*, 593(1-3):79–88, 2005.

[36] M. Heinen, Y. X. Chen, Z. Jusys, and R. J. Behm. In situ ATR-FTIRS coupled with on-line DEMS under controlled mass transport conditions - A novel tool for electrocatalytic reaction studies. *ELECTROCHIMICA ACTA*, 52(18, SI):5634–5643, 2007.

[37] M Wilms, M Kruft, G Bermes, and K Wandelt. A new and sophisticated electrochemical scanning tunneling microscope design for the investigation of potentiodynamic processes. *REVIEW OF SCIENTIFIC INSTRUMENTS*, 70(9):3641–3650, 1999.

[38] W Weiss and M Ritter. Metal oxide heteroepitaxy: Stranski-Krastanov growth for iron oxides on Pt(111). *PHYSICAL REVIEW B*, 59(7):5201–5213, 1999.

[39] W Weiss and W Ranke. Surface chemistry and catalysis on well-defined epitaxial iron-oxide layers. *PROGRESS IN SURFACE SCIENCE*, 70(1-3):1–151, 2002.

[40] R Meyer, SK Shaikhutdinov, and HJ Freund. CO oxidation on a Pd/Fe3O4(111) model catalyst. *ZEITSCHRIFT FUR PHYSIKALISCHE CHEMIE-INTERNATIONAL JOURNAL OF RESEARCH IN PHYSICAL CHEMISTRY & CHEMICAL PHYSICS*, 218(8):905–914, 2004.

[41] A. Sala, H. Marchetto, Z. H. Qin, S. Shaikhutdinov, Th Schmidt, and H. J. Freund. Defects and inhomogeneities in Fe3O4(111) thin film growth on Pt(111). *PHYSICAL REVIEW B*, 86(15), 2012.

[42] M Ritter, W Ranke, and W Weiss. Growth and structure of ultrathin FeO films on Pt(111) studied by STM and LEED. *PHYSICAL REVIEW B*, 57(12):7240–7251, 1998.

[43] Hui-Feng Wang, William E. Kaden, Rhys Dowler, Martin Sterrer, and Hans-Joachim Freund. Model oxide-supported metal catalysts - comparison of ultrahigh vacuum and solution based preparation of Pd nanoparticles on a single-crystalline oxide substrate. *PHYSICAL CHEMISTRY CHEMICAL PHYSICS*, 14(32):11525–11533, 2012.

[44] T Schalow, B Brandt, DE Starr, M Laurin, S Schauermann, SK Shaikhutdinov, J Libuda, and HJ Freund. Oxygen-induced restructuring of a Pd/Fe3O4 model catalyst. *CATALYSIS LETTERS*, 107(3-4):189–196, 2006.

[45] Y. N. Sun, Z. H. Qin, M. Lewandowski, S. Shaikhutdinov, and H. J. Freund. CO adsorption and dissociation on iron oxide supported Pt particles. *SURFACE SCIENCE*, 603(20):3099–3103, 2009.

[46] SK Shaikhutdinov, M Ritter, XG Wang, H Over, and W Weiss. Defect structures on epitaxial Fe3O4(111) films. *PHYSICAL REVIEW B*, 60(15):11062–11069, 1999.

[47] K Okada and A Kotani. Theory of core-level x-ray photoemission and photoabsorption in Ti compounds. *JOURNAL OF ELECTRON SPECTROSCOPY AND RELATED PHENOMENA*, 62(1-2):131–140, 1993.

[48] J Moulder, W Stickle, P Sobol, and K Bomben. *Handbook of X-ray Photoelectron Spectroscopy*. Perkin-Elmer Corporation, 1992.

[49] WJ Carter, GK Schweitzer, and TA Carlson. Experimental evaluation of a simple model for quantitative-analysis in x-ray photoelectron-spectroscopy. *JOURNAL OF ELECTRON SPECTROSCOPY AND RELATED PHENOMENA*, 5(NOV-D):827–835, 1974.

[50] M.P. Seah and W.A. Dench. Quantitative electron spectroscopy of surfaces: a standard data base for electron inelastic mean free paths in solids. *Surface and Interface Analysis*, 1:2–11, 1979.

[51] Wei Ping Zhou, Adam Lewera, Robert Larsen, Rich I. Masel, Paul S. Bagus, and Andrzej Wieckowski. Size effects in electronic and catalytic properties of unsupported palladium nanoparticles in electrooxidation of formic acid. *JOURNAL OF PHYSICAL CHEMISTRY B*, 110(27):13393–13398, 2006.

[52] B Richter, H Kuhlenbeck, HJ Freund, and PS Bagus. Cluster core-level binding-energy shifts: The role of lattice strain. *PHYSICAL REVIEW LETTERS*, 93(2), 2004.

[53] AE Hughes and CC Phillips. An experimental and theoretical-study of the transmission function of a commercial hemispherical electron-energy analyzer. *SURFACE AND INTERFACE ANALYSIS*, 4(5):220–226, 1982.

[54] TH Ong, PB Davies, and CD Bain. Sum-frequency spectroscopy of monolayers of alkoxy-terminated alkanethiols in contact with liquids. *LANGMUIR*, 9(7):1836–1845, 1993.

[55] AG Lambert, PB Davies, and DJ Neivandt. Implementing the theory of sum frequency generation vibrational spectroscopy: A tutorial review. *APPLIED SPECTROSCOPY REVIEWS*, 40(2):103–145, 2005.

[56] R Superfine, P Guyotsionnest, JH Hunt, CT Kao, and YR Shen. Surface vibrational spectroscopy of molecular adsorbates on metals and semiconductors by infrared visible sum-frequency generation. *SURFACE SCIENCE*, 200(1):L445–L450, 1988.

[57] YR Shen. Surface-properties probed by 2nd-harmonic and sum-frequency generation. *NATURE*, 337(6207):519–525, 1989.

[58] P Guyotsionnest, JH Hunt, and YR Shen. Sum-Frequency Vibrational Spectroscopy of a Langmuir Film - Study of Molecular-Orientation of a Two-Dimensional System. *PHYSICAL REVIEW LETTERS*, 59(14):1597–1600, 1987.

[59] CD Bain. Sum-frequency vibrational spectroscopy of the solid-liquid interface. *JOURNAL OF THE CHEMICAL SOCIETY-FARADAY TRANSACTIONS*, 91(9):1281–1296, 1995.

[60] R Superfine, JY Huang, and YR Shen. Experimental-determination of the sign of molecular dipole-moment derivatives - An infrared visible sum frequency generation absolute phase measurement study. *CHEMICAL PHYSICS LETTERS*, 172(3-4):303–306, 1990.

[61] Na Ji, Victor Ostroverkhov, Chao-Yuan Chen, and Yuen-Ron Shen. Phase-sensitive sum-frequency vibrational spectroscopy and its application to studies of interfacial alkyl chains. *JOURNAL OF THE AMERICAN CHEMICAL SOCIETY*, 129(33):10056+, 2007.

[62] XD Zhu, H Suhr, and YR Shen. Surface vibrational spectroscopy by infrared-visible sum frequency generation. *PHYSICAL REVIEW B*, 35(6):3047–3050, 1987.

[63] G Binnig and H Rohrer. Scanning Tunneling Microscopy. *HELVETICA PHYSICA ACTA*, 55(6):726–735, 1982.

[64] N. Nilius, M. V. Ganduglia-Pirovano, V. Brazdova, M. Kulawik, J. Sauer, and H-J. Freund. Electronic properties and charge state of gold monomers and chains adsorbed on alumina thin films on NiAl(110). *PHYSICAL REVIEW B*, 81(4), 2010.

[65] H. Ariga, T. Taniike, H. Morikawa, R. Tero, H. Kondoh, and Y. Iwasawa. Lattice-work structure of a TiO2(001) surface studied by STM, core-level spectroscopies and DFT calculations. *CHEMICAL PHYSICS LETTERS*, 454(4-6):350–354, 2008.

[66] D Drakova. Theoretical modelling of scanning tunnelling microscopy, scanning tunnelling spectroscopy and atomic force microscopy. *REPORTS ON PROGRESS IN PHYSICS*, 64(2):205–290, 2001.

[67] J Bardeen. Tunnelling from a Many-Particle Point of View. *PHYSICAL REVIEW LETTERS*, 6(2):57–&, 1961.

[68] J Tersoff and DR Hamann. Theory and application for the scanning tunneling microscope. *PHYSICAL REVIEW LETTERS*, 50(25):1998–2001, 1983.

[69] J Tersoff and DR Hamann. Theory of the scanning tunneling microscope. *PHYSICAL REVIEW B*, 31(2):805–813, 1985.

[70] J Wintterlin, J Wiechers, H Brune, T Gritsch, H Hofer, and RJ Behm. Atomic-Resolution Imaging of Close-Packed Metal Surfaces by Scanning Tunneling Microscopy. *PHYSICAL REVIEW LETTERS*, 62(1):59–62, 1989.

[71] Francisco Zaera. Surface chemistry at the liquid/solid interface. *SURFACE SCIENCE*, 605(13-14):1141–1145, 2011.

[72] Francisco Zaera. Probing Liquid/Solid Interfaces at the Molecular Level. *CHEMICAL REVIEWS*, 112(5):2920–2986, 2012.

[73] Y Shingaya, H Matsumoto, H Ogasawara, and M Ito. In-situ and ex-situ IRAS, LEED and EC-STM studies of underpotentially deposited copper on a Pt(111) electrode in sulfuric-acid-solution - Coadsorption of sulfate ion with copper. *SURFACE SCIENCE*, 335(1-3):23–31, 1995.

[74] Y Gonzalez-Garcia, GT Burstein, S Gonzalez, and RM Souto. Imaging metastable pits on austenitic stainless steel in situ at the open-circuit corrosion potential. *ELECTROCHEMISTRY COMMUNICATIONS*, 6(7):637–642, 2004.

[75] A Bewick, K Kunimatsu, and BS Pons. Infrared-spectroscopy of the electrode-electrolyte interphase. *ELECTROCHIMICA ACTA*, 25(4):465–468, 1980.

[76] Paul Fenter and Neil C. Sturchio. Mineral-water interfacial structures revealed by synchrotron X-ray scattering. *PROGRESS IN SURFACE SCIENCE*, 77(5-8):171–258, 2004.

[77] F Ohnesorge and G Binnig. True atomic-resolution by atomic force microscopy through repulsive and attractive forces. *SCIENCE*, 260(5113):1451–1456, 1993.

[78] J Clavilier, R Faure, G Guinet, and R Durand. Preparation of mono-crystalline Pt microelectrodes and electrochemical study of the plane surfaces cut in the direction of the (111) and (110) plants. *JOURNAL OF ELECTROANALYTICAL CHEMISTRY*, 107(1):205–209, 1980.

[79] JS Hammond and N Winograd. XPS Spectroscopy study of potentiostatic and galvanostatic oxidation of Pt electrodes in H2SO4 and HClO4. *JOURNAL OF ELECTROANALYTICAL CHEMISTRY*, 78(1):55–69, 1977.

[80] D Aberdam, R Durand, R Faure, and F Elomar. Structural-changes of a Pt(111) electrode induced by electrosorption of oxygen in acidic solutions - A coupled voltammetry, LEED and AES study. *SURFACE SCIENCE*, 171(2):303–330, 1986.

[81] SG Sun, DF Yang, SJ Wu, J Ociepa, and J Lipkowski. Electrochemical, auger-electron spectroscopy and low-energy-electron diffraction studies of the stability of the Au(210) electrode surface in the presence of adsorbed pyridine. *JOURNAL OF ELECTROANALYTICAL CHEMISTRY*, 349(1-2):211–222, 1993.

[82] K Brandt, E Vogler, M Parthenopoulos, and K Wandelt. In situ and ex situ FTIR characterization of a cyanate adlayer on Cu(111). *JOURNAL OF ELECTROANALYTICAL CHEMISTRY*, 570(1):47–53, 2004.

[83] M Lennartz, M Arenz, C Stuhlmann, and K Wandelt. Cyanide adlayers on Pt(111) in chloride containing electrolytes studied by in situ, ex situ IRAS and LEED. *SURFACE SCIENCE*, 461(1-3):98–106, 2000.

[84] Davide Ferri and Alfons Baiker. Advances in Infrared Spectroscopy of Catalytic Solid-Liquid Interfaces: The Case of Selective Alcohol Oxidation. *TOPICS IN CATALYSIS*, 52(10):1323–1333, 2009.

[85] Bas Hulsken, Richard Van Hameren, Jan W. Gerritsen, Tony Khoury, Pall Thordarson, Maxwell J. Crossley, Alan E. Rowan, Roeland J. M. Nolte, Johannes A. A. W. Elemans, and Sylvia Speller. Real-time single-molecule imaging of oxidation catalysis at a liquid-solid interface. *NATURE NANOTECHNOLOGY*, 2(5):285–289, 2007.

[86] Changyong Park, P.A. Fenter, N.C. Sturchio, and J.R. Regalbuto. Probing outer-sphere adsorption of aqueous metal complexes at the oxide-water interface with resonant anomalous X-ray reflectivity. *Physical Review Letters*, 94:076104/1–4, 2005.

[87] Hui-Feng Wang, Hiroko Ariga, Rhys Dowler, Martin Sterrer, and Hans-Joachim Freund. Surface science approach to catalyst preparation - Pd deposition onto thin Fe3O4(111) films from PdCl2 precursor. *JOURNAL OF CATALYSIS*, 286:1–5, 2012.

[88] Y. H. Jiang, W. D. Xiao, L. W. Liu, L. Z. Zhang, J. C. Lian, K. Yang, S. X. Du, and H. J. Gao. Self-Assembly of Metal Phthalocyanines on Pb(111) and Au(111) Surfaces at Submonolayer Coverage. *JOURNAL OF PHYSICAL CHEMISTRY C*, 115(44):21750–21754, 2011.

[89] Xiao Lin and Niklas Nilius. Self-assembly of MgPc molecules on polar FeO thin films. *JOURNAL OF PHYSICAL CHEMISTRY C*, 112(39):15325–15328, 2008.

[90] S Narasimhan and D Vanderbilt. Elastic stress domains and the herringbone reconstruction on Au(111). *PHYSICAL REVIEW LETTERS*, 69(10):1564–1567, 1992.

[91] W Mizutani, A Ohi, M Motomatsu, and H Tokumoto. Field evaporation of gold by scanning-tunneling-microscopy. *APPLIED SURFACE SCIENCE*, 87-8(1-4):398–404, 1995.

[92] Franziska Ringleb, Yuichi Fujimori, Hui-Feng Wang, Hiroko Ariga, Esther Carrasco, Martin Sterrer, Hans-Joachim Freund, Livia Giordano, Gianfranco Pacchioni, and Jacek Goniakowski. Interaction of Water with FeO(111)/Pt(111): Environmental Effects and Influence of Oxygen. *JOURNAL OF PHYSICAL CHEMISTRY C*, 115(39):19328–19335, 2011.

[93] J Kubota, Z Ma, and F Zaera. In situ characterization of adsorbates in solid-liquid interfaces by reflection-absorption infrared spectroscopy. *LANGMUIR*, 19(8):3371–3376, 2003.

[94] Frank Hoebel. *Pd und Au Nanoteilchen auf verschiedenen Oxidtraegern - Stabilitaet und CO-Adsorptionseigenschaften.* PhD thesis, Technical University Berlin, 2008.

[95] T. Schalow, B. Brandt, D. E. Starr, M. Laurin, S. K. Shaikhutdinov, S. Schauermann, J. Libuda, and H. J. Freund. Particle size dependent adsorption and reaction kinetics on reduced and partially oxidized Pd nanoparticles. *PHYSICAL CHEMISTRY CHEMICAL PHYSICS*, 9(11):1347–1361, 2007.

[96] K Wolter, O Seiferth, H Kuhlenbeck, M Baumer, and HJ Freund. Infrared spectroscopic investigation of CO adsorbed on Pd aggregates deposited on an alumina model support. *SURFACE SCIENCE*, 399(2-3):190–198, 1998.

[97] F Moreau, GC Bond, and AO Taylor. Gold on titania catalysts for the oxidation of carbon monoxide: control of pH during preparation with various gold contents. *JOURNAL OF CATALYSIS*, 231(1):105–114, 2005.

[98] ED Park and JS Lee. Effects of pretreatment conditions on CO oxidation over supported Au catalysts. *JOURNAL OF CATALYSIS*, 186(1):1–11, 1999.

[99] CT Campbell. Ultrathin metal films and particles on oxide surfaces: Structural, electronic and chemisorptive properties. *SURFACE SCIENCE REPORTS*, 27(1-3):1–111, 1997.

[100] G Ertl, H Knoezinger, and J Weitkamp, editors. *Handbook of Heterogeneous Catalysis*, volume 1. VCH Weinheim, 1 edition, 1997.

[101] G Deroos, JM Fluit, Lam Hermans, and JW Geus. Investigation of the interaction of precipitation nickel(II) hydroxide with silica surfaces by rutherford back scattering (RBS). *ZEITSCHRIFT FUR ANORGANISCHE UND ALLGEMEINE CHEMIE*, 449:115–126, 1979.

[102] J Regalbuto, editor. *Catalyst preparation: Science and engineering.* CRC Press, 2007.

[103] M Haruta. Size- and support-dependency in the catalysis of gold. *CATALYSIS TODAY*, 36(1):153–166, 1997.

[104] R Zanella, L Delannoy, and C Louis. Mechanism of deposition of gold precursors onto TiO2 during the preparation by cation adsorption and deposition-precipitation with NaOH and urea. *APPLIED CATALYSIS A-GENERAL*, 291(1-2):62–72, 2005.

[105] YJ Chen and CT Yeh. Deposition of highly dispersed gold on alumina support. *JOURNAL OF CATALYSIS*, 200(1):59–68, 2001.

[106] Giovanni Agostini, Elena Groppo, Andrea Piovano, Riccardo Pellegrini, Giuseppe Leofanti, and Carlo Lamberti. Preparation of Supported Pd Catalysts: From the Pd Precursor Solution to the Deposited Pd2+ Phase. *LANGMUIR*, 26(13):11204–11211, 2010.

[107] M Haruta, S Tsubota, T Kobayashi, H Kageyama, MJ Genet, and B Delmon. Low-temperature oxidation of CO over gold supported on TiO2, alpha-Fe2O3, and Co3O4. *JOURNAL OF CATALYSIS*, 144(1):175–192, 1993.

[108] T Schalow, M Laurin, B Brandt, S Schauermann, S Guimond, H Kuhlenbeck, DE Starr, SK Shaikhutdinov, J Libuda, and HJ Freund. Oxygen storage at the metal/oxide interface of catalyst nanoparticles. *ANGEWANDTE CHEMIE-INTERNATIONAL EDITION*, 44(46):7601–7605, 2005.

[109] Markus Wilde, Katsuyuki Fukutani, Wiebke Ludwig, Bjoern Brandt, Jan-Henrik Fischer, Swetlana Schauermann, and Hans-Joachim Freund. Influence of Carbon Deposition on the Hydrogen Distribution in Pd Nanoparticles and Their Reactivity in Olefin Hydrogenation. *ANGEWANDTE CHEMIE-INTERNATIONAL EDITION*, 47(48):9289–9293, 2008.

[110] ML Toebes, JA van Dillen, and YP de Jong. Synthesis of supported palladium catalysts. *JOURNAL OF MOLECULAR CATALYSIS A-CHEMICAL*, 173(1-2):75–98, 2001.

[111] N Mahata and V Vishwanathan. Influence of palladium precursors on structural properties and phenol hydrogenation characteristics of supported palladium catalysts. *JOURNAL OF CATALYSIS*, 196(2):262–270, 2000.

[112] DO Simone, T Kennelly, NL Brungard, and RJ Farrauto. Reversible poisoning of palladium catalysts for methane oxidation. *APPLIED CATALYSIS*, 70(1):87–100, 1991.

[113] H-F Wang. *Surface Science Approach to Catalyst Preparation: Palladium Deposition onto Iron Oxide Films from the Liquid Phase*. PhD thesis, Freie Universitaet Berlin, 2012.

[114] Martin Sterrer and Hans-Joachim Freund. Towards Realistic Surface Science Models of Heterogeneous Catalysts: Influence of Support Hydroxylation and Catalyst Preparation Method. *CATALYSIS LETTERS*, 143(5):375–385, 2013.

[115] J. J. Cruywagen and R. J. Kriek. Complexation of palladium(II) with chloride and hydroxide. *JOURNAL OF COORDINATION CHEMISTRY*, 60(4):439–447, 2007.

[116] M Sakashita and N Sato. Ion selectivity of precipitate films affecting passivation and corrosion of metals. *CORROSION*, 35(8):351–355, 1979.

[117] S Shaikhutdinov, M Heemeier, J Hoffmann, I Meusel, B Richter, M Baumer, H Kuhlenbeck, J Libuda, HJ Freund, R Oldman, SD Jackson, C Konvicka, M Schmid, and P Varga. Interaction of oxygen with palladium deposited on a thin alumina film. *SURFACE SCIENCE*, 501(3):270–281, 2002.

[118] T. Schalow, B. Brandt, M. Laurin, S. Schauermann, S. Guilmond, H. Kuhlenbeck, J. Libuda, and H. J. Freund. Formation of interface and surface oxides on supported Pd nanoparticles. *SURFACE SCIENCE*, 600(12):2528–2542, 2006.

[119] Matthias Peter, Jose Manuel Flores Camacho, Serguey Adamovski, Luis K. Ono, Karl-Heinz Dostert, Casey P. O'Brien, Beatriz Roldan Cuenya, Swetlana Schauermann, and Hans-Joachim Freund. Trends in the Binding Strength of Surface Species on Nanoparticles: How Does the Adsorption Energy Scale with the Particle Size? *ANGEWANDTE CHEMIE-INTERNATIONAL EDITION*, 52(19):5175–5179, 2013.

[120] Francois Moreau and Geoffrey C. Bond. Preparation and reactivation of Au/TiO2 catalysts. *CATALYSIS TODAY*, 122(3-4):260–265, 2007.

[121] GC Bond and DT Thompson. Catalysis by gold. *CATALYSIS REVIEWS-SCIENCE AND ENGINEERING*, 41(3-4):319–388, 1999.

[122] T Akita, M Okumura, K Tanaka, and M Haruta. SEM and RHEED-REM study of au particles deposited on rutile TiO2 (110) by deposition precipitation and gas-phase grafting methods. *JOURNAL OF CATALYSIS*, 212(1):119–123, 2002.

[123] M Tschapek, C Wasowski, and RM Torressanchez. PZC and IEP of gamma-Al2O3 and TiO2. *JOURNAL OF ELECTROANALYTICAL CHEMISTRY*, 74(2):167–176, 1976.

[124] Chengming Zhang, Lequan Liu, Xinjiang Cui, Lirong Zheng, Youquan Deng, and Feng Shi. Chlorine as an Indicator in the Controllable Preparation of Active Nano-Gold Catalyst. *SCIENTIFIC REPORTS*, 3, 2013.

[125] S Tsubota, DAH Cunningham, Y Bando, and M Haruta. Preparation of nanometer gold strongly interacted with TiO2 and the structure sensitivity in low-temperature oxidation of CO. In Poncelet, G and Martens, J and Delmon, B and Jacobs, PA and Grange, P, editor, *PREPARATION OF CATALYSTS VI: SCIENTIFIC BASES FOR THE PREPARATION OF HETEROGENEOUS CATALYSTS*, volume 91 of *STUDIES IN SURFACE SCIENCE AND CATALYSIS*, pages 227–235. ELSEVIER SCIENCE PUBL B V, 1995.

[126] Lin Li, Aiqin Wang, Botao Qiao, Jian Lin, Yanqiang Huang, Xiaodong Wang, and Tao Zhang. Origin of the high activity of Au/FeOx for low-temperature CO oxidation: Direct evidence for a redox mechanism. *JOURNAL OF CATALYSIS*, 299:90–100, 2013.

[127] M Haruta. Gold as a novel catalyst in the 21st century: Preparation, working mechanism and applications. *GOLD BULLETIN*, 37(1-2):27–36, 2004.

[128] Zbynek Novotny, Giacomo Argentero, Zhiming Wang, Michael Schmid, Ulrike Diebold, and Gareth S. Parkinson. Ordered Array of Single Adatoms with Remarkable Thermal Stability: Au/Fe3O4(001). *PHYSICAL REVIEW LETTERS*, 108(21), 2012.

[129] JMC Soares, P Morrall, A Crossley, P Harris, and M Bowker. Catalytic and noncatalytic CO oxidation on Au/TiO2 catalysts. *JOURNAL OF CATALYSIS*, 219(1):17–24, 2003.

[130] T Kendelewicz, P Liu, CS Doyle, GE Brown, EJ Nelson, and SA Chambers. Reaction of water with the (100) and (111) surfaces of Fe3O4. *SURFACE SCIENCE*, 453(1-3):32–46, 2000.

[131] R Zanella, S Giorgio, CR Henry, and C Louis. Alternative methods for the preparation of gold nanoparticles supported on TiO2. *JOURNAL OF PHYSICAL CHEMISTRY B*, 106(31):7634–7642, 2002.

[132] SK Shaikhutdinov, R Meyer, M Naschitzki, M Baumer, and HJ Freund. Size and support effects for CO adsorption on gold model catalysts. *CATALYSIS LETTERS*, 86(4):211–219, 2003.

[133] M Haruta, BS Uphade, S Tsubota, and A Miyamoto. Selective oxidation of propylene over gold deposited on titanium-based oxides. *RESEARCH ON CHEMICAL INTERMEDIATES*, 24(3):329–336, 1998.

[134] B.V. Crist. *The Handbooks of Monochromatic XPS Spectra Series: Commercially Pure Binary Oxides.* Number Bd. 2. XPS International, 2004.

[135] Luis K. Ono and Beatriz Roldan-Cuenya. Effect of interparticle interaction on the low temperature oxidation of CO over size-selected Au nanocatalysts supported on ultrathin TiC films. *CATALYSIS LETTERS*, 113(3-4):86–94, 2007.

[136] Luis K. Ono and Beatriz Roldan Cuenya. Formation and thermal stability of Au2O3 on gold nanoparticles: Size and support effects. *JOURNAL OF PHYSICAL CHEMISTRY C*, 112(12):4676–4686, 2008.

Selbständigkeitserklärung

Hiermit erkläre ich, die vorliegende Arbeit selbstständig ohne fremde Hilfe verfaßt und keine weiteren Hilfsmittel als die angegebenen verwendet zu haben.

Rhys Montgomery Dowler
Berlin, 4. November 2013